INVESTIGATIONS ON FORMABILITY OF TAILOR WELDED BLANKS OF ALUMINIUM ALLOY IN WARM WORKING

Thesis Submitted
in Fulfillment of the Requirements for the
Degree of

DOCTOR OF PHILOSOPHY

In
Mechanical Engineering

by

Rakesh Kumar
(Roll No. 2K18/PHDME/05)

Under the Supervision of
Prof. Vijay Gautam
Professor, Department of Mechanical Engineering
Delhi Technological University

To the
Department of Mechanical Engineering

DELHI TECHNOLOGICAL UNIVERSITY
(Formerly Delhi College of Engineering)
Shahbad Daulatpur, Main Bawana Road, Delhi-110042, India

September, 2026

DELHI TECHNOLOGICAL UNIVERSITY

(Formerly Delhi College of Engineering)
Shahbad Daulatpur, Main Bawana Road, Delhi-110042

CANDIDATE DECLARATION

I, **Rakesh Kumar,** hereby certify that the work which is being presented in the thesis entitled "**Investigations on Formability of Tailor Welded Blanks of Aluminium Alloy in Warm Working"** in fulfillment of the requirements for the award of the Degree of Doctor of Philosophy, submitted in the Department of Mechanical Engineering, Delhi Technological University is an authentic record of my own work carried out during the period from August 2018 to July 2026 under the supervision of Prof Vijay Gautam, Department of Mechanical Engineering, Delhi Technological University, Delhi. The matter presented in the thesis has not been submitted by me for the award of any other degree of this or any other Institute.

Rakesh Kumar
(Roll No.- 2K18/PHDME/05)

DELHI TECHNOLOGICAL UNIVERSITY

(Formerly Delhi College of Engineering)
Shahbad Daulatpur, Main Bawana Road, Delhi-110042

CERTIFICATE BY THE SUPERVISOR

Certified that **Rakesh Kumar (**2K18/PHDME/05) has carried out the research work presented in his thesis entitled "**Investigations on Formability of Tailor Welded Blanks of Aluminium Alloy in Warm Working"** for the award of **Doctor of Philosophy** from Department of Mechanical Engineering, Delhi Technological University, Delhi, under my supervision. The thesis embodies results of original work, and studies are carried out by the student himself and the contents of the thesis do not form the basis for the award of any other degree to the candidate or to anybody else from this or any other University/Institution.

Prof. Vijay Gautam
Professor
Department of Mechanical Engineering
Delhi Technological University, New Delhi

Date:

ACKNOWLEDGEMENTS

I would like to convey my deep sense of gratitude and sincere thanks to my supervisor Professor Vijay Gautam, Department of Mechanical Engineering, Delhi Technological University, for giving me an opportunity to pursue this research work under his guidance. He has been a tremendous mentor for me. Perseverance, exuberance, positive approaches are just some of the traits they have imprinted on my personality.

He steered me through this journey with his invaluable advice, positive criticism, stimulating discussions and consistent encouragement. If I will stand proud of my achievements, then undeniably he is the main creditor. It is my privilege to be under his guidance. His advice on both research as well as on my career have been priceless. Words are short to suffice his favour and cooperation. I am grateful to him in all respects.

I would like to express my gratitude to Prof. Prateek Sharma, Vice chancellor, Delhi Technological University, Delhi for providing this opportunity to carry out this work in this prestigious institute.

I would like to thank Prof. B.B. Arora, Head of the Department of Mechanical Engineering, and Prof. Akhilesh Arora, DRC Chairman, for their support in finishing this work.

I wish to record my thanks and gratitude to my Internal SRC expert, Prof. Raj Kumar Singh, Department of Mechanical Engineering (Delhi Technological University); and External SRC experts Prof. P. M. Pandey, Department of Mechanical Engineering (IIT Delhi), Prof. Mohammed Suhaib, Department of Mechanical Engineering (JMI New

Delhi), and Prof. M. Jayasimhadri, Department of Applied Physics (Delhi Technological University), for their valuable guidance, critical and constructive discussion during this work.

I would like to thank my senior fellow research scholar, Dr. Pankaj Kumar Sharma, for his support and guidance during my PhD work. Special thanks to my elder brother and senior fellow research scholar, Dr. Ravi Datt Yadav, for his continuous support and guidance throughout my research. I would also like to express my special thanks to my senior fellow research scholars, Dr. Bijendra Prasad, Dr. Subhajit Konar, and Dr. Praveen Kumar Singh, for their support, guidance, and encouragement during my research work. Also, I would like to thank my fellow research scholars, Mr. Gaurav Ranjan and Mr. Jayant, for helping and encouraging me throughout my research. Without their support and motivation, pursuit of this PhD work would have never been possible.

I would like to thank Lab Assistant/ Senior Technician Mr. Ignatius Francis, Mr. Om Prakash and Mr. Tek Chand for their help and support during the experimental work in the Metal Forming Laboratory.

I sincerely thank the anonymous reviewers whose insightful and constructive comments and suggested revisions improved the organization and clarity of the research.

I am greatly indebted to my parents Mr. Lal Singh and Mrs. Prem Lata and my parents-in-law Dr. Kamal Singh Yadav and Mrs. Manju Yadav for their love and blessings to see me scaling greater heights of life. I would like to express my sincere gratitude to my sisters-in-law, Mrs. Renuka Yadav and Ms. Kanishka Yadav, for their love and

support. I also appreciate my niece, Yashvi, and my nephew, Rudransh, for bringing happiness during my PhD journey.

With immense pleasure and delight, I would like to thank my life partner Ms. Riya Yadav for giving me mental and moral support in my highs and lows of this PhD journey.

Ultimately, I acknowledge the quiet inner voice and resilience that kept me grounded, focused, and moving forward during moments of doubt.

ABSTRACT

This study offers a methodical examination of the mechanical properties, microstructural changes, and heated formability of laser-welded AA6082 Aluminium alloy tailor welded blanks (TWBs). Commercially obtainable sheets with thicknesses of 1.5, 2.0, 2.5, and 3.0 mm were utilized to create tailored welded blanks (TWB) including various thickness combinations (1.5×2.0 mm, 1.5×2.5 mm, and 1.5×3.0 mm) employing an industrial robotic fiber laser welding apparatus. Initial annealing trials determined 350°C to be the optimal pre-welding thermal treatment, achieving an excellent equilibrium between strength (94 MPa yield strength) and ductility (19.8% elongation). Subsequent tensile analysis at high temperatures indicated that 300°C is the optimal temperature for warm forming. At this temperature, the substance demonstrated its peak elongation (28.2%) and a significant rise in the strain-hardening exponent (n = 0.18), which is essential for facilitating uniform strain distribution and postponing localized necking.

The refinement of laser welding parameters (3700-4000 W) resulted in flawless joints. Tensile tests validated exceptional weld integrity, with failure consistently manifesting in the thinner (1.5 mm) base sheet instead of the fusion zone. Microhardness assessments revealed concentrated hardening in the fusion zone (72-73 HV0.5) in contrast to the base metals (47-54 HV0.5), thereby effectively relocating the "weakest link" to the parent material. The assessment of stretch formability was conducted by Limit Dome Height (LDH) and Forming Limit Diagrams (FLD) at ambient temperature and under warm forming scenarios. Findings revealed that weld bead orientation is a more influential variable than temperature by itself; longitudinal weld alignment markedly enhanced LDH at 300°C, specifically by 49.6% for the 1.5 × 3.0 mm configuration, whereas transverse alignment exhibited minimal enhancement. The combinations examined, the 1.5 × 3.0 mm TWB exhibited the superior forming capability, attaining the maximum LDH (17.5 mm) and the most advantageous FLD at 300°C.

Microstructural analysis by Electron Backscatter Diffraction (EBSD) demonstrated grain

enlargement in the fusion zone (29.25 μm) relative to the base metals and heat affected zones (HAZs). Notwithstanding the bigger grains, the fusion zone retained its strength owing to a modest density of Geometrically Necessary Dislocations (GND) and its crystallographic texture. Ultimately, finite element analyses utilizing Abaqus/Explicit effectively forecasted strain distributions and failure sites, validating that warm forming at 300°C yields a more uniform strain distribution. This research indicates that the 1.5 × 3.0 mm longitudinal TWB created at 300°C yields the best balance of welding quality, mechanical properties, and warm forming characteristics.

Keywords: AA6082 aluminium alloy, Annealing, Tailor welded blanks, Laser welding, Warm forming, Electron Backscatter Diffraction, Limiting Dome Height, Forming Limit Diagram, Finite Element Analysis.

TABLE OF CONTENTS

Topics	Page No.
Candidate Declaration	i
Certificate by the Supervisor	ii
Acknowledgements	iii-v
Abstract	vi-vii
Table of Contents	viii-xi
List of Figures	xii-xv
List of Tables	xvi
List of Abbreviations	xvii
Nomenclatures	xviii
Chapter 1: Introduction	**1-39**
1.1 Aluminium Alloys	1
1.1.1 Importance of Light Weight Sheet Materials	2
1.1.2 Aluminium Alloys Application in Automobile Body Parts	4
1.1.3 Sheet Materials for Weight Reduction of Autobody	6
1.1.4 Characteristics of Aluminium Alloy Sheets	7
1.1.5 Other Lightweight Materials and Their Automotive Challenges	7
1.2 Tailor Welded Blanks (TWBs)	8
1.3 Laser Welding	14
1.4 Work Hardening of Aluminium Alloys	19
1.4.1 Work Hardening	20
1.4.2 Precipitation Hardening	21
1.4.3 Annealing	22

1.5 Sheet Metal Forming 24

1.6 Formability 26

1.6.1 Erichsen Cup Test 26

1.6.2 Limiting Dome Height Test 27

1.6.3 Hydraulic Bulge Test 28

1.6.4 Swift Cup Drawing Test 29

1.7 Warm Forming 29

1.8 Forming Limit Diagram 34

1.9 Important Material Parameters Which Affect Formability 36

1.9.1 Strain Hardening Exponent 36

1.9.2 Anisotropy 36

1.9.3 Sheet Thickness 37

1.9.4 Ductility 38

1.10 Summary 38

Chapter 2: Literature Review **40-86**

2.1 Aluminium Alloys 40

2.2 Annealing 46

2.3 Tailor Welded Blanks 50

2.4 Laser Welding 56

2.5 Formability 64

2.6 Warm Forming 69

2.7 Formability of TWBs 76

2.8 Research Gaps 83

2.9. Research Novelty and Contributions 84

2.10. Research Objectives 86

Chapter 3: Methodology **87-106**

3.1 Material Selection 88

3.2 Determination of Annealing Temperature of Parent Sheet 88

3.3 Fabrication of Tailor Welded Blanks 89

3.3.1 Laser Welding System and Fixture 89

3.3.2 Welding Parameters and TWB Combinations 90

3.4 Tensile Characterization 93

3.4.1 Tensile Specimen Preparation 93

3.4.2 Tensile Testing of AA6082-O 94

3.4.3 Normal Anisotropy (r-value) Measurement 97

3.4.4 Tensile Testing of Laser Welded Tailor Welded Blanks 99

3.5 Microhardness Measurement 99

3.6 Formability Evaluation 101

3.7 Microstructural Characterization 103

3.7.1 Sample Preparation 103

3.7.2 Electron Backscatter Diffraction (EBSD) 104

3.8 Finite Element Simulation 104

Chapter 4: Results and Discussion **107-145**

4.1 Optimization of Annealing Temperature 107

4.2 Tensile Properties of AA 6082-O 110

4.3 Laser Weld Quality 114

4.3.1 Weld Integrity 114

4.3.2 Weld Strength 117

4.4 Hardness Distribution 119

4.5 Formability (Limit Dome Height) 121

4.6 Forming Limit Diagram 126

4.7 Microstructural Characterization 129

4.7.1 Base Metals 129

4.7.2 Heat Affected Zones (HAZs) 133

4.7.3 Fusion Zone (Weld Zone) 136

4.8 Finite Element Analysis 139

4.9 Summary 143

Chapter 5: Conclusions and Future Research Scope **146-151**

5.1 Conclusions 146

5.2 Future Research Scope 150

References **152-173**

Plagiarism Report **174-175**

Publications Based on the Research Work **176**

Proof of Publications **177-179**

Biodata **180**

LIST OF FIGURES

Figure No.	Title	Page No.
Figure 1.1	Growth in the use of aluminium and its alloys in the automotive industry	3
Figure 1.2	Applications of aluminium alloys in automobiles	4
Figure 1.3	Growth of Aluminium in car body application	5
Figure 1.4	Principle of tailor welded blanks	9
Figure 1.5	Tailor welded blanks applications in white body	11
Figure 1.6	Application of a TWB in inner door panel for an automobile	12
Figure 1.7	Schematic diagram of laser welding set-up	15
Figure 1.8	Effect of annealing on the structure and mechanical property changes of a cold-worked metal	23
Figure 1.9	Sheet metal forming operations	24
Figure 1.10	Schematic of the setup for Erichsen test and a tested sample	27
Figure 1.11	Schematic of the setup for limiting dome height test	27
Figure 1.12	Hydraulic bulge test	28
Figure 1.13	Swift cup test and a drawn cup	29
Figure 1.14	Schematic illustration of the warm forming (HFQ) process	33
Figure 1.15	Forming-limit diagrams (FLD) for various sheet metals and strains in deformed circular grid patterns	35
Figure 3.1	Schematic representation of the overall research methodology adopted in the present study.	87
Figure 3.2	Experimental setup of the laser welding system and clamping fixture used for butt welding to fabricate TWBs	90
Figure 3.3	Schematic representation of the AA 6082 aluminium alloy	92

	TWB combinations	
Figure 3.4	ASTM E8/E8M sub-size tensile specimen geometry and dimensions	93
Figure 3.5	Laser-cut tensile specimens prepared for (a) anisotropy (b) weld integrity and (c) weld strength	94
Figure 3.6	Tinius Olsen H50KS bench top universal tensile testing machine with environmental chamber	95
Figure 3.7	Struers DURAMIN 40 microhardness tester	100
Figure 3.8	FLD specimens of laser welded tailor welded blanks showing (a) transverse and (b) longitudinal weld bead orientations	101
Figure 3.9	100 tonne hydraulic press with integrated heating system	102
Figure 3.10	Finite element model of the blank, spacer, punch, die, and blank holder used for formability simulation in ABAQUS	105
Figure 4.1	Effect of annealing temperature on the tensile strength of AA 6082	107
Figure 4.2	Effect of annealing temperature on the elongation of AA 6082	108
Figure 4.3	Effect of annealing temperature on the Vickers hardness of AA 6082	109
Figure 4.4	(a) Engineering and (b) true stress–strain curves of annealed AA 6082-O tested at room temperature, 180°C, 240°C, and 300°C	113
Figure 4.5	Engineering stress–strain curves of laser-welded tailor welded blanks for weld integrity evaluation	115
Figure 4.6	Tensile-tested laser-welded tailor welded blank specimens used for weld integrity evaluation	115

Figure 4.7	Engineering stress–strain curves of laser-welded tailor welded blanks for weld strength evaluation	118
Figure 4.8	Vickers hardness distribution across the weld region of laser-welded tailor welded blanks with different thickness combinations	119
Figure 4.9	LDH specimens of the 1.5 × 2.0 mm TWB under (a) transverse and (b) longitudinal weld bead orientation	122
Figure 4.10	LDH specimens of the 1.5 × 2.5 mm TWB under (a) transverse and (b) longitudinal weld bead orientation	123
Figure 4.11	LDH specimens of the 1.5 × 3.0 mm TWB under (a) transverse and (b) longitudinal weld bead orientation	124
Figure 4.12	Forming limit diagrams of the (a) 1.5 × 2.0 mm, (b) 1.5 × 2.5 mm and (c) 1.5 × 3.0 mm TWB	128
Figure 4.13	EBSD characterization of the 1.5 mm base metal: (a) inverse pole figure (IPF) map, (b) pole figures, (c) geometrically necessary dislocation (GND) distribution map, and (d) GND density distribution	130
Figure 4.14	EBSD characterization of the 3.0 mm base metal: (a) inverse pole figure (IPF) map, (b) pole figures, (c) geometrically necessary dislocation (GND) distribution map, and (d) GND density distribution	132
Figure 4.15	EBSD characterization of the heat-affected zone (HAZ) adjacent to the 1.5 mm sheet: (a) inverse pole figure (IPF) map, (b) pole figures, (c) geometrically necessary dislocation (GND) distribution map, and (d) GND density distribution	134

Figure 4.16	EBSD characterization of the heat-affected zone (HAZ) adjacent to the 3.0 mm sheet: (a) inverse pole figure (IPF) map, (b) pole figures, (c) geometrically necessary dislocation (GND) distribution map, and (d) GND density distribution	135
Figure 4.17	EBSD characterization of the fusion zone (weld zone): (a) inverse pole figure (IPF) map, (b) pole figures, (c) geometrically necessary dislocation (GND) distribution map, and (d) GND density distribution	137
Figure 4.18	Maximum in-plane principal strain distribution predicted by FEA for the 1.5 × 2.0 mm tailor welded blank at (a) room temperature and (b) 300°C	140
Figure 4.19	Maximum in-plane principal strain distribution predicted by FEA for the 1.5 × 2.5 mm tailor welded blank at (a) room temperature and (b) 300°C	141
Figure 4.20	Maximum in-plane principal strain distribution predicted by FEA for the 1.5 × 3.0 mm tailor welded blank at (a) room temperature and (b) 300°C	142

LIST OF TABLES

Table No.	Title	Page No.
Table 3.1	Chemical composition of AA 6082 aluminium alloy (in wt.%).	88
Table 4.1	Mechanical properties of annealed AA 6082-O at room temperature	111

LIST OF ABBREVIATIONS

AA	Aluminium Alloy
ASTM	American Society for Testing and Materials
CAE	Computer Aided Engineering
EBSD	Electron Backscattered Diffraction
FEA	Finite Element Analysis
FLD	Forming Limit Diagram
GND	Geometrically Necessary Dislocations
HAZ	Heat Affected Zone
HV	Hardness on Vickers Scale
IPF	Inverse Pole Figure
LBW	Laser Beam Welding
LDH	Limiting Dome Height
MRD	Multiples of Random Distribution
RD	Rolling Direction
SEM	Scanning Electron Microscopes
TD	Transverse Direction
TWB	Tailor Welded Blank
UTS	Ultimate Tensile Strength
WI	Weld Integrity
WS	Weld Strength
XRD	X-ray diffraction
YS	Yield Strength

NOMENCLATURES

n	Strain Hardening Exponent
K	Strength Coefficient
P	Laser Power
σ_e	Engineering Stress
ε_e	Engineering Strain
σ_t	True Stress
ε_t	True Strain
ε_w	True Width Strain
ε_l	True Longitudinal Strain
ε_t	True Thickness Strain
r	Plastic Strain Ratio
$\overline{r}$	Normal Anisotropy

CHAPTER 1

INTRODUTION

1.1 Aluminium Alloys

Aluminium and its alloys are extensively utilized engineering materials due to their lightweight nature, favorable strength-to-weight ratio, resistance to corrosion, malleability, weldability, and recyclability. Aluminium, possessing a density of roughly 2.7 g/cm^3, is approximately one-third as dense as steel, rendering it especially appealing for lightweight constructions in the automotive, aerospace, marine, and transportation industries. Its capacity to generate a stable and cohesive oxide layer also offers substantial resistance to atmospheric and various environmental factors. Moreover, Aluminium alloys can be easily manipulated by rolling, extrusion, forging, stamping, and various other manufacturing techniques, facilitating the creation of components with varied shapes. Aluminium alloys are generally categorized into eight primary series based on their main alloying constituents. The 1xxx series comprises economically pure Aluminium, noted for its excellent corrosion resistance and superior electrical and thermal conductivity, albeit with comparatively low strength. The 2xxx series is predominantly alloyed with copper and exhibits elevated strength post-heat treatment, rendering it appropriate for heavily loaded structural uses. The 3xxx series features manganese as the primary alloying component and provides moderate strength, excellent formability, and resistance to corrosion. The 4xxx series is predominantly alloyed with silicon and is extensively utilized for welding and brazing due to its comparatively low melting point. The 5xxx series incorporates magnesium and offers excellent strength, resistance to corrosion, and weldability, especially suited for marine uses. The 6xxx series has magnesium and silicon as the primary alloying

constituents, which create Mg_2Si and allow these alloys to undergo heat treatment. These alloys offer a beneficial blend of moderate strength, formability, weldability, machinability, and corrosion resistance, rendering them appealing for automobile structural and body uses. Within the 6xxx series, AA6082 is a heat-treatable alloy comprising magnesium and silicon, and it is frequently regarded for structural uses that necessitate a blend of strength, formability, and corrosion resistance. The attributes of AA6082 render it especially pertinent for the production and shaping of tailor welded blanks (TWBs). The 7xxx series is predominantly alloyed with zinc, typically alongside magnesium and additional elements, and exhibits exceptional strength following heat treatment. These alloys are widely utilized in components subjected to significant stress in aerospace and structural applications. The 8xxx family encompasses Aluminium alloys featuring various alloying methods tailored for certain uses, including those with lithium or iron-based dispersoids.

The 6xxx series of alloy families is notably significant for this study because to its amalgamation of strength, formability, weldability, and resistance to corrosion. Consequently, AA6082 has been chosen as the material to examine the forming characteristics of laser-welded tailor welded blanks in heated forming scenarios.

1.1.1 Importance of Light Weight Sheet Materials

Minimizing weight is a crucial goal in contemporary vehicle engineering since it enhances fuel efficiency, decreases energy usage and emissions, and reduces material consumption and production expenses. A decrease in vehicle weight can lead to an enhancement in fuel efficiency and a decline in emissions [1–2]. Aluminium alloys are progressively regarded as lightweight substitutes for traditional steels in automotive

uses due to their low density, superior strength-to-weight ratio, resistance to corrosion, recyclability, and favorable manufacturability [3–4]. Their amalgamation of mechanical and functional attributes has facilitated their application in vehicle chassis, enclosures, and various lightweight elements. The utilization of Aluminium in vehicles has significantly risen over the years, particularly in the applications of Aluminium sheets and plates. Enhanced mechanical characteristics of Aluminium alloys by alloying and thermal processing have broadened their use in automotive and aerospace frameworks [5]. The rising utilization of Aluminium sheet materials has generated a demand for effective joining and shaping methods that can manufacture lightweight components with customized thickness and characteristics. In this scenario, tailor welded blanks (TWBs) offer a proficient method for amalgamating sheets of varying thicknesses and/or materials before shaping, thereby allowing for the strategic placement of material where it is most needed. Figure 1.1 depicts the rising utilization of Aluminium and its alloys in automotive applications throughout the years, including components like heat exchangers, bumpers, hoods, and body-in-white structures [6].

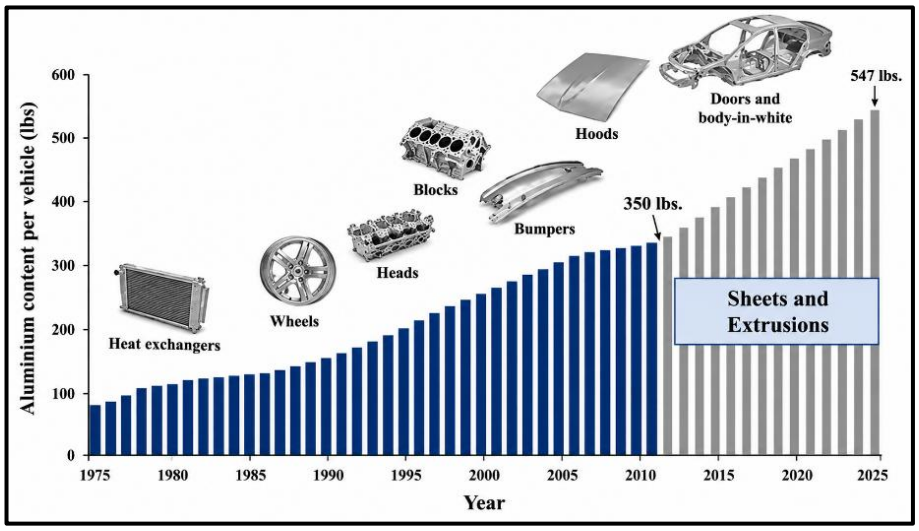


Figure 1.1 Growth in the use of aluminium alloys in the automotive industry [6].

Figure 1.2 depicts multiple utilizations of Aluminium alloys within the automobile industry. Notwithstanding their lightweighting capabilities, the constrained formability of numerous Aluminium alloys at ambient temperature may limit their application in intricate sheet-metal parts. Consequently, appropriate forming techniques are necessary to enhance their formability and facilitate the production of lightweight vehicle parts. Various methodologies examined for improving the formability of Aluminium sheets include sophisticated forming techniques and, crucially for this research, warm forming, which facilitates shaping at higher temperatures.

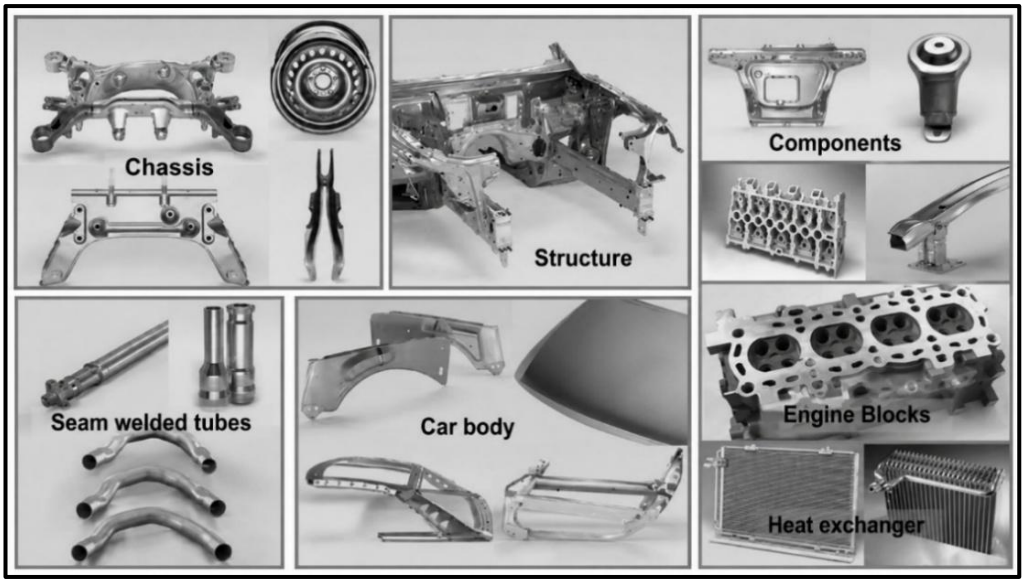


Figure 1.2 Applications of aluminium alloys in automobiles [7].

1.1.2 Aluminium Alloys Application in Automobile Body Parts

The rise in environmental rules and the necessity to diminish fuel usage and CO_2 emissions have spurred the advancement of lightweight automotive frameworks. Minimizing vehicle mass can be accomplished via enhanced structural design, diminished component sizes, and substituting traditional materials with lighter options

(Figure 1.3). Among these methodologies, replacing steel with Aluminium alloys presents considerable promise due to their reduced density and advantageous strength-to-weight ratio. As a result, Aluminium alloys are progressively utilized in automotive body parts and various structural applications where minimizing weight is a key design goal.

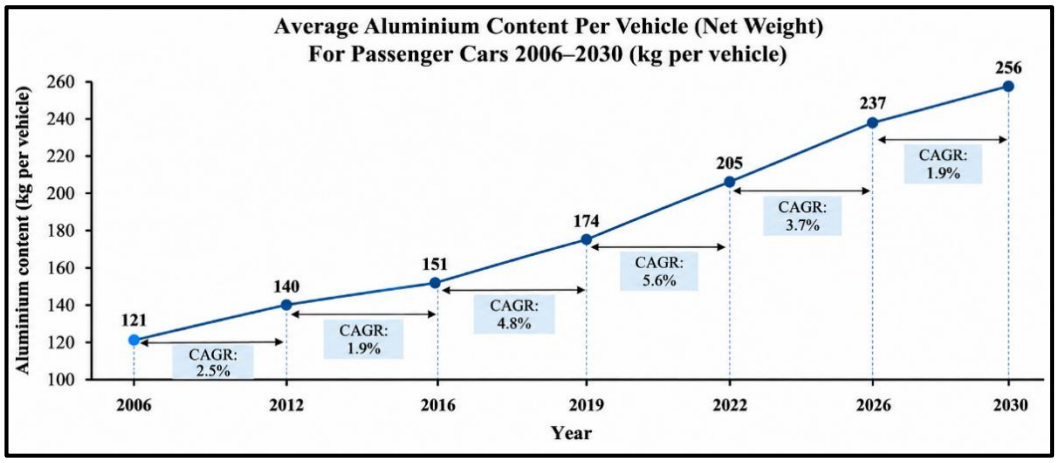


Figure 1.3 Growth of Aluminium in car body application [8].

Figure 1.1 depicts the historical expansion and variety of Aluminium uses within the automotive sector, while Figure 1.3 showcases the historical and anticipated rise in the average Aluminium composition per passenger vehicle. Although reducing vehicle dimensions can contribute to weight alleviation, enhanced safety regulations, greater passenger comfort, and the addition of extra equipment have generally resulted in an escalation of vehicle weight. Consequently, car manufacturers have increasingly relied on structural improvements and lightweight materials to reduce vehicle weight. The transition from conventional body structures to monocoque designs and the progressive integration of high-strength steels marked notable progress in reducing vehicle weight. However, further reduction in weight requires the utilization of

materials with lower density while maintaining adequate mechanical characteristics and manufacturability. This has increased enthusiasm for lightweight sheet materials, particularly Aluminium alloys, in automotive body and structural components.

1.1.3 Sheet Materials for Weight Reduction of Automotive Body

The rising necessity for vehicle lightweighting has encouraged the utilization of Aluminium alloy sheets in automotive body and structural elements. Aluminium sheets are utilized in parts like hoods, fenders, and roof or sunroof panels, where their lightweight nature offers considerable weight savings over traditional steel sheets. Nonetheless, their elevated material expenses and variations in forming and joining characteristics relative to steel may restrict their broader utilization. Consequently, choosing a suitable sheet material necessitates evaluating mechanical characteristics, formability, manufacturability, longevity, expense, and recyclability. Formability holds significant importance in the production of extensive and intricately shaped automotive sheet parts. It delineates the capacity of a sheet material to experience the necessary plastic deformation devoid of flaws like fractures, excessive thinning, wrinkling, dimensional errors, or surface distortion. The comprehensive forming efficacy can thus be evaluated based on fracture resistance, shape preservation, and the capacity of the sheet to adapt to the specified component geometry [9–10]. From the viewpoint of sheet metal forming, fracture-associated formability encompasses deformation techniques like deep drawing, stretching, stretch flanging, and bending [9]. The attributes of the material and the conditions of forming both affect the ultimate quality of stamped parts. Specifically, elastic recovery post-forming can cause springback and dimensional discrepancies, whereas inadequate formability may result

in localized thinning, necking, or rupture. Consequently, a suitable amalgamation of material characteristics and fabrication parameters is crucial for the creation of flawless automobile sheet components.

1.1.4 Characteristics of Aluminium Alloy Sheets

Automotive body applications predominantly utilize heat-treatable 6xxx series Al–Mg–Si alloys and non-heat-treatable 5xxx series Al–Mg alloys, with 2xxx series Al–Cu alloys employed in specific instances. The 5xxx and 6xxx series are especially pertinent to automotive sheet applications due to its advantageous blend of strength, formability, corrosion resistance, and manufacturability. In contrast to steel, Aluminium alloys possess a reduced elastic modulus and typically demonstrate distinct yielding and plastic deformation characteristics. Their reaction during formation is additionally affected by plastic anisotropy, work hardening, and the propensity for localized deformation under specific forming circumstances. Thus, the fabrication of Aluminium alloy sheets, especially for intricate automotive parts, may encounter difficulties like localized thinning, wrinkling, springback, and early fracture. The advancement of Aluminium alloys exhibiting enhanced strength and ductility has broadened their use in automotive body frameworks. The 6xxx series alloys provide an advantageous equilibrium of strength, malleability, corrosion resistance, and heat-treatment adaptability, rendering them ideal for lightweight sheet parts and custom welded blanks.

1.1.5 Other Lightweight Materials and Their Automotive Challenges

Apart from Aluminium alloys and TWBs, many lightweight materials are utilized in aircraft and other transportation sectors due to their elevated specific strength and

rigidity. Titanium alloys provide exceptional specific strength, resistance to corrosion, and reliable performance under high temperatures; yet, their considerable expense and stringent manufacturing and shaping demands restrict their extensive adoption in automotive sectors. Magnesium alloys offer a reduced density compared to Aluminium, although they may have challenges with corrosion resistance and formability, especially at ambient temperatures. Fibre-reinforced polymer composites, including carbon-fibre-reinforced polymers (CFRPs), offer remarkable specific strength and rigidity; nonetheless, their elevated cost, anisotropic characteristics, joining and repair necessities, and recycling difficulties may limit their wider use in the automotive sector. High-strength steels continue to be prevalent due to their robustness, established production systems, and comparatively low expense, despite their increased density restricting potential weight reduction [9], [37]. Consequently, the selection of materials for lightweight vehicle constructions necessitates a balance between density, specific mechanical characteristics, formability, manufacturability, durability, joining criteria, cost, and recyclability. In this context, Aluminium alloys provide an advantageous blend of low density, mechanical properties, corrosion resistance, and manufacturing flexibility, rendering them appealing for lightweight automobile sheet parts.

1.2 Tailor Welded Blanks (TWBs)

Tailor-welded blanks (TWBs) are semi-finished metal sheets created by fusing two or more sheets before to the shaping process as shown in Figure 1.4. The individual sheets may possess the same or varying thicknesses, material classifications, mechanical characteristics, or surface treatments based on the functional specifications of the ultimate component. Subsequent to welding, the combined blank is then shaped by

traditional sheet metal forming techniques like deep drawing or stamping to create intricate structural elements. This production method allows engineers to position material exclusively where necessary, thus attaining an ideal balance of strength, rigidity, weight minimization, and cost efficiency. Due to these benefits, tailor-welded blanks have emerged as a crucial lightweight production technology utilized by the automobile sector [11–14]. The rising need for lightweight automobiles, enhanced fuel efficiency, and rigorous environmental standards has expedited the advancement of TWB technology in recent decades. Standard sheet elements produced from consistent sheet thickness may possess surplus material in areas experiencing comparatively minimal stresses. Tailor-welded blanks address this constraint by enabling localized differences in thickness and material characteristics within a singular component. Consequently, considerable decreases in vehicle mass can be attained without jeopardizing structural integrity. Supplementary benefits encompass superior crashworthiness, heightened dimensional precision, diminished assembly processes, minimized material waste, decreased production expenses, increased design adaptability, and enhanced corrosion resistance, rendering TWBs exceptionally appealing for contemporary automotive body frameworks [13-14].

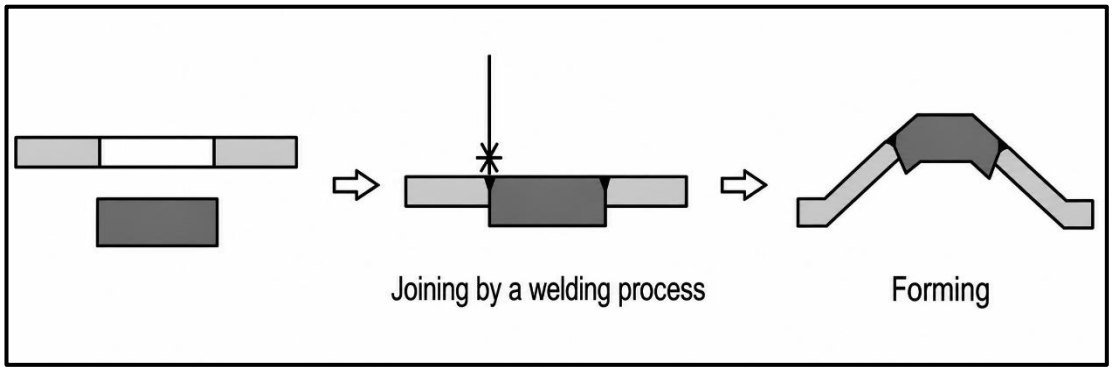


Figure 1.4 Principle of tailor welded blanks [14].

The commercial utilization of tailor-welded blanks commenced in the late twentieth century and has consistently grown alongside improvements in welding technologies. Initial fabrication methods encompassed resistance mash seam welding, electron beam welding, and gas tungsten arc welding. Nonetheless, laser beam welding (LBW) swiftly became the favored joining method due to its rapid welding speed, outstanding accuracy, minimal heat-affected zone (HAZ), reduced distortion, and straightforward automation. Friction stir welding (FSW) has lately attracted significant interest for aluminium alloys due to its solid-state joining process, which reduces fusion-related imperfections and enhances weld quality. As a result, both LBW and FSW are extensively utilized in the production of Aluminium tailor-welded blanks for lightweight structural purposes [14-16]. As shown in Figure 1.5 and 1.6, the tailor-welded blanks are widely utilized in the automobile sector for the production of door inner panels, floor panels, side members, roof rails, wheel housings, bumper reinforcements, engine compartment parts, B-pillars, frame rails, and deck lids. Their potential to amalgamate sheets of varying thicknesses or material classifications within a singular component allows engineers to enhance load-bearing strength while concurrently minimizing total vehicle weight. The removal of various spot welds and reinforcement components enhances structural integrity and manufacturing efficiency. These benefits have positioned TWBs as a pivotal enabling technology for the construction of lightweight vehicles [13-14].

Primarily, the majority of tailor-welded blanks were produced from steel due of its superior weldability and established manufacturing framework. Nevertheless, the rising focus on lightweight conveyance has markedly augmented the utilization of aluminium alloys in the automotive and aerospace sectors. Aluminium alloys exhibit

a low density, elevated specific strength, remarkable corrosion resistance, and exceptional recyclability, rendering them appealing substitutes for traditional steels. Recent advancements in heated shaping and sophisticated joining techniques have broadened the industrial utilization of aluminium tailor-welded blanks. The 6xxx series of commercial aluminium alloys has garnered significant interest due to its advantageous blend of strength, malleability, and resistance to corrosion [16-17].

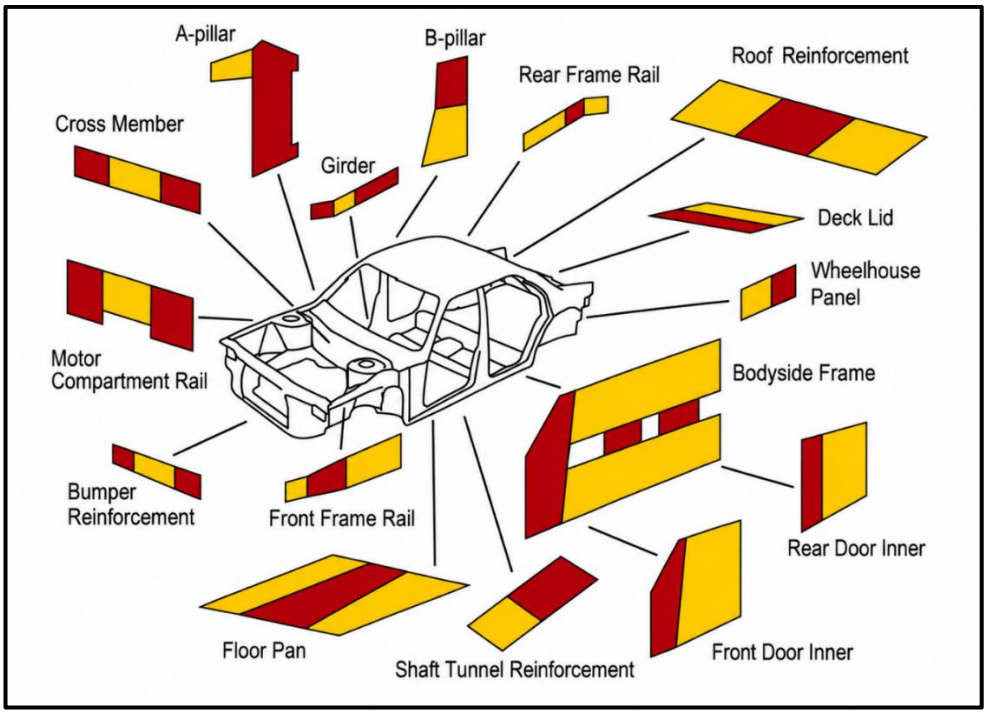


Figure 1.5 Tailor welded blanks applications in white body [9].

Despite the significant weight reduction advantages of aluminium alloys, their effective use as tailor-welded blanks presents difficulties due to their elevated thermal conductivity, high laser reflectivity, low molten viscosity, and persistent oxide layer. These traits commonly result in welding imperfections like porosity, hot cracking, depletion of alloying elements, and softening in the heat-affected zone. Thus, the mechanical characteristics and deformability of welded blanks are significantly

affected by the welding technique and its parameters. Merklein et al. highlighted the necessity of optimizing welding parameters to enhance the structural integrity of aluminium tailored welded blanks [14], whereas Wang et al. illustrated that satisfactory joints can be achieved through both laser beam welding and friction stir welding when suitable process conditions are applied [16]. Numerous scholars have examined the impact of welding methods on the deformation characteristics of aluminium tailor-welded blanks. Shakeri et al. indicated that formability diminishes as the thickness ratio increases and that fracture characteristics are significantly influenced by the welding technique [12] and the direction of loading Friedman and Kridli noted that blanks produced from sheets of uniform thickness typically failed in the weld area due to a diminished weld cross-section, while varying thickness combinations demonstrated enhanced deformation capacity owing to the development of a transition zone. Similarly, Stasik and Wagoner shown that aligning the weld line with the loading direction markedly enhances ductility in contrast to transverse loading, underscoring the significance of weld orientation in component design [14].

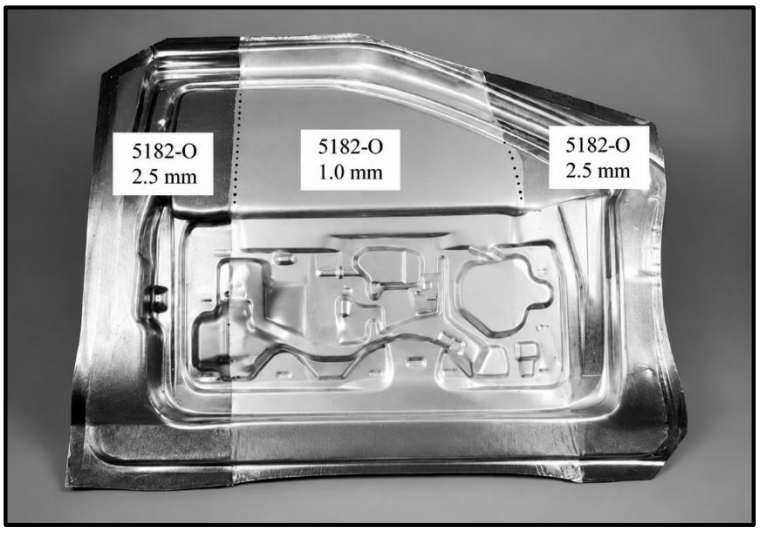


Figure 1.6 Application of a TWB in inner door panel for an automobile [10].

The impact of weld quality on formability has been thoroughly investigated. Bayley and Pilkey shown that interior weld flaws like porosity are significantly more harmful than exterior surface defects as they encourage early strain localization and fracture. In a similar vein, Davies et al. examined the ductility of weld metal and the forming limit behavior of Aluminium tailor-welded blanks, concluding that the weld zone displays deformation properties markedly distinct from the base material. Chien et al. additionally shown that strain localization typically begins at geometric irregularities in the weld profile, leading to reduced forming limits under biaxial loading compared to uniaxial tension [18]. As industrial demand escalates, numerical simulation has emerged as a crucial instrument for examining the deformation characteristics of tailor-welded blanks. Finite element analysis facilitates the forecasting of strain distribution, weld-line displacement, material thinning, springback, and failure onset before to actual manufacturing, thus minimizing both development duration and production expenses. Lamprecht illustrated that precise depiction of weld-zone attributes greatly enhances the correlation between experimental and simulated outcomes, while further studies validated that authentic modeling of weld features is crucial for dependable forecasting of forming behavior [19-21]. Recently, advanced computer methods have significantly improved the analysis and design of tailor-welded blanks. Veera Babu et al. created an expert system utilizing an artificial neural network (ANN) to forecast the tensile properties of steel and aluminium tailored welded blanks (TWB) through finite element simulation data. Their model effectively forecasted yield strength, ultimate tensile strength, uniform elongation, strain-hardening exponent, and strength coefficient across diverse welding and material scenarios, illustrating that ANN

methodologies can considerably diminish experimental labor while facilitating enhanced TWB design [22-23].

Prior studies unequivocally illustrate that tailor-welded blanks offer significant benefits in lightweight structural design via optimal material usage, superior crash performance, and increased manufacturing efficiency. Nonetheless, the formability of Aluminium tailor-welded blanks is significantly influenced by welding quality, weld orientation, sheet thickness combinations, characteristics of the heat-affected zone, and forming conditions. These obstacles persist in driving research into sophisticated welding methods, warm forming technologies, computational modeling, and intelligent optimization strategies to enhance the structural integrity and industrial utility of Aluminium tailor-welded blanks.

1.3 Laser Welding

Laser welding has become one of the most sophisticated fusion joining techniques due to its capacity to create high-quality joints with exceptional precision, profound penetration, reduced heat input, rapid welding speed, and little distortion. Due to these benefits, the technique has attained considerable significance in contemporary manufacturing sectors, especially in automotive, aircraft, railway, shipbuilding, and precision engineering, where lightweight constructions and elevated production efficiency are essential demands. In contrast to traditional arc welding methods, laser welding employs a highly focused laser beam as its heat source, leading to a narrow fusion zone, less heat-affected zone (HAZ), enhanced dimensional precision, and greater surface quality. Moreover, the non-contact characteristic of the procedure facilitates seamless automation, robotic incorporation, and adaptable manufacturing,

rendering laser welding a compelling joining technique for both mass production and high-value engineering applications [24-26]. The swift advancement of high-power laser technologies, such as CO_2, Nd: YAG, disk, diode, and fiber lasers, has significantly broadened the industrial utilization of laser welding. Fiber lasers have garnered significant interest due to their superior beam quality, remarkable electrical efficiency, adaptable beam delivery, and capacity to perform deep penetration welding. The enhanced features of contemporary laser systems have facilitated the welding of both thin sheets and thick sections with remarkable efficiency and outstanding consistency. As a result, laser welding has emerged as a favored method for combining lightweight Aluminium structures where precision and mechanical integrity are paramount (Figure 1.7).

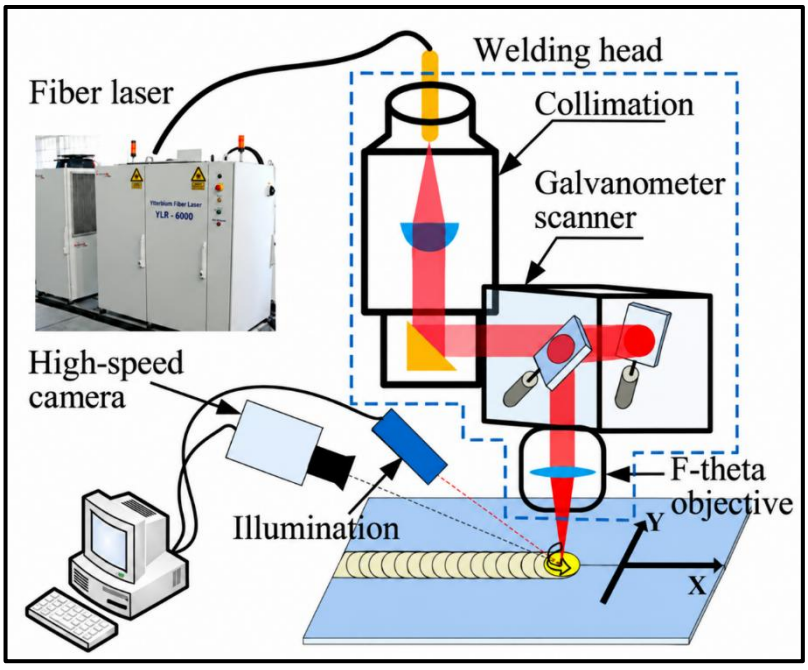


Figure 1.7 Schematic diagram of laser welding set-up (28).

The operational mechanism of laser welding relies on the transformation of focused laser energy into heat energy at the surface of the workpiece. Two distinct welding

modes are typically seen based on the density of laser power. At low power density, heat conduction welding takes place, resulting in superficial weld penetration. Nevertheless, when the laser power density beyond a threshold, localized vaporization of the substance leads to the creation of a keyhole. The numerous reflections of the laser beam within the keyhole greatly enhance energy absorption, resulting in deep and slender welds with a high aspect ratio. This keyhole mode is extensively utilized in structural applications due to its enhanced penetrating ability and greater welding efficiency compared to traditional fusion welding techniques [24-25]. Laser welding has gained significant relevance for aluminium alloys due to the rising need for lightweight transportation solutions that focus on decreasing vehicle mass, enhancing fuel efficiency, and minimizing carbon emissions. Aluminium alloys have a remarkable blend of elevated specific strength, resistance to corrosion, and recyclability, rendering them desirable materials for automotive and aerospace applications. Nonetheless, the effective fusion of aluminium alloys continues to pose difficulties owing to their elevated thermal conductivity, significant reflectivity to laser light, low viscosity of the liquefied metal, and the vaporization of volatile alloying constituents like magnesium. These traits frequently result in erratic keyhole dynamics, the emergence of porosity, solidification flaws, and diminished joint integrity if suitable welding conditions are not utilized. Numerous studies have consequently concentrated on comprehending the welding characteristics of aluminium alloys under varying laser processing parameters. Research on AA2024 aluminium alloy has shown that effective laser welding necessitates appropriate shielding gas selection, sufficient irradiation for steady keyhole development, and meticulous regulation of magnesium evaporation to reduce pore formation and

mitigate strength deterioration. Empirical studies focusing on microstructural analysis, hardness assessment, and tensile evaluation have demonstrated that refined laser settings can considerably diminish the extent of the heat-affected zone while preserving adequate mechanical properties. These results underscore the significance of parameter tuning in enhancing the quality of welds for precipitation-hardened Aluminium alloys [27]. Recent advancements have used beam oscillation methods to enhance weld quality in the laser welding of Aluminium alloys. Various oscillation patterns, including as transverse, longitudinal, and circular beam movements, have been documented to enhance the stability of the molten pool, optimize weld morphology, refine grain structure, and facilitate the development of equiaxed grains in the fusion zone. Despite the fact that beam oscillation might exert a minimal effect on ultimate tensile strength, it markedly enhances ductility by diminishing weld imperfections and optimizing solidification characteristics. Among the several oscillation techniques, circular beam oscillation has demonstrated the ability to yield superior welds with higher mechanical properties, attributed to better agitation of the molten pool and more consistent keyhole dynamics [28]. A significant domain of investigation has concentrated on the refinement of laser welding settings for high-strength Aluminium alloys like AA7075-T6. Due to the frequent inadequacy of traditional welding methods in achieving flawless joints in these alloys, fiber laser welding has been explored through statistical optimization approaches including Taguchi design and VIKOR analysis. Parameters such as laser intensity, welding velocity, and laser frequency have been refined to enhance tensile strength and hardness while reducing welding imperfections. These investigations illustrate that the

judicious selection of parameters is essential for attaining dependable joints acceptable for structural uses in lightweight vehicles [29].

Beyond process optimization, much focus has been directed on comprehending the essential physical processes involved in laser welding. Sophisticated experimental research has examined the behavior of laser-induced plumes, laser absorption, melt flow, keyhole dynamics, and the creation of porosity. These studies have demonstrated that consistent keyhole development, effective laser absorption, and regulated molten pool dynamics are crucial for achieving high-quality welds with significant penetration. Moreover, recent advancements like vacuum laser welding, tandem laser systems, and the laser joining of heterogeneous materials, such as metal-to-polymer and metal-to-composite connections, illustrate the growing potential of laser-based joining technologies for forthcoming lightweight manufacturing applications [30]. The increasing use of laser welding in industry has generated a need for dependable quality oversight and process management solutions. Contemporary investigations in laser welding have progressively concentrated on immediate quality evaluation through the utilization of optical sensors, infrared cameras, thermal imaging, acoustic emission analysis, photodiodes, and machine vision methodologies. These non-intrusive monitoring techniques provide ongoing surveillance of weld pool configuration, keyhole consistency, thermal distribution, and defect emergence throughout the welding process. Recently, multi-sensor monitoring systems combined with machine learning algorithms have demonstrated significant promise in forecasting weld quality and facilitating intelligent manufacturing systems that enable adaptive process control [31]. In conjunction with experimental studies, numerical modeling has emerged as a crucial instrument for examining laser welding techniques. Finite element modeling

has been extensively utilized to replicate temperature cycles, residual stresses, deformation, damage progression, fatigue characteristics, and hybrid laser welding techniques. Numerical simulation allows researchers to examine the impact of process parameters on weld quality, hence minimizing experimental expenses and development duration. The amalgamation of finite element analysis with empirical observations yields an extensive comprehension of laser welding dynamics and aids in the enhancement of industrial joining techniques [32].

Due to its capacity to provide accurate, high-quality, and low-distortion connections, laser welding has emerged as one of the most promising joining methods for lightweight Aluminium frameworks. Ongoing progress in laser sources, beam delivery mechanisms, process oversight, numerical simulation, and intelligent process regulation is broadening its industrial uses. As a result, laser welding has emerged as a crucial manufacturing technique for creating dependable welded connections in contemporary lightweight engineering components, especially within the automotive and aerospace industries where minimizing weight, ensuring structural integrity, and enhancing manufacturing efficiency are paramount.

1.4 Work Hardening of Aluminium Alloys

Work hardening, known as strain hardening, is a process where a material's strength increases during plastic deformation due to accumulation of dislocations. This segment commences with a summary of the impacts of work hardening on the material's behaviour. Work hardening is intimately linked to the interactions between individual dislocations and the barriers present within the material. The extent of strain hardening depends on the alloy composition, temper condition, and amount of plastic strain. Non-

heat-treatable alloys (e.g., AA1xxx, AA3xxx, and AA5xxx) derive much of their strength from strain hardening, whereas heat-treatable alloys (e.g., AA2xxx, AA6xxx, and AA7xxx) obtain additional strength through precipitation hardening.

1.4.1 Work Hardening

Work hardening is frequently characterized by the stress-strain deformation behaviour of a material, illustrating the progression of deformation processes during plastic deformation. At first, deformation transpires by simple glide (Stage I), wherein dislocations predominantly traverse a singular active slip system and face negligible opposition aside from lattice friction and pre-existing impediments. As plastic deformation escalates, more slip systems are activated, facilitating the interaction of dislocations on intersecting planes. These interactions impede dislocation movement, leading to a fast escalation in the work hardening rate, referred to as Stage II. The manifestation and degree of this phase are heavily influenced by crystal orientation, and in certain orientations where numerous slip systems are simultaneously engaged, Stage I can be non-existent. As deformation persists, the dislocation density escalates markedly until healing processes, including dislocation annihilation and reorganization, commence. This active recovery diminishes the frequency of dislocation build-up, resulting in a progressive decline in the work hardening rate throughout Stage III. At elevated strains, deformation progresses into Stage IV, noted for its comparatively mild and largely uniform hardening rate. In exceptionally pure aluminium, especially at high temperatures, dynamic recovery becomes increasingly evident and may ultimately lead to a state of stress saturation where additional work hardening is minimal. The phenomenon of work hardening is frequently assessed by

the work hardening rate (θ) in relation to stress. In FCC metals and alloys, the rate of hardening often escalates as temperature diminishes, whereas the shift from Stages III to IV is dictated by unique material properties and dislocation interactions [33].

1.4.2 Precipitation Hardening

Precipitation hardening serves as the principal strengthening mechanism in Al–Mg–Si alloys, wherein finely distributed precipitates inside the ductile aluminium matrix markedly improve the mechanical characteristics. This process, referred to as age hardening, encompasses solution heat treatment, subsequent quenching, and aging. During the solution treatment, the alloy is elevated above the solvus temperature to create a uniform solid solution (α), facilitating the complete dissolution of alloying elements and the eradication of pre-existing secondary phase particles and chemical segregations. Rapid quenching that follows inhibits atomic diffusion, resulting in a supersaturated solid solution owing to the diminished solubility of magnesium and silicon at reduced temperatures. The supersaturated alloy undergoes artificial aging, generally at temperatures ranging from 160 to 200°C, facilitating controlled atomic diffusion that encourages the nucleation and development of finely dispersed precipitates. These precipitates obstruct dislocation movement, thereby enhancing the alloy's strength and hardness. In Al-Mg-Si alloys, the precipitation process consists of the emergence of Guinier-Preston zones (GP zones), succeeded by metastable β″ and β′ precipitates, culminating in the stable β (Mg_2Si) phase. The β″ precipitates yield the most significant strengthening impact because to their small dimensions, coherent structure, and robust resistance to dislocation motion, thus being chiefly accountable for the optimal mechanical characteristics of 6xxx series aluminium alloys [34].

1.4.3 Annealing

When a metal is subjected to cold working, its crystals become elongated and distorted, leading to a higher dislocation density and the emergence of flaws, which improve the material's strength but diminishing its ductility. A reduction in ductility is detrimental in metal shaping procedures. To achieve a more ductile substance, cold-worked metal is heated in a furnace. Should the material experience extended heating, the cold-worked metal undergoes multiple changes, such as recovery, recrystallization, and grain enlargement. Figure 1.8 depicts the effect of temperature on the mechanical characteristics of the materials. This process of reheating, referred to as annealing, is utilized to alleviate the material's stress. When a substance experiences cold working, strain energy is released within the substance due to plastic deformation, leading to an elevation in the internal energy of the substance. Consequently, the inherent energy of a strain-hardened substance consistently surpasses that of an unstrained counterpart [35]. When a cold-worked substance is heated again beneath its recrystallization threshold, particularly within the recovery temperature spectrum, internal and residual stresses are reduced. Throughout the recuperation phase, dislocations rearrange into a more stable energy state aided by the supplied heat energy. As a result of material recovery, sub-grain boundaries emerge, identified as low-angle grain boundaries referred to as polygonization, which takes place before recrystallization. The internal energy diminishes when dislocations are eliminated and restructured into a more stable energy configuration, resulting in a slight fall in strength but a significant enhancement in ductility. Throughout recrystallization, the distorted configuration produced by cold working is completely replaced by fresh, recrystallized grains. Primary recrystallization occurs via two main mechanisms: an independent nucleus may

develop alongside a distorted grain. A primary high-angle grain boundary can advance into a portion of the metal that has undergone greater deformation. The annealing process consists of three phases: elevating to designated temperatures, sustaining the temperature while soaking, and reducing to ambient room temperature. Time is an essential factor in this procedure. Throughout the heating and cooling phases, a temperature differential is present between the furnace's inside and exterior, affected by the dimensions and shape of the workpiece.

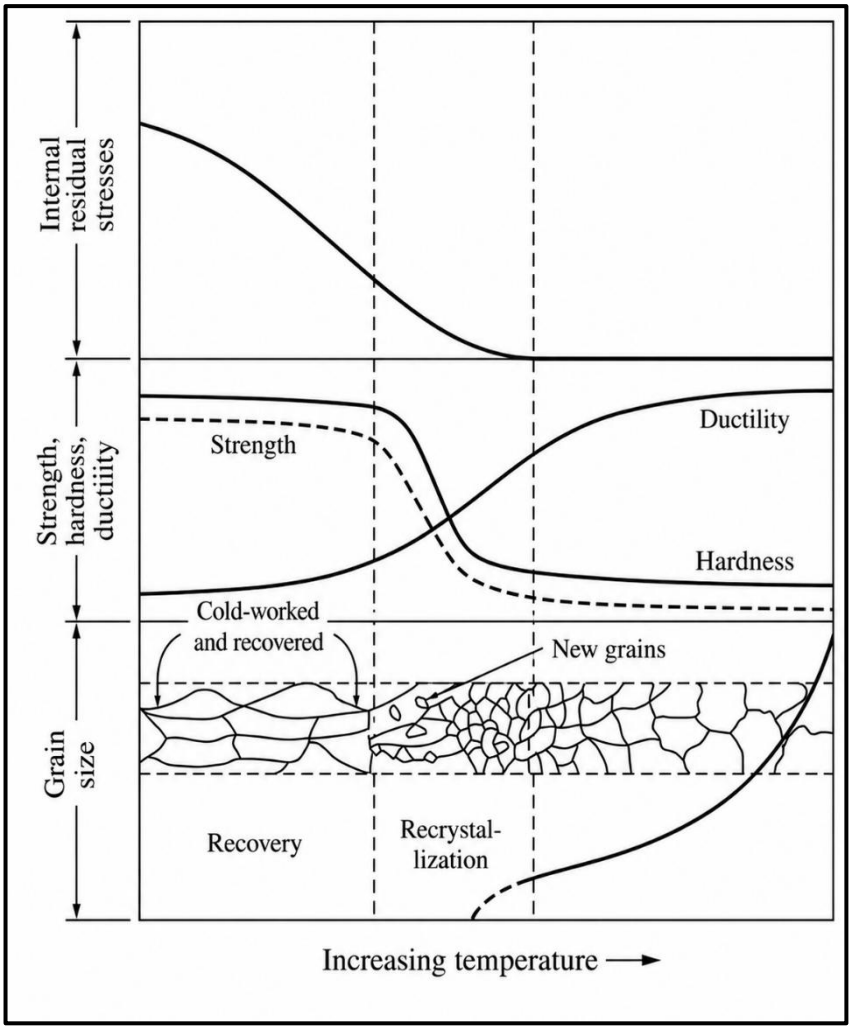


Figure 1.8 Effect of annealing on the structure and mechanical property changes of a cold-worked metal [35].

1.5 Sheet Metal Forming

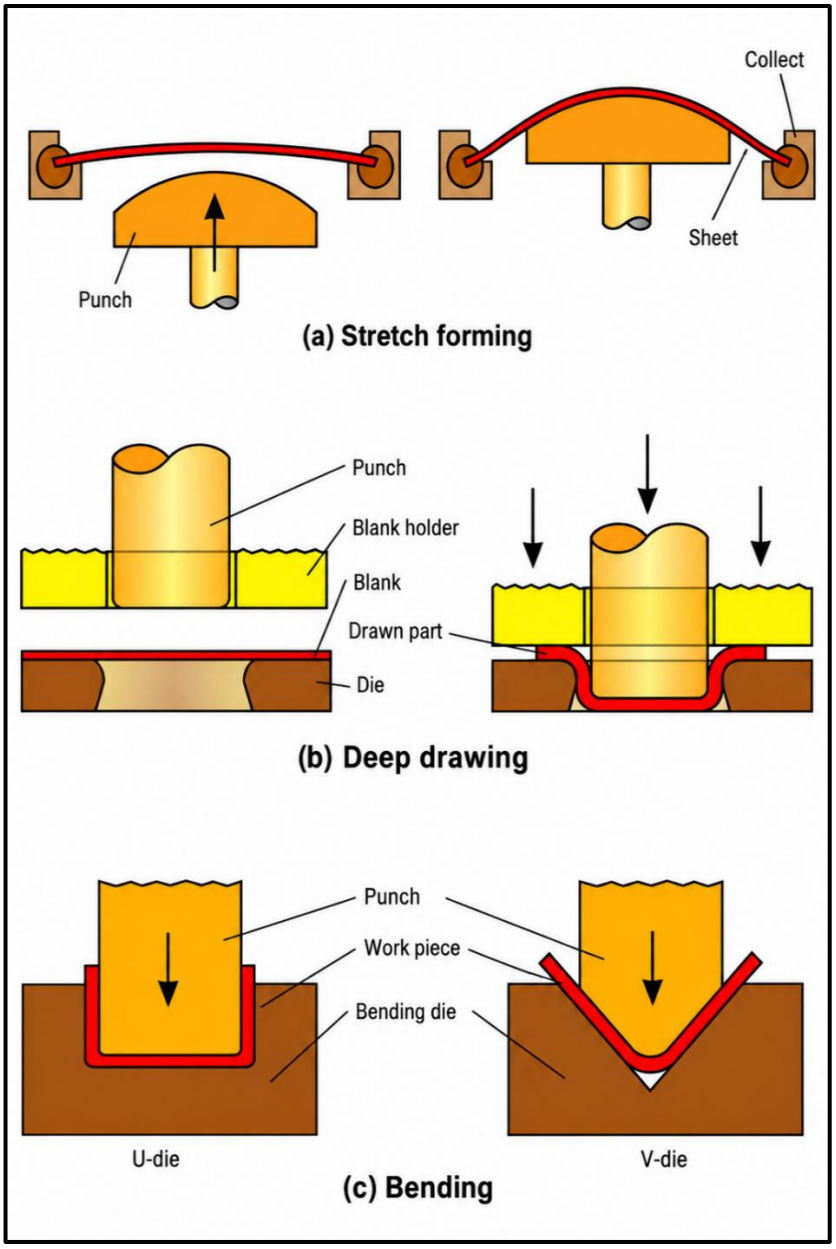


Figure 1.9 Sheet metal forming operations [36].

Sheet metal forming is among the most prevalent manufacturing techniques utilized in the creation of components for sectors including automotive, aircraft, electronic devices, and cookware. It encompasses the plastic deformation of metal sheets into

specified forms without the elimination of material, rendering it a cost-efficient and effective method for large-scale manufacturing. Typical sheet metal processes encompass bending, deep drawing, stretching, spinning, hydroforming, and stamping as shown in Figure 1.9. The capacity to create intricate shapes with precise dimensions and robust structural integrity renders sheet metal forming an essential technology in contemporary manufacturing. Plastic deformation in sheet metal transpires when the material is exposed to external forces, either tensile, compressive, or a mix of both, to attain the desired configuration of the component without fracturing. Numerous prevalent sheet metal fabrication techniques utilize these concepts, such as stretch forming, deep drawing, and bending, each tailored for various applications and shapes. These procedures are depicted in Figure 1.9. A primary technique is stretch forming, which involves securely clamping a sheet metal blank at its borders with considerable blank holding power. After being firmly secured, a solid punch exerts pressure on the sheet to mold it into the intended shape [37]. In contrast to other shaping processes that may entail compressive or bending forces, stretch forming primarily exposes the material to uniaxial or biaxial tensile stresses, leading to the elongation of the material's surface. This procedure can yield components with exceptional dimensional precision, consistent thickness distribution, and excellent surface finishes. As a result of these advantages, stretch forming is widely employed in the aerospace sector, where accurate and seamless shapes are essential, particularly in the production of aircraft skin panels, fuselage parts, and wing coverings. In contrast to alternative forming techniques, stretch forming provides superior regulation of the ultimate shape and diminishes the likelihood of surface imperfections like wrinkling. Deep drawing is an additional sheet metal fabrication technique employed to create hollow parts by

utilizing a punch to pull a sheet metal blank into a die. In contrast to stretch forming, it encompasses both tensile and compressive forces, especially in the flange area where radial tensile and circumferential compressive stresses prevail. Excessive compressive stress may result in wrinkling, which can be managed by implementing a sufficient blank holding force. The wall of the cup undergoes plane strain and thinning, but the center of the blank experiences biaxial tensile stress due to contact with the punch. Deep drawing is frequently employed in the automotive, aerospace, and packaging sectors to produce deep hollow components via single or multi-stage processes [38].

1.6 Formability

In sheet metal forming, formability denotes the ability of a sheet metal to be plastically deformed into a particular intended shape without undergoing failure. The degree of deformation achievable in one stage is limited by the onset of tensile instability (necking) and/or fracture due to excessive thinning of the blank. The necking and, excessive thinning phenomenon are the principal constraints in sheet metal processes. The malleability of sheet metals is generally evaluated by laboratory simulation tests. In experimental simulations, the material undergoes deformation that closely resembles a certain shaping procedure. This segment offers a brief overview of some commonly employed simulated testing techniques.

1.6.1 Erichsen Cup Test

Figure 1.10 illustrates the diagram of the Erichsen cup experiments. The preliminary evaluation for assessing the formability of sheet metals was proposed by Erichsen [39]. A circular sample of 27 mm in diameter is held between two clamps and subjected to deformation by a hemispherical punch with a diameter of 20 mm until necking or

failure transpires, at which moment the height of the cup is recorded. The taller the cup, the more excellent the material's malleability during elongation.

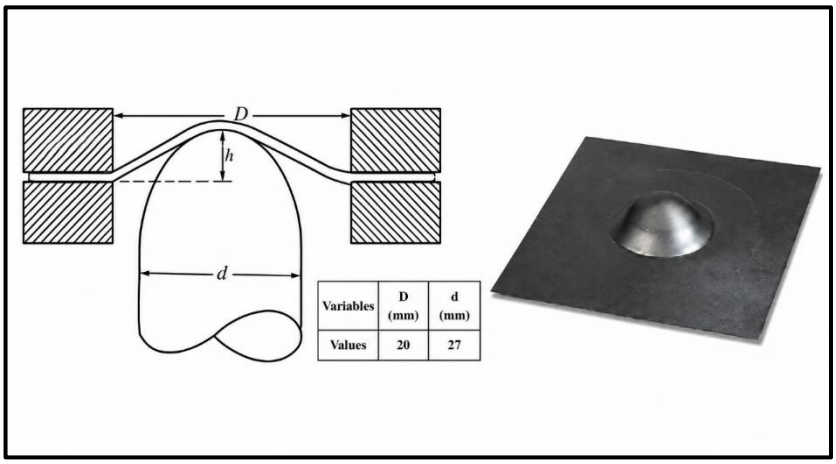


Figure 1.10 Schematic of the setup for Erichsen test and a tested sample [40].

1.6.2 Limiting Dome Height Test

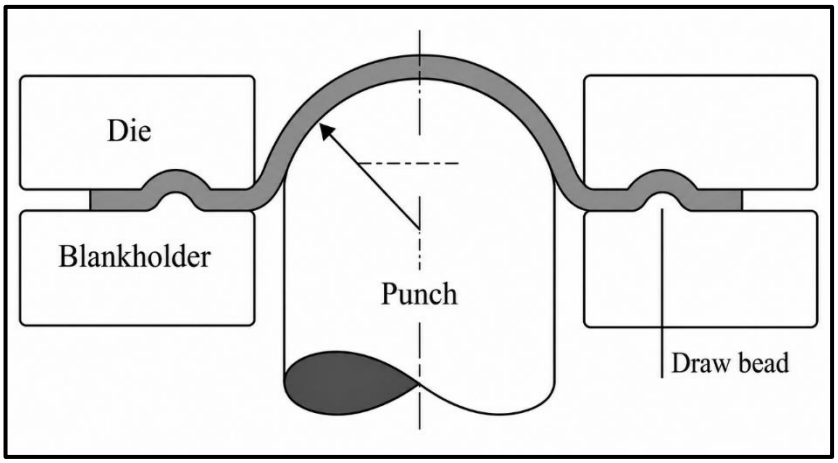


Figure 1.11 Schematic of the setup for limiting dome height test [41].

Hecker presented a formability assessment in which the blank is shaped over a hemispherical punch measuring 101.6 mm in diameter, featuring a drawbead integrated into the die plates. In the limit dome height assessment, the material is fully restrained using a drawbead, which inhibits the material from being pulled into the die,

leading to unadulterated biaxial stretching throughout the evaluation [41]. Figure 1.11 illustrates the diagram of the apparatus with a sample that has been evaluated. The formability is evaluated by gauging the dome height at the onset of necking or failure. This evaluation is commonly known as the limiting dome height (LDH) examination.

1.6.3 Hydraulic Bulge Test

A hydraulic bulging test [42] serves as an alternative technique for evaluating the formability of a sheet subjected to biaxial strain. The assembly consists of a pressure vessel and a clamping mechanism. Pressure can be produced using a liquid or gas as seen in Figure 1.12.

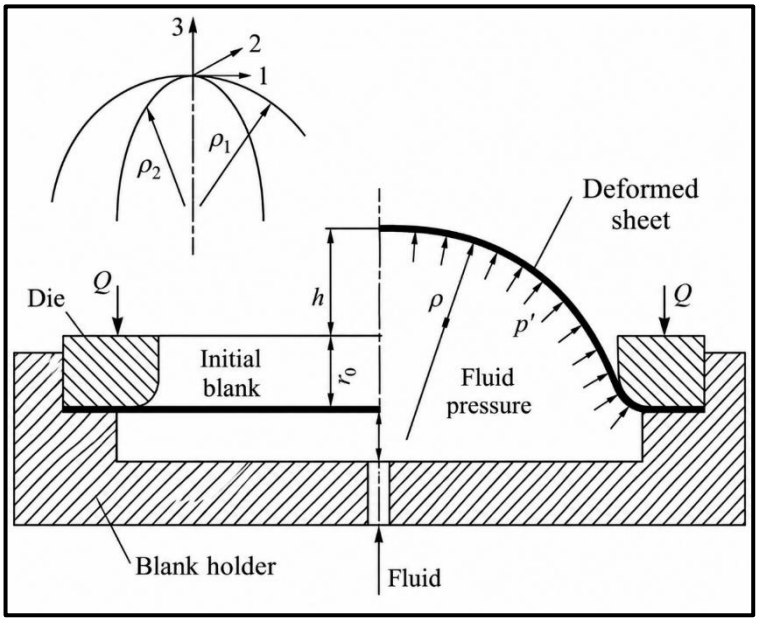


Figure 1.12 Hydraulic bulge test [43].

The height of the bulge at which material failure transpires is employed to evaluate formability. The benefit of this test is found in the lack of friction between the instrument and the workpiece, promoting equibiaxial stretching and leading to heightened total strain.

1.6.4 Swift Cup Drawing Test

All the above-described evaluations are utilized to gauge the formability of a sheet in stretching scenarios. The Swift flat bottom cup test [44] is a traditional technique for evaluating the drawability of a sheet. This examination utilizes a flat-bottom punch of 50 mm in diameter to form circular blanks of differing sizes into the die, as illustrated in Figure 1.13. The blank diameter is gradually increased to determine the limiting draw ratio (LDR), which is defined as the ratio of the maximum blank diameter that may be drawn without failure to the punch diameter.

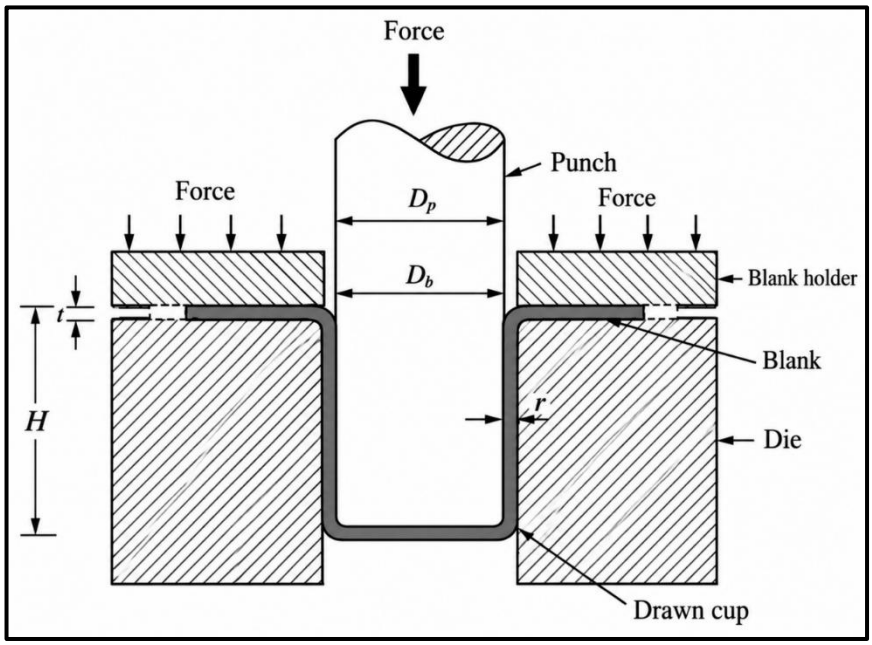


Figure 1.13 Swift cup test and a drawn cup [45].

1.7 Warm Forming

The rising need for lightweight constructions in the automotive, aerospace, and transportation sectors has hastened the adoption of aluminium alloys in place of traditional steel sheets. Due to their minimal density, elevated specific strength,

remarkable corrosion resistance, and recyclability, aluminium alloys are extensively utilized in the production of lightweight structural elements. Nonetheless, their comparatively inadequate formability at ambient temperature constrains the manufacturing of intricate sheet components due to early localized necking, restricted ductility, excessive springback, and fracturing during the forming process. As a result, extensive studies have concentrated on creating sophisticated forming methods that enhance the formability of aluminium sheets without compromising their mechanical characteristics and dimensional precision. Among these methods, warm forming has surfaced as one of the most advantageous production procedures due to its substantial improvement in sheet formability without necessitating the excessively high temperatures typical of traditional hot forming [46-48]. Warm forming is a thermo-mechanical method for shaping sheet metal, executed below the recrystallization temperature, generally between 150–300 °C for Aluminium alloys, contingent upon the alloy's composition and temper state. At these fairly high temperatures, aluminium alloys demonstrate diminished flow stress, enhanced ductility, heightened strain-rate sensitivity, and postponed strain localization, leading to much greater forming limits compared to traditional cold forming conditions. As the procedure occurs beneath the recrystallization temperature, it prevents excessive grain formation while generally maintaining favorable microstructural attributes. These characteristics provide warm forming a compelling manufacturing method for creating intricate aluminium parts with enhanced quality and diminished forming imperfections [49].

The automotive sector has significantly propelled the advancement of heated forming technology due to the rising need for lightweight automobiles that enhance fuel efficiency and lower emissions. Despite the prevalent utilization of 5xxx and 6xxx

series Aluminium alloys in automotive applications, its constrained formability at room temperature frequently limits their applicability in components with intricate geometries. Warm forming mitigates this constraint by diminishing forming forces, minimizing springback, enhancing material flow, and augmenting the permissible deformation prior to fracture. As a result, intricate aluminium parts that pose challenges for traditional cold forming can be effectively fabricated by heated forming methods [50]. Empirical studies have consistently shown that increased forming temperatures markedly enhance the mechanical properties of aluminium alloys. Elevated temperatures diminish yield strength and ultimate tensile strength due to thermal softening, while concurrently enhancing total elongation and strain-rate sensitivity. The improved strain-rate sensitivity postpones localized necking, encourages more consistent plastic deformation, and elevates the limiting dome height and forming limit diagrams in contrast to room-temperature forming. These enhancements offer increased operational flexibility and diminish the chances of early failure in industrial sheet forming processes [51].

The influence of warm forming has also been extensively evaluated using forming limit diagrams (FLDs) and limiting dome height (LDH) tests. Studies on AA5754, AA6061, and AA6082 aluminium alloys have reported significant increases in forming limit strains and limiting dome height with increasing temperature. Elevated temperatures promote more uniform strain distribution, reduce localized thinning, and improve overall deformation behaviour. In addition, lower punch speeds have been shown to further improve forming limits because of the increased contribution of strain-rate sensitivity during deformation. These investigations confirm that forming temperature and deformation rate are among the most influential parameters

controlling the warm formability of aluminium alloy sheets [52-54]. Besides improving ductility, warm forming enhances dimensional accuracy by reducing springback, which is one of the principal limitations of cold forming aluminium sheets. The reduction in flow stress lowers residual stresses generated during deformation, thereby decreasing elastic recovery after unloading. Elevated temperatures also promote more homogeneous thickness distribution and reduce localized thinning, resulting in improved component quality and manufacturing reliability. These advantages are particularly beneficial in producing precision automotive components where dimensional accuracy is critical [50], [52].

Precise execution of heated forming necessitates dependable forecasting of the thermo-mechanical properties of aluminium alloys during deformation. Given that the material's behaviour varies considerably with temperature and strain rate, temperature-sensitive constitutive models have been integrated into finite element analyses to forecast material flow, strain localization, thickness distribution, and failure. Empirical validation has shown that these numerical models can reliably forecast limiting dome heights, strain distributions, and failure sites, rendering them essential instruments for process enhancement and die configuration [54]. Recent studies have additionally applied warm forming techniques to high-strength 7xxx series Aluminium alloys, which demonstrate inadequate formability in the T6 temper at ambient temperature. Warm forming significantly enhances the ductility and drawability of these alloys by thermal softening, while preserving a reasonably high strength after forming. Nonetheless, excessively elevated forming temperatures might induce over-ageing and lead to coarsening, consequently diminishing the ultimate mechanical characteristics.

Thus, choosing a suitable forming temperature is crucial for attaining a harmony between improved formability and the preservation of strength [55].

A notable advancement is the HFQ (Solution Heat Treatment–Forming–In-Die Quenching) technique, which amalgamates solution heat treatment, swift transfer, forming, and in-die quenching into one manufacturing pathway. A diagrammatic representation of the warm forming (HFQ) procedure is depicted in Figure 1.14. This method facilitates the creation of intricate aluminium parts with superior dimensional precision while preserving significant post-forming strength upon aging. Numerical analyses indicate that precise forecasting of temperature changes, heat transfer, material movement, and springback is crucial for the effective execution of the HFQ process, thus broadening the industrial use of Aluminium alloys in lightweight automotive frameworks [56].

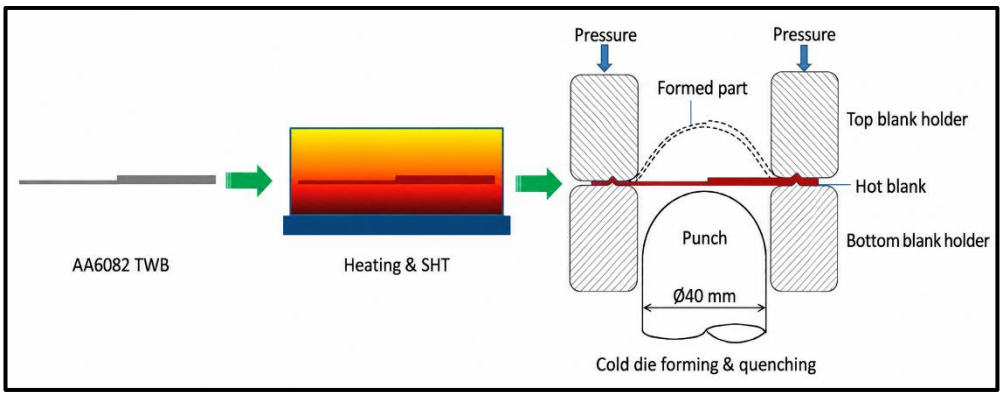


Figure 1.14 Schematic illustration of the warm forming (HFQ) process [56].

The available research indicates that warm forming is a proficient production technique for enhancing the formability of aluminium alloy sheets. Diminished flow stress, augmented ductility, heightened strain-rate sensitivity, postponed localized necking, enhanced forming limits, and decreased springback synergistically facilitate

the effective fabrication of intricate lightweight components that are challenging to produce at ambient temperatures. Ongoing advancements in experimental characterization, constitutive modeling, numerical simulation, and sophisticated forming technologies have bolstered the utilization of warm forming in the production of high-performance aluminium alloy components, establishing a robust basis for investigating the warm formability of aluminium alloy tailor welded blanks.

1.8 Forming Limit Diagram

A forming limit diagram, often called the Forming Limit Curve (FLC), is employed to predict the deformation characteristics of sheet metal. This chart predicts the region of material failure. Circular indicators are affixed to the sheets to perform the Forming Limit Diagram experiment. The sheet is then deformed in a press prior to the blank holder securing the sheet and aiding in material locking to permit sufficient deep drawing. Upon achieving the necessary pressure on the blank, the punch progresses towards the sheet and alters its shape. When the sheet is elongated, circles get distorted, transforming into an ellipse, as depicted in Figure 1.15. Designate the original diameter of the circle as d1, whereas the final diameters of the altered circle, referred to as the ellipse, are d2 minor (minor diameter) and d2 major (major diameter). Principal strains can be calculated in the following manner: the principal strain, oriented along the major axis of the ellipse, is denoted as ln (d2 major/d_1), the secondary strain is shown as ln (d2 minor/d_1). The metrics at failure and necking denote the conditions of failure and necking, whereas strain levels removed from necking suggest a secure scenario. A chart illustrating the combination of significant and minor strain linked to failure, necking, and the safe zone culminates in the formation of the limit diagram, often

known as the Keeler-Goodwin diagram [57]. The strain data above the curve signifies the areas of failure. The curve on the left illustrates the limit stresses documented from specimens exposed to simultaneous tension and compression deformation. The graph on the right depicts the maximum stresses observed from specimens subjected to biaxial tension. The primary strain value, with the secondary strain at zero, indicates a state of plain strain [58].

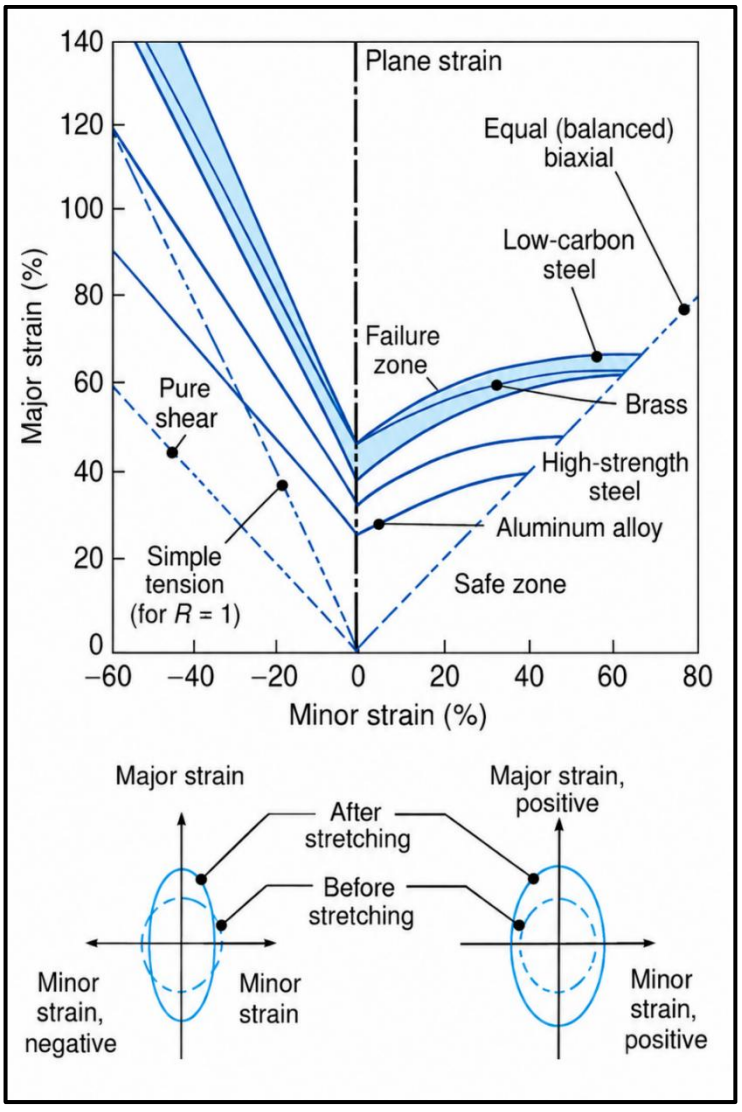


Figure 1.15 Forming-limit diagrams (FLD) for various sheet metals and strains in deformed circular grid patterns [59].

1.9 Important Material Parameters Affecting Formability

1.9.1 Strain Hardening Exponent

The strain hardening exponent (n) indicates a material's ability to evenly distribute strain when subjected to tensile stress. It demonstrates a material's capacity for work hardening, which transpires when flow stress escalates with rising plastic strain. An increased n value indicates a greater capacity for uniform plastic deformation, as the material can more efficiently distribute strain and delay the onset of localized necking. This enhances formability by enabling the sheet to endure greater strains before to failure, which is particularly advantageous in forming techniques such as deep drawing and stretch forming. Conversely, materials with a diminished strain hardening exponent exhibit rapid localization of deformation, leading to premature necking and inferior formability. Consequently, a heightened strain hardening exponent is generally associated with enhanced stability, augmented forming limits, and superior performance in sheet metal forming operations [60].

1.9.2 Anisotropy

The standard anisotropy ($\bar{R}$) and planar anisotropy (ΔR) affect the drawability and earing of sheets in deep drawing processes [60]. The R value (plastic strain ratio) denotes the proportion of true strain in width to true strain in thickness. The R value, characterized as the proportion of true strain in the lateral direction to true strain in the vertical direction, offers a direct evaluation of a material's capacity to resist thinning during tensile stress. Elevated average normal anisotropy ($\bar{R}$) indicates enhanced drawability, since the sheet can experience increased plastic deformation with reduced thickness reduction, hence lessening the risk of tearing or fracture. Planar anisotropy

(ΔR) refers to the variation of R values based on orientation in relation to the rolling direction, resulting in uneven material flow during drawing. Elevated ΔR values lead to considerable flaws in the ear along the cup rim, culminating in greater material wastage and additional post-processing needs. Consequently, attaining a superior $\bar{R}$ alongside a minimal ΔR is crucial for improving deep drawability and mitigating earing tendencies in sheet metal forming processes.

1.9.3 Sheet Thickness

Augmented sheet thickness improves formability. It directly influences stress distribution, strain adaptation, and failure resilience throughout the forming procedure. Denser sheets exhibit superior formability as they can withstand greater forming forces and endure larger plastic deformations prior to encountering localized necking or fracture. Increased thickness enhances resistance to thinning, bolsters through-thickness stress support, and reduces tearing during processes like as deep drawing and stretching. Thinner sheets, conversely, are more prone to fast reductions in thickness, strain localization, and premature failure, particularly under complex stress scenarios. Augmented sheet thickness leads to heightened forming forces and material usage, necessitating a balance with design and production constraints. Consequently, a suitable sheet thickness is necessary to enhance formability while maintaining efficiency and structural integrity in forming processes. In the necking region, heightened limiting stresses occur as a result of the augmented thickness of the sheet metal [61]. The design of the neck depends on the strain rate sensitivity index (m) of the substance. Necks display a more gradual contour in substances possessing a higher modulus. Aluminium alloys exhibiting reduced m-values demonstrate markedly more

pronounced necking. The existence of a more defined neck probably reduces the importance of the thickness effect.

1.9.4 Ductility

Sheet ductility measured by percentage elongation in a uniaxial tension test is a critical material characteristic that significantly affects formability, as it dictates the extent of plastic deformation a sheet may endure prior to failure. Substances exhibiting elevated ductility can endure greater deformations via continuous plastic deformation, facilitating the creation of intricate geometries without fracturing or rupturing during fabrication techniques such deep drawing, bending, and stretching. Augmented ductility facilitates strain redistribution in multiaxial stress conditions, mitigates the onset of localized necking, and elevates the forming limit of the sheet. Sheets exhibiting low ductility possess limited capacity for plastic deformation, leading to early fracture and diminished formability, particularly in areas experiencing elevated tensile stresses. Enhanced sheet ductility is intrinsically linked to superior formability, consistent forming dependability, and increased design versatility [61].

1.10 Summary

This chapter laid the scientific groundwork for the current study by examining aluminium alloys, tailor welded blanks (TWBs), laser welding, mechanisms of strengthening, and the formability of sheet metal. The increasing need for lightweight constructions in the automotive and aerospace sectors has expedited the use of 6xxx series aluminium alloys due to their superior specific strength, resistance to corrosion, recyclability, and advantageous strength-to-weight ratio. The notion of aluminium TWBs was examined, emphasizing their benefits in minimizing weight, optimizing

materials, and enhancing structural efficiency, while also addressing issues such welding imperfections, softening in the heat-affected zone, and diminished formability. The significance of weld quality, sheet thickness combination, weld orientation, and numerical modeling in assessing TWB performance was likewise highlighted. The section moreover examined laser welding as a sophisticated joining method for fabricating aluminium TWBs, highlighting its exceptional accuracy, profound penetration, minimal thermal input, and appropriateness for automated manufacturing. The influence of welding settings on weld quality, microstructural development, and mechanical characteristics was examined, emphasizing the necessity for process refinement. Furthermore, the reinforcement methods of aluminium alloys, such as work hardening, precipitation hardening, and annealing, were analyzed to elucidate their impact on microstructural development, strength, hardness, ductility, and deformation characteristics during forming processes. Ultimately, the principles of sheet metal forming and its formability were discussed, encompassing the processes of strain localization, necking, and fracture, alongside widely utilized formability assessment methods like the Erichsen cup test, Limiting Dome Height (LDH) test, and Forming Limit Diagram (FLD). This chapter delineates the conceptual connection among aluminium alloy metallurgy, laser welding technology, tailor welded blank design, and sheet metal forming, laying the theoretical groundwork for examining the formability characteristics of laser-welded AA6082 aluminium alloy tailor welded blanks under warm forming conditions, particularly focusing on the impact of welding parameters, weld attributes, and forming temperature on their mechanical performance and deformation behavior.

CHAPTER 2

LITERATURE REVIEW

2.1 Aluminium Alloys

The increasing need for lightweight automobiles has hastened the utilization of aluminium alloys in vehicle body frameworks owing to its superior strength-to-weight ratio, resistance to corrosion, recyclability, and malleability. In this regard, Miller et al. examined recent advancements in aluminium alloys for lightweight automotive uses, highlighting the applicability of 5xxx and 6xxx series alloys in body-in-white (BIW) frameworks [4]. The research assessed the characteristics of alloys, encompassing formability, bake-hardening, corrosion resistance, and mechanical performance. The writers indicated that 5xxx alloys exhibit enhanced formability for inner panels, while 6xxx alloys deliver more strength and superior surface quality for outside panels. Aluminium-rich vehicle frameworks were discovered to markedly decrease vehicle mass while enhancing fuel efficiency, resistance to corrosion, and recyclability. In a similar vein, Lahaye et al. examined the function of aluminium within the Super Light-Car (SLC) initiative by assessing multi-material Body-in-White (BIW) configurations. Their research illustrated that the tactical amalgamation of advanced 5xxx and 6xxx series aluminium alloys with additional lightweight materials significantly diminished vehicle mass while preserving crash safety, rigidity, and manufacturability, positioning aluminium as a crucial component for eco-friendly lightweight vehicles [62]. Similarly, Hirsch examined progress in lightweight vehicle construction utilizing aluminium, emphasizing enhancements in 5xxx and 6xxx series alloys, fabrication techniques, and multi-material body-in-white concepts. The

research determined that sophisticated aluminium alloys, when paired with contemporary production methods, facilitate significant weight reduction without compromising crash safety, durability, or manufacturability [63]. Moreover, Hirsch investigated contemporary advancements in sophisticated 5xxx and 6xxx series alloys as well as multi-material Body-in-White (BIW) configurations, emphasizing alloy innovation, processing techniques, and novel vehicle design strategies. The results indicated that sophisticated aluminium alloys, in conjunction with techniques such custom welded blanks, warm shaping, and multi-material fabrication, considerably diminish vehicle weight while preserving structural integrity and cost-effectiveness. The writer determined that ongoing progress in aluminium alloy technology will be crucial for the development of future lightweight, fuel-efficient, and ecological vehicle frameworks [9].

The AA6XXX series of aluminium alloys has garnered considerable interest for automotive and structural uses owing to its superior mechanical characteristics, resistance to corrosion, weldability, and ability to undergo age-hardening. In this context, Mukhopadhyay examined the categorization, treatment, enhancement methods, and uses of AA6XXX alloys. The research investigated the effects of alloy composition, thermomechanical processing, and precipitation hardening on microstructure and mechanical characteristics, emphasizing that Mg_2Si precipitation, along with suitable heat treatment, markedly improves strength, ductility, corrosion resistance, and formability. The writer determined that AA6XXX alloys are predominantly favored for lightweight automotive and structural uses due to their exceptional mechanical properties and weldability. Due to the significant impact of thermomechanical processing on their mechanical properties, numerous researchers

have explored the impacts of deformation parameters and crystallographic texture [64]. Singh et al. examined the effect of crystallographic texture on the microstructure and anisotropic mechanical characteristics of an AA6013-equivalent Al–Mg–Si–Cu alloy. Hot rolling at 400 °C resulted in a more refined microstructure and enhanced tensile strength compared to rolling at 520 °C, while preserving comparable ductility, indicating that crystallographic texture and thermomechanical processing significantly affect anisotropic behavior [65]. In a similar vein, Tajally and Emadoddin examined the influence of plastic deformation on the mechanical characteristics and anisotropy of AA7075 sheets using tensile testing at various rolling-direction angles. The findings indicated that texture evolution during rolling had a considerable impact on yield strength, tensile strength, elongation, and anisotropic characteristics, highlighting the significance of deformation-induced anisotropy in forecasting formability and structural efficacy. These investigations collectively illustrate that the alloy composition, precipitation hardening, thermomechanical processing, and crystallographic texture collaboratively influence the microstructure, anisotropic mechanical properties, and formability of aluminium alloys for lightweight engineering purposes [66].

The correlation between microstructural development and the mechanical properties of aluminium alloys has been thoroughly examined by sophisticated characterization methods including EBSD, X-ray diffraction (XRD), SEM, and dislocation-based assessments. Thermomechanical processing is essential for regulating grain boundary properties, dislocation density, residual stress development, and fracture characteristics. Kumar et al. examined the influence of grain boundary misorientation, deformation temperature, and AlFeMnSi intermetallic particles on the fatigue

characteristics of AA6082 aluminium alloy by EBSD, XRD, SEM, EDS, tensile, hardness, and fatigue assessments. The findings indicated that warm rolling at 100 °C yielded the most extended fatigue life due to an elevated dislocation density, an increased proportion of low-angle grain boundaries, and smaller AlFeMnSi and Mg_2Si precipitates, while a rise in deformation temperature facilitated recovery, grain coarsening, and diminished fatigue resistance. The researchers determined that regulated thermomechanical treatment is crucial for improving the fatigue and mechanical characteristics of AA6082 alloys [67]. In a similar vein, Lodh et al. examined the progression of residual stress and substructural alterations during the tensile deformation of AA3003 alloy by EBSD, grazing-incidence X-ray diffraction, residual stress assessments, and discrete dislocation dynamics (DDD) simulations. The research demonstrated that crystallographic direction significantly affected grain fragmentation, the accumulation of geometrically required dislocations (GND), and the progression of residual stress, whereas dislocation dynamics (DDD) simulations effectively linked orientation-specific stress development to dislocation evolution [68]. Additionally, Tomstad et al. investigated the effect of constituent particle composition on the ductile fracture characteristics of 6000-series aluminium alloys by tensile testing, optical microscopy, SEM, EBSD, and X-ray diffraction. The findings indicated that a rise in constituent particles diminished ductility due to expedited microvoid development, while extrusion enhanced fracture resistance by purifying and redistributing the particles. These studies collectively illustrate that the characteristics of grain boundaries, accumulation of dislocations, crystallographic orientation, morphology of constituent particles, and thermomechanical processing collaboratively

influence microstructural evolution and dictate the mechanical response, fatigue resistance, residual stress formation, and fracture behavior of aluminium alloys [69].

The malleability and deformation characteristics of aluminium sheet alloys have been extensively studied due to their significance in producing intricate automotive parts via sheet metal forming. Prior research indicates that the composition of alloys, strain-hardening characteristics, grain morphology, crystallographic orientation, and strain distribution significantly affect sheet formability. In this regard, Bhargava et al. examined the formability of AA5182 aluminium alloy sheets by forming limit diagrams (FLDs), tensile testing, and microstructural examination. The findings indicated that AA5182 had remarkable formability owing to its superior strain-hardening properties and advantageous strain distribution, rendering it appropriate for intricate press-forming tasks. The authors determined that AA5182 is a suitable material for lightweight vehicle body panels that necessitate excellent formability and sufficient strength [70]. In a similar vein, Kumar and Gautam investigated the effect of magnesium concentration on the tensile characteristics, formability, and deformation behavior of Al–Mg–Si alloy sheets using tensile testing, FLD analysis, SEM, EBSD, and texture characterization. The alloy with 3.1 wt.% Mg demonstrated more refined equiaxed grains, enhanced crystallographic texture, elevated yield and tensile strengths, increased ductility, and superior formability attributed to the consistent dispersion of Mg_2Si particles. The investigators determined that augmenting magnesium levels markedly improves the mechanical characteristics and deformation behavior of Al–Mg–Si alloys for lightweight sheet uses. These investigations reveal that the tensile characteristics and formability of aluminium alloy sheets are collectively influenced by alloy composition, grain refinement, crystallographic

texture, precipitate distribution, strain-hardening behavior, and strain distribution, underscoring the necessity of optimizing composition and microstructure for advanced lightweight automotive uses [71].

The effective utilization of aluminium alloys in lightweight vehicle frameworks relies on the strength and mechanical characteristics of welded connections, especially in tailor welded blanks (TWBs), where welding greatly affects microstructure and deformation properties. In this context, Baig et al. examined the influence of fabrication methods and welding processes, such as gas tungsten arc welding (GTAW) and friction stir welding (FSW), on the mechanical properties of AA5182-O and AL6111-T4 tailor-welded blanks. Tensile testing across a broad spectrum of strain rates, alongside EBSD analysis and Khan–Huang–Liang (KHL) constitutive modeling, revealed that AA5182-O demonstrated negative strain-rate sensitivity, while AL6111-T4 exhibited positive strain-rate sensitivity. Friction stir welded connections exhibited superior strength compared to GTAW joints, and the KHL model effectively forecasted the trial outcomes. The researchers determined that the method of manufacture and the welding technique significantly affect the mechanical characteristics, texture development, and deformation behavior of aluminium TWBs [72]. In a similar vein, Sheikhi et al. investigated the onset and progression of solidification fissures during pulsed laser welding of AA2024 aluminium alloy by experimental welding tests and finite element modeling. The findings indicated that preheating markedly diminished crack initiation by decreasing cooling and strain rates, although it was less successful in inhibiting crack propagation along the fusion line. The investigators determined that the strain rate predominantly influences crack initiation, while localized strain concentration and limited liquid supply dictate crack

propagation. These investigations collectively illustrate that welding methods, processing parameters, temperature cycles, and deformation characteristics significantly influence the microstructural development, mechanical properties, and structural robustness of aluminium TWBs. Nonetheless, the cumulative impact of laser welding, warm forming, thickness discrepancies, and microstructural changes on the formability of aluminium tailor welded blanks is not yet fully comprehended, therefore prompting this study [73].

2.2 Annealing

Annealing serves as a potent thermomechanical process for altering the microstructure of aluminium alloys by recovery, recrystallization, and grain development, thus enhancing formability and mechanical properties. Numerous research efforts have examined its impact on the deformation characteristics of aluminium sheet alloys. In this context, Drysdale and Bahrani investigated the impact of full and inter-stage annealing on the strain thresholds of L166-F aluminium alloy during multi-stage forming by uniaxial tensile testing, punch stretching, and forming limit diagrams (FLDs). The findings indicated that both annealing processes enhanced the limit strain, with inter-stage annealing yielding a more significant enhancement than full annealing. The authors determined that integrating annealing into strain prediction models improves formability evaluation and refines multi-stage sheet forming processes [74]. Similarly, Go et al. examined the recovery and recrystallization characteristics of cold-rolled AA5754 aluminium alloy during continuous annealing through isothermal annealing tests and a physically grounded microstructure model. The research indicated that elevated annealing temperatures and increased previous

cold reduction expedited recovery and recrystallization, resulting in smaller recrystallized grains. The suggested model precisely forecasted softening behavior and served as a valuable instrument for enhancing the continuous annealing of AA5754 sheets. These investigations collectively illustrate that regulated annealing facilitates recovery and recrystallization, augments strain accommodation, boosts formability, and allows for more dependable forecasting of deformation behavior in sheet metal forming [75].

The impact of annealing on crystallographic texture, recrystallization, and the ensuing mechanical and formability properties has been extensively studied in aluminium alloys. Annealing profoundly influences anisotropy, strength, ductility, and corrosion resistance by altering grain structure and texture via recovery and recrystallization. In this context, Narayanasamy et al. examined the influence of annealing temperature on the texture, anisotropy, and formability of AA5052 aluminium alloy sheets subjected to annealing at temperatures ranging from 200 to 350 °C. Tensile testing, forming limit diagrams (FLDs), X-ray diffraction, and orientation distribution function investigations indicated that elevating the annealing temperature facilitated recovery and recrystallization, enhanced grain refinement, augmented normal anisotropy, and elevated forming limit stresses. The sheet subjected to annealing at 350 °C demonstrated optimal formability due to its recrystallized microstructure, advantageous texture, and enhanced anisotropic characteristics [76]. In a similar vein, Lin et al. investigated the annealing characteristics of Er-modified AA5083 aluminium alloy across a temperature spectrum of 125–375 °C. The mechanical characteristics, resistance to corrosion, and microstructural development were assessed using tensile testing, potentiodynamic polarization, and transmission electron microscopy (TEM).

The findings indicated that the annealing temperature exerted a more significant effect than the holding duration, with optimal characteristics attained after annealing at 225 °C for 4 hours, attributed to regulated recovery, recrystallization, and advantageous distribution of β-phase precipitates. These investigations illustrate that fine-tuning the annealing temperature is crucial for regulating recrystallization, crystallographic texture, precipitate development, and grain refinement, thus attaining an ideal equilibrium of strength, ductility, anisotropy, corrosion resistance, and sheet formability in aluminium alloys [77].

The annealing characteristics of 6xxx series aluminium alloys have been extensively examined due to the significant impact of recovery, recrystallization, precipitation, and grain development on their mechanical properties and microstructural stability during thermal processing. Rao et al. examined the influence of annealing on cryorolled AA6061 aluminium alloy by TEM, XRD, EBSD, hardness, and tensile assessments following annealing at temperatures ranging from 150 to 350 °C. The findings indicated that annealing at 150 °C yielded the optimal equilibrium of strength and ductility via β′ precipitation and recovery, while elevated temperatures facilitated recrystallization and grain enlargement, diminishing strength. The researchers determined that ultrafine-grained AA6061 exhibited thermal stability up to 250 °C owing to the Zener pinning influence of Mg_2Si precipitates [78]. In a similar vein, Kumar et al. investigated the impact of annealing on cryorolled AA6082 aluminium alloy by EBSD, TEM, tensile, hardness, and corrosion assessments. Recovery transpired within the temperature range of 110–250 °C, recrystallization took place between 250–300 °C, and grain enlargement happened at temperatures over 300 °C. Annealing at 150 °C yielded the ideal strength-ductility equilibrium, whereas 350 °C

delivered enhanced corrosion resistance, illustrating that regulated annealing improves the thermal stability and overall efficacy of AA6082 [79]. Moreover, Fröck et al. investigated the effects of solution-annealing temperature and soaking duration on the precipitation characteristics of EN AW-6082 alloy by SEM, TEM, and hardness assessments. The research indicated that insufficient dissolution expedited Mg_2Si precipitation, heightened quench sensitivity, and diminished age-hardening potential, underscoring the necessity of proper solution treatment [80]. Similarly, Kumar et al. examined the influence of annealing on ultrafine-grained AA6082 aluminium alloy and discovered that annealing at 150 °C yielded optimal hardness and tensile strength via β″ precipitation, but thermal stability persisted up to 300 °C due to Zener drag. These investigations collectively indicate that recovery, recrystallization, precipitation, grain growth, and precipitate pinning collectively dictate the annealing behavior of 6xxx series aluminium alloys, thus rendering optimized annealing parameters crucial for attaining an ideal equilibrium of strength, ductility, thermal stability, corrosion resistance, and microstructural enhancement [81].

Essential research on recrystallization has improved comprehension of microstructural development during annealing and its influence on the mechanical properties of aluminium alloys. Zhao et al. examined the effect of ultra-fast annealing temperature on the recrystallization characteristics, microstructure, and mechanical attributes of severely cold-rolled commercially pure aluminium by EBSD, TEM, and tensile assessments. The findings indicated that full recrystallization transpired within the temperature range of 410–435 °C, yielding fine equiaxed grains that exhibited an ideal equilibrium of strength and ductility, whereas elevated temperatures led to grain coarsening and diminished strength. The authors determined that meticulous

regulation of annealing temperature is crucial for attaining full recrystallization while preventing excessive grain expansion. The existing literature indicates that annealing is a crucial thermomechanical process for modifying the microstructure and mechanical properties of aluminium alloys via regulated recovery, recrystallization, precipitation, and grain development. These microstructural alterations dictate crystallographic texture, grain dimensions, anisotropic behavior, strength, ductility, corrosion resistance, and sheet malleability. Nonetheless, although considerable study has been conducted on certain aluminium alloys, there is a paucity of studies aimed at refining annealing parameters for laser-welded tailor welded blanks and their ensuing warm shaping. Consequently, additional examination is necessary to comprehend the synergistic effect of annealing on microstructural development, mechanical characteristics, and formability, which underpins the current study [82].

2.3 Tailor Welded Blanks

Tailor welded blanks (TWBs) have emerged as a significant lightweight manufacturing technique in the automotive sector, facilitating the amalgamation of sheets with varying thicknesses, strengths, or material grades prior to forming, thus enhancing structural efficiency while decreasing vehicle weight and production expenses. As a result, considerable investigation has concentrated on their welding quality, malleability, and mechanical characteristics. In this context, Davies et al. examined the characteristics and malleability of AA5182-O aluminium tailor-welded blanks created using gas tungsten arc welding (GTAW) and non-vacuum electron beam welding. The research assessed weld geometry, microstructure, chemical composition, tensile characteristics, and weld porosity, indicating that weld porosity and geometric

imperfections considerably diminished ductility and formability, while reducing weld flaws enhanced weld dependability. The writers determined that the quality of welding is essential for the effective industrial utilization of aluminium TWBs [11]. In a similar vein, Merklein et al. examined the production techniques, characteristics, formability, and automotive uses of bespoke blanks, encompassing tailor welded, tailor rolled, patchwork, and tailor heat-treated blanks. The research emphasized that tailored blanks offer considerable weight savings, superior structural integrity, better crash performance, and optimal material use, however issues persist regarding welding quality, thickness discrepancies, and forming characteristics. These investigations collectively illustrate that custom welded blanks provide considerable benefits for lightweight vehicle design; yet, attaining superior weld quality and comprehending their deformation characteristics are crucial for effective industrial use [14].

Subsequent to the production of custom welded blanks, precise assessment and forecasting of their mechanical properties are crucial for guaranteeing dependable performance in later forming processes. Consequently, numerous scholars have examined the tensile characteristics of TWBs and formulated techniques for forecasting their mechanical attributes. In this context, Abdullah et al. investigated the tensile deformation characteristics of aluminium tailor-welded blanks (TWB) of similar gauge, employing the rule of mixtures to assess the properties of the weld metal. Tensile examinations of base metals and welded samples of varying dimensions indicated that specimen size and presumed weld width markedly affected prediction precision, with smaller specimens yielding more dependable outcomes. The authors determined that the rule of mixtures serves as a reliable method for predicting weld metal characteristics when suitable specimen sizes are employed [83]. In a similar

vein, Veera Babu et al. created an expert system utilizing an artificial neural network (ANN) to forecast the tensile characteristics of TWBs. Finite element analyses conducted in PAM-STAMP 2G produced training data for various thickness ratios, strength ratios, weld orientations, and weld attributes. The artificial neural network precisely forecasted yield strength, ultimate tensile strength, uniform elongation, strain-hardening exponent, and strength coefficient with tolerable inaccuracies. In summary, these investigations reveal that experimental characterization and computational forecasting are proficient in assessing the tensile response of tailor welded blanks, while precise estimation of weld metal characteristics and tensile behavior is crucial for enhancing TWB design and refining numerical simulations in sheet metal forming [13].

The deformation characteristics and formability of custom welded blanks are significantly affected by the quality of the weld, its orientation, the thickness ratio, and the mechanical properties of the weld area. As a result, much investigation has concentrated on comprehending fracture mechanics and creating dependable numerical models for forecasting TWB forming behavior. In this context, Shakeri et al. examined the onset of damage and fracture characteristics in AA5754 aluminium tailor welded blanks (TWB) fabricated using non-vacuum electron beam (NVEB) and Nd laser welding. Dome height assessments, optical microscopy, scanning electron microscopy, and image analysis indicated that weld imperfections, gauge ratio, and weld orientation considerably influenced failure behavior, whereas Nd laser welds had superior formability and fewer flaws compared to NVEB welds. The authors determined that reducing weld imperfections is crucial for enhancing the formability and fracture resistance of aluminium TWBs [12]. In a similar vein, Shi et al. assessed

weld-line modeling techniques for forecasting the impact performance of custom welded blanks by finite element simulations. The suggested dual-beam model forecasted deformation, failure sites, plastic strain, and energy absorption with greater precision than traditional models by integrating weld geometry and material characteristics [84]. Similarly, Gautam and Kumar examined the springback characteristics of laser-welded interstitial-free steel tailored blank (TWB) during V-bending via experimental methods and finite element analysis. The findings indicated that springback was mostly influenced by the thicker sheet, while the characteristics of the weld zone had a more substantial effect than material anisotropy, greatly enhancing springback prediction. These studies collectively illustrate that the integrity of welds, geometric design, and precise characterization of weld zone attributes are crucial for enhancing the forecasting of deformation behavior, fracture, impact performance, and springback in tailor welded blanks during sheet metal forming [19].

The mechanical characteristics of custom welded blanks are intricately linked to the microstructural changes occurring in the weld area, especially in the nugget zone, thermo-mechanically affected zone (TMAZ), and heat-affected zone (HAZ). Consequently, numerous research efforts have examined the impact of welding methodologies on the microstructure, texture, hardness, and mechanical properties of aluminium joints. In this context, Costa et al. investigated the link between hardness and localized tensile characteristics of friction stir welded AA6082-T6 joints by microhardness assessments, tensile testing, and digital image correlation. The findings demonstrated a direct correlation between hardness and stress, affirming that the strength of the weld is significantly influenced by the local distribution of hardness [15]. In a similar vein, Wang et al. examined the microstructure and textural

development of friction stir welded AA5052-O/AA6061-T6 joints by optical microscopy, EBSD, and TEM. The research indicated that dynamic recrystallization enhanced the grain structure of the nugget zone, as low-angle grain boundaries progressively converted into high-angle grain boundaries owing to dislocation buildup, hence augmenting the metallurgical properties of the joints [16]. Similarly, Liu et al. assessed the mechanical properties of AA6082 tailor welded blanks produced using laser and friction stir welding by employing tensile tests, hardness evaluations, digital image correlation, and a post-weld strength prediction (PWSP) model. The findings indicated that yield strength augmented with specimen dimensions, whereas ultimate tensile strength stayed relatively stable, and the PWSP model effectively forecasted post-weld tensile characteristics [17]. Moreover, Jula et al. examined the alterations in softening and precipitation within the heat-affected zone (HAZ) of GTAW-welded AA6082-T651 before to and subsequent to post-weld heat treatment (PWHT). SEM, TEM, DSC, thermal modeling, and hardness assessments indicated that HAZ softening was due to the coarsening of precipitates and over-aging, while PWHT reinstated hardness by generating fine β″-Mg_2Si precipitates. These investigations together indicate that the welding method, weld geometry, hardness distribution, microstructural evolution, texture development, and post-weld heat treatment significantly affect the strength, ductility, and structural integrity of aluminium tailor welded blanks. Sophisticated characterisation methods including EBSD, TEM, digital image correlation, and microhardness testing offer significant understanding of the association between weld microstructure and mechanical properties [18].

Recent studies have concentrated on sophisticated welding techniques to enhance the quality, microstructure, and mechanical properties of aluminium alloy connections, while reducing welding imperfections and residual stresses. In this context, Koli et al. conducted a comparative analysis of Cold Metal Transfer (CMT), MIG pulse synergic, and traditional MIG welding techniques on AA6061-T6 aluminium alloy utilizing optical microscopy, FESEM, XRD, residual stress, and microhardness evaluations. The findings indicated that CMT achieved superior weld penetration, less heat input, fewer imperfections, lower residual stresses, and enhanced microstructural properties compared to alternative welding methods [20]. In a similar vein, Svoboda et al. examined the residual stress distribution in both analogous and heterogeneous friction stir welded AA5083 and AA6061 joints by X-ray diffraction (XRD). The research uncovered distinctive M-shaped residual stress patterns, whereas alterations in lattice spacing and FWHM validated recrystallization and precipitate development [21]. Moreover, Koli et al. assessed various AA6061-T6/AA6082-T6 joints produced using CMT welding employing optical microscopy, FESEM, EDX, XRD, tensile tests, hardness measurements, and residual stress evaluations. An ideal heat input of 120–130 J/mm resulted in enhanced tensile strength, advantageous microstructure, and compressive residual stresses, while the elimination of weld reinforcing further augmented joint efficiency [22]. Similarly, Koli et al. examined ultrasonic-assisted CMT (U-CMT) welding of AA6061-T6 and AA6082-T6 alloys. The findings indicated that ultrasonic vibration enhanced weld grain structure, diminished porosity, facilitated Al–Si eutectic development, and markedly improved tensile strength and hardness in contrast to traditional CMT welding. These investigations together illustrate that sophisticated welding techniques, enhanced heat application, ultrasonic support, and

management of residual stresses are essential for improving weld microstructure, minimizing flaws, and augmenting the mechanical properties of aluminium alloy connections. Nonetheless, few investigations have thoroughly analyzed the synergistic impacts of laser welding parameters, thickness discrepancies, following annealing, microstructural development, and warm formability of aluminium tailor welded blanks. Consequently, additional studies are necessary to elucidate the connections between welding parameters, microstructural features, and formability behavior, which serves as the impetus for this research [23].

2.4 Laser Welding

Laser welding has surfaced as a sophisticated joining technique for lightweight constructions due to its elevated energy density, profound penetration, restricted heat-affected zone, minimal deformation, and compatibility with automation. The caliber of laser-welded connections is determined by the interaction between laser and material, energy absorption, keyhole stability, molten pool dynamics, shielding settings, and process regulation. As a result, many research efforts have explored the essential mechanics of laser welding. Huntington and Eagar investigated the influence of surface treatment, alloy composition, and joint configuration on laser power absorption in the welding of pure aluminium and AA5456 alloy. The findings indicated that joint geometry exerted the most substantial effect on laser energy absorption, whereas surface pretreatment markedly enhanced absorption efficiency. The scientists determined that bevel-groove junctions facilitated consistent keyhole development and enhanced weld integrity [85]. Similarly, Katayama et al. examined the influences of laser intensity, power density, shielding gas, plume dynamics, keyhole behavior, and

welding speed in CO_2, YAG, disk, and fiber laser welding by high-speed imaging, X-ray transmission, and spectroscopic analysis. The research indicated that the depth of weld penetration and the occurrence of defects were significantly influenced by laser settings and keyhole stability, whereas optimum processing reduced porosity, spatter, humping, and cracking [86]. In a similar vein, Katayama et al. examined laser-induced plumes, laser absorption, deep-penetration welding, and laser direct joining, demonstrating that plume dynamics, keyhole configuration, laser absorption, and vacuum conditions considerably influence weld penetration and joint stability [25]. Moreover, Katayama examined the principles of laser welding and emphasized that fiber and disk lasers offer enhanced beam quality, increased efficiency, greater penetration depth, and reduced welding imperfections compared to traditional laser systems [87]. Furthermore, Quintino et al. examined the utilization of CO_2, Nd, fiber, and disk lasers in structural aluminium welding, determining that refined laser settings and suitable welding techniques are crucial for achieving flawless, high-strength connections. These investigations collectively demonstrate that the absorption of laser energy, beam attributes, keyhole stability, shielding circumstances, and process refinement collaboratively dictate weld penetration, defect occurrence, and overall joint integrity, laying the scientific groundwork for laser welding of lightweight aluminium constructions and tailor welded blanks [88].Extensive research has explored the laser welding of aluminium alloys, namely the 5xxx and 6xxx series utilized in automotive and aerospace sectors, based on a foundational comprehension of laser-material interaction. Due to their elevated heat conductivity, significant reflection, and vulnerability to welding imperfections, it is crucial to optimize laser welding conditions to achieve robust connections with enhanced mechanical

properties. In this context, Zhao et al. examined the difficulties, processes, and progress in laser welding of 2xxx, 5xxx, and 6xxx automotive aluminium alloys. The research investigated laser energy absorption, thermal transfer, fluid dynamics, alloy vaporization, weld microstructure, mechanical characteristics, and flaws including porosity and hot cracking, concluding that weld quality is chiefly determined by keyhole stability, process parameters, and alloy composition [89]. In a similar vein, Cao et al. conducted a review on the laser welding of wrought aluminium alloys, emphasizing the effects of laser type, wavelength, power, welding speed, shielding gas, filler material, and joint configuration. The research indicated that Nd laser welding offers enhanced process adaptability, increased penetration depth, and superior weld quality when optimal process parameters are utilized [90]. Similarly, Cao et al. examined the metallurgical properties, welding imperfections, and mechanical attributes of laser-welded 5xxx and 6xxx alloys, revealing that refined welding parameters and defect management enhance microstructure, tensile strength, fatigue resistance, and structural robustness [91]. Moreover, Hong and Shin examined laser welding techniques pertinent to automotive uses concerning aluminium and several lightweight alloys. The research underscored that laser welding provides superior productivity, more penetration, less heat-affected zones, and enhanced structural integrity compared to traditional joining techniques, while stressing the necessity of process improvement and defect minimization for broader industrial implementation. These studies collectively illustrate that effective laser welding of aluminium alloys necessitates meticulous optimization of alloy properties, laser settings, thermal dynamics, and metallurgical changes to achieve flawless joints with enhanced mechanical strength and enduring structural integrity [30].

Notwithstanding the benefits of laser welding, the integrity and dependability of aluminium alloy connections are frequently compromised by imperfections like porosity, keyhole instability, solidification cracking, and incomplete fusion. As a result, considerable investigation has concentrated on comprehending the mechanisms of defect creation and devising efficient mitigation measures. In this context, Matsunawa examined the creation of porosity and keyhole instability in deep-penetration continuous-wave laser welding by the use of X-ray radiography, weld pool imaging, scanning electron microscopy, and gas analysis. The research demonstrated that erratic keyhole oscillations ensnared metal vapor and shielding gas, resulting in spherical and elongated voids, whereas refined pulse modulation successfully stabilized the keyhole and diminished porosity [92]. In a similar vein, Haboudou et al. investigated the development of porosity during continuous-wave Nd laser welding of AA5083 and A356 alloys by X-ray radiography, CT, SEM, EDS, and high-speed imaging. The findings indicated that laser surface cleaning diminished hydrogen-induced porosity, while dual-beam welding enhanced keyhole stability and weld quality without markedly altering the microstructure or mechanical characteristics [93]. Similarly, Hu and Richardson examined transverse solidification cracking in AA2024 and AA7075 alloys during laser and hybrid laser/GMA welding. Experimental findings and thermo-mechanical simulations indicated that extensive temperature differentials induced tensile stresses in the semi-solid phase, leading to cracking, whereas diminished welding velocity or supplementary heating significantly mitigated crack development [94]. Moreover, Katayama et al. investigated the impact of fibre laser welding settings on the depth of penetration and the occurrence of defects in A5083 alloy. Rapid imaging and X-ray transmission demonstrated that elevated

power density enhanced penetration, while nitrogen shielding gas and an ideal laser tilt angle diminished porosity and undercut [95]. El-Batahgy and Kutsuna similarly examined the laser welding of AA5052, AA5083, and AA6061 alloys, demonstrating that adequate surface preparation, enhanced argon shielding, and the use of filler wire or backing strips reduced porosity and eradicated solidification cracking, although AA6061 necessitated post-weld aging to regain weld strength [96]. Furthermore, Zhang et al. investigated the dynamics of the molten pool in full-penetration fibre laser welding of 5083 aluminium alloy by numerical simulations and high-speed photography. The research indicated that consistent keyhole behavior facilitated gas release, markedly decreasing porosity in contrast to partial-penetration welding. These investigations collectively illustrate that porosity, keyhole instability, and solidification cracking are influenced by the interaction between laser and material, dynamics of the molten pool, shielding settings, and process factors. Consequently, meticulous regulation of keyhole stability, thermal input, shielding atmosphere, and welding parameters is crucial for achieving flawless laser-welded aluminium connections with enhanced structural integrity and mechanical properties [97].

The microstructural changes that occur during laser welding significantly influence the mechanical characteristics, hardness distribution, corrosion resistance, and overall efficacy of aluminium alloy joints. As a result, numerous scholars have explored the metallurgical changes linked to laser welding across various processing parameters. In this context, Braun et al. conducted a comparison of laser beam welding (LBW) and friction stir welding (FSW) on 6013-T6 aluminium alloy through assessments of hardness, tensile strength, microstructure, and corrosion resistance. The findings indicated that FSW attained more than 80% joint efficiency with reduced flaws, while

LBW joints displayed porosity and diminished strength, especially with Al–5%Mg filler. The authors determined that FSW offers enhanced mechanical characteristics and corrosion resistance in comparison to traditional LBW [98]. In a similar vein, Sánchez-Amaya et al. examined conduction-mode laser welding of AA5083-T0 and AA6082-T6 with a high-power diode laser. The research revealed that welding speed significantly influenced weld penetration more than laser power, resulting in robust connections with superior corrosion resistance and dependable penetration forecasting in ideal circumstances [99]. Similarly, Zhou et al. investigated the influence of laser power on the microstructure and corrosion characteristics of hybrid laser–gas metal arc welded AA6061-T6 joints. Elevating laser intensity facilitated grain coarsening, augmented dendritic spacing, and intensified corrosion owing to alterations in the distribution of Al–Fe–Si intermetallic particles [100]. Additionally, Srinivas et al. examined continuous-wave Nd laser welding of dissimilar AA5083-H111 and AA6061-T6 alloys utilizing various laser power levels, welding velocities, and beam spot dimensions. The findings indicated that the cooling rate and temperature gradient had a substantial impact on grain structure and mechanical characteristics, achieving a peak tensile strength of 241 MPa at a laser power of 3.5 kW, a welding speed of 3.5 m/min, and a beam spot size of 180 μm. These investigations together illustrate that the parameters of laser welding significantly affect grain refinement, microstructural development, hardness, tensile properties, corrosion resistance, and fracture characteristics of aluminium alloy joints. Consequently, meticulous refinement of welding parameters is crucial for attaining desirable metallurgical properties and enhanced mechanical performance in laser-welded aluminium alloys [26].

The utilization of laser welding for custom welded blanks has attracted significant interest due to its integration of superior laser joining and the structural and weight-reducing benefits of TWB technology. Nonetheless, the effective execution of laser-welded aluminium tailored welded blanks necessitates high weld quality, few imperfections, and sufficient mechanical performance and formability. In this context, Enz et al. examined the laser beam welding of homogeneous AA7075-T6 and heterogeneous AA7075-T6/AA5182-O aluminium tailor welded blanks for sheet metal fabrication. Optical microscopy, SEM, X-ray analysis, microhardness assessments, and limit dome height (LDH) evaluations demonstrated that employing vanadium foil with 5087 filler wire markedly diminished porosity and enhanced weld integrity, despite the welded blanks displaying inferior formability compared to the original materials. The researchers determined that additional refinement of laser welding is necessary to enhance the formability of high-strength aluminium tailored welded blanks [101]. In a similar vein, Enz et al. assessed the mechanical properties of laser beam welded junctions, both analogous (AA7075–AA7075) and heterogeneous (AA7075–AA5182), utilizing vanadium foil with filler wire and a large-beam fibre laser. The research indicated that fibre laser welding resulted in enhanced tensile strength and improved formability, whilst dissimilar joints showed greater mechanical performance than identical joints. These investigations together indicate that the efficacy of laser-welded aluminium tailor welded blanks is determined by factors such as weld integrity, porosity, microstructural changes, hardness variation, and welding methodology. Despite notable advancements, sustaining excellent formability while reducing welding-related imperfections continues to pose a considerable problem, especially for high-strength aluminium alloys. These results

underscore the necessity to refine laser welding parameters to attain a suitable equilibrium among weld integrity, mechanical characteristics, and formability in aluminium tailor welded blanks [102].

In recent years, much attention has been directed on refining laser welding settings, advancing intelligent process monitoring methodologies, and broadening industrial applications to enhance weld quality and dependability. In this context, Park et al. examined Nd laser welding of AA5182 aluminium alloy with AA5356 filler wire for automotive purposes. The research demonstrated using ANOVA that filler wire diminished welding imperfections and enhanced tensile strength and Erichsen ratio at optimal heat input, with laser power being the most significant process variable [103]. In a similar vein, Sathish et al. refined Nd laser welding settings for AA7068 aluminium alloy with the application of the Taguchi method and ANOVA. The findings demonstrated that wire feed rate exerted the most significant impact on tensile strength, succeeded by traverse speed, while laser power had a very minor effect [104]. Similarly, Dhanaraj and Rathinasuriyan enhanced fibre laser welding of AA7075-T6 alloy through Taguchi's L9 design, VIKOR analysis, tensile assessments, hardness evaluations, and microstructural examination. The ideal settings (0.9 kW laser power, 8 mm/s travel speed, and 1000 Hz frequency) yielded around 75% welding efficiency with flawless welds [29]. Additionally, Qi et al. utilized Response Surface Methodology (RSM) to enhance the continuous fibre laser welding of incompatible AA4047/AA6061 connections. The ideal settings (800 W, 17.5 mm/s, and 0 mm defocus) yielded flawless welds with a forecast accuracy above 97% and a tensile strength of 260.45 MPa [105]. Furthermore, Sibillano et al. illustrated that correlation spectroscopy proficiently tracked magnesium deficiency and shielding gas efficacy

during CO_2 laser welding of AA5083 alloy [106]. Tušek et al. conducted a comparison of laser and MIG welding for tailor welded blanks, determining that laser welding is preferable for analogous materials, while MIG welding offers superior toughness for heterogeneous steels [107]. Similarly, Wu et al. examined the laser welding of car steel sheets and custom welded blanks, demonstrating that refined shielding gas and processing parameters reduced flaws and enhanced deep-drawing performance and mechanical characteristics. These studies collectively illustrate that process optimization, statistical design techniques, real-time surveillance, and sophisticated characterisation markedly improve the quality and industrial relevance of laser welding. Nonetheless, few investigations have thoroughly analyzed the synergistic impacts of laser welding parameters, thickness discrepancies, annealing processes, microstructural development, and warm formability of aluminium tailor welded blanks. Consequently, additional inquiry is necessary to ascertain these interconnections, thereby offering the scientific foundation and impetus for the current study [108].

2.5 Formability

Formability is an essential attribute that influences the effective production of sheet metal parts for lightweight automotive, aeronautical, and engineering uses. The capacity of a material to experience significant plastic deformation without localized necking or rupture strongly influences component quality, dimensional precision, and production efficacy. As a result, considerable investigation has concentrated on the determinants affecting sheet metal formability and the advancement of sophisticated forming techniques. In this context, Kleiner et al. examined the significance of metal

forming techniques in the fabrication of lightweight parts, such as custom welded blanks, warm forming, superplastic forming, incremental forming, and hydroforming. The research emphasized that sophisticated forming techniques optimize material usage, augment formability, decrease component mass, and boost structural integrity while preserving manufacturing efficiency. The authors determined that sophisticated metal forming techniques are crucial for producing lightweight, high-strength parts. Given that dependable formability evaluation is essential for the design and enhancement of sheet metal forming processes, various experimental methods have been established to analyze deformation characteristics [37]. In this context, Reddy et al. conducted a comprehensive study of sheet metal formability assessments, encompassing tensile, cruciform biaxial, Erichsen, Olsen, Fukui conical cupping, hole expansion, limiting dome height (LDH), Swift cup, hydraulic bulging, forming limit curve (FLC), and draw-bend evaluations. The analysis examined the benefits, drawbacks, and industrial uses of various techniques for assessing stretchability, drawability, and failure characteristics, ultimately determining that choosing a suitable formability test is crucial for enhancing sheet metal forming and reducing production flaws. These studies collectively illustrate that sophisticated forming technologies and dependable formability evaluation techniques are essential for the creation of lightweight sheet metal components and the enhancement of material selection, process design, and deformation characteristics [109].

Precise forecasting of sheet metal formability is crucial for reducing manufacturing flaws and enhancing forming procedures prior to production. As a result, considerable investigation has concentrated on experimental, theoretical, and finite element techniques for forecasting forming limit diagrams (FLDs) and forming limit curves

(FLCs) [109]. In this context, Ahmadi et al. examined FLD prediction for low-carbon and ultra-low-carbon steel sheets using experimental testing and ABAQUS finite element analysis employing Hill's yield criterion and the Atkins fracture criterion. The anticipated FLDs demonstrated strong concordance with experimental results, whereas anisotropic modeling yielded superior precision. The research determined that the strain-hardening exponent (n) and plastic strain ratio (r) significantly affect sheet formability and forming limitations [110]. In a similar vein, Mishra et al. included microstructural characteristics into finite element calculations to forecast FLCs for AA1050, AISI 316L, and AISI 304L sheets. The application of a variable strain-hardening exponent (n) and anisotropy (r) markedly enhanced forecast precision, especially in biaxial loading conditions [111]. Similarly, Abspoel et al. formulated an empirical approach for forecasting the forming limit curves of steel sheets based on tensile characteristics. Validation with experimental data demonstrated enhanced precision compared to the Keeler and Cayssials models, particularly for advanced high-strength steels [112]. Additionally, Habibi et al. assessed two altered finite element models derived from the Marciniak–Kuczynski (M–K) methodology for forecasting FLDs of ST14 steel sheets. The revised Nakazima model forecasted FLDs with under 10% divergence from empirical findings, showcasing enhanced precision compared to the flat model. These works collectively illustrate that precise prediction of FLD and FLC necessitates careful consideration of material anisotropy, strain-hardening characteristics, microstructural development, and constitutive modeling. The amalgamation of experimental characterisation with sophisticated finite element analysis establishes a dependable framework for assessing sheet metal formability and refining forming procedures [113].

AA6082 is a prominent aluminium alloy in lightweight sheet metal applications due to its advantageous blend of strength, corrosion resistance, and formability. As a result, numerous scholars have examined the impact of welding methods, material thickness, strain rates, and processing parameters on its formability. In this context, Simoncini et al. examined a double-sided friction stir welding (DS-FSW) method to enhance the post-weld formability of AA6082 joints. Tensile assessments, microstructural examinations, LDH evaluations, and forming limit curve (FLC) analyses indicated that DS-FSW yielded smaller recrystallized grains and markedly enhanced LDH and FLC metrics in comparison to traditional FSW, hence augmenting the formability of AA6082 custom welded blanks [114]. In a similar vein, Nghishiyeleke et al. assessed the formability of AA6082-O sheets by tensile and Erichsen cupping examinations. The findings revealed that thicker sheets had elevated forming limit curves and enhanced drawability, whereas rolling direction markedly affected anisotropy and formability [115]. Similarly, Çavuşoğlu et al. investigated the influence of sheet thickness on the yielding characteristics and formability of AA6082-T6 by experimental and numerical analyses. Augmenting sheet thickness enhanced anisotropy and formability, whereas the Barlat-89 yield criterion provided a more precise prediction of yielding behavior and forming limits compared to the Hill-48 model [116]. Moreover, Simoncini et al. examined the effect of strain rate on the formation limit curves of AA6082-T6 via experimental testing and finite element analysis. The research indicated that elevated strain rates markedly enhanced the forming limit curve, indicating superior formability in high-velocity forming scenarios. These investigations together illustrate that welding methods, grain refinement, sheet thickness, rolling direction, constitutive modeling, and strain rate

significantly affect the formability of AA6082 aluminium alloy. Consequently, refining these parameters is crucial for enhancing deformation characteristics and broadening the industrial utilization of AA6082 in lightweight sheet metal constructions [117].

Beyond inherent material characteristics, the workability of aluminium alloy sheets is significantly affected by processing variables like blank holder force, friction, lubrication, forming temperature, strain trajectory, and tool design. As a result, a multitude of research endeavors have examined their impacts through both experimental and computational methods. In this context, Pranavi et al. examined the deep drawability of the AA6061 aluminium alloy by finite element analysis. The findings indicated that diminished friction, decreased strain trajectories, and enhanced blank holder force facilitated material flow and increased dome height, whereas failure consistently originated at the cup's side wall. The authors determined that numerical simulation accurately forecasts formability and aids in the selection of ideal deep drawing settings [118]. In a similar manner, Gautam and Konar integrated experimental characterization with finite element simulation to assess interstitial-free (IF) and deep draw quality (DDQ) steels intended for vehicle fuel tanks. Should steel provide enhanced ductility, increased normal anisotropy, reduced thinning, and improved formability, it would illustrate the efficacy of combining material characterization with numerical simulation for the purpose of material selection [119]. Similarly, Ramulu examined the deformation characteristics of aluminium alloys during hot forming, deep drawing, incremental forming, hydroforming, and biaxial forming. The evaluation underscored that high-temperature shaping boosts ductility, diminishes flow stress, and improves formability, stressing the necessity of refining

processing settings [120]. Moreover, He et al. examined AA5052-H24 sheets through tensile and Erichsen cupping assessments, revealing that augmented blank holder force, elevated punch velocity, and enhanced lubrication improved formability, whereas rolling direction markedly influenced anisotropy [121]. In a similar vein, Hodžić et al. investigated the effects of alloy composition and lubrication on Al–Mg–Si alloys using deep drawing tests and finite element analysis. The research indicated that while increased silicon levels enhanced formability, lubrication exerted a significantly more substantial influence, underscoring the necessity for optimum lubrication and precise friction modeling. These studies collectively illustrate that effective sheet metal forming relies on the interplay of material characteristics, process variables, lubrication, strain trajectory, and forming temperature [122]. Nevertheless, few studies have thoroughly examined the synergistic effects of laser welding, annealing processes, thickness discrepancies, microstructural changes, and warm forming on the formability of aluminium tailor welded blanks. Consequently, additional inquiry is necessary to ascertain these interconnections, thereby offering the scientific impetus for the current study.

2.6 Warm Forming

Warm forming has become a proficient manufacturing method for enhancing the formability of aluminium alloys while preserving acceptable mechanical characteristics and dimensional precision. Processing at intermediate temperatures beneath the recrystallization threshold diminishes flow stress, postpones localized necking, augments ductility, and facilitates material flow during deformation. As a result, extensive studies have concentrated on the concepts and uses of heated forming

for lightweight aluminium parts. In this context, Bolt et al. examined the warm forming of 1050-H14, 5754-O, and 6016-T4 aluminium alloys via deep drawing and stretch drawing utilizing a heated die and a punch at ambient temperature. The findings indicated that heated forming markedly enhanced drawing depth, diminished wrinkling, and augmented formability while having a negligible impact on hardness. The authors determined that heated forming is a proficient method for producing intricate aluminium parts [123]. In a similar vein, Tebbe and Kridli assessed the present comprehension and prospective advancements of heated forming for 5xxx and 6xxx series aluminium alloys. The research examined constitutive models, experimental analyses, heating techniques, lubrication, and numerical simulations, emphasizing that intermediate-temperature forming significantly enhances ductility, drawability, and overall formability while preventing excessive recrystallization. The authors determined that the amalgamation of experimental research with numerical modeling is crucial for enhancing warm formation and broadening its industrial utilization. These studies collectively illustrate that warm forming successfully addresses the restricted room-temperature formability of aluminium alloys by enhancing material flow, minimizing forming defects, and augmenting manufacturing potential, thus establishing a scientific foundation for its industrial use in lightweight sheet metal components [124].

Comprehensive studies have examined the impact of elevated forming temperatures on the deformation characteristics and forming thresholds of aluminium alloys. Given that temperature and strain rate significantly influence strain hardening, strain-rate sensitivity, and localized deformation, several investigations have explored their collective impacts on forming limit diagrams (FLDs), forming limit curves (FLCs),

and tensile properties. In this context, Naka et al. investigated the influence of temperature and forming velocity on the forming limit diagrams (FLDs) of 5083-O Al–Mg alloy by punch stretch tests and Marciniak–Kuczynski (M–K) model. The findings indicated that formability markedly improved at elevated temperatures, especially at 573 K and reduced forming velocities, due to greater strain-rate sensitivity. The authors determined that warm forming significantly enhances the formability of aluminium sheets and that the M–K model reliably forecasts FLDs [125]. In a similar vein, Li and Ghosh examined the tensile properties of Al 5182+1%Mn, Al 5754, and Al 6111-T4 alloys within the temperature range of 200–350 °C with varying strain rates. The research indicated that ductility rose with temperature yet diminished with strain rate, with strain-hardened 5xxx alloys demonstrating superior warm formability compared to precipitation-hardened Al 6111-T4 [46]. Similarly, Li and Ghosh assessed the biaxial warm forming characteristics of Al 5754, Al 5182+Mn, and Al 6111-T4 alloys, revealing those elevated temperatures markedly improved formability, especially for the 5xxx series alloys, while preserving mechanical qualities [47]. Additionally, Hsu et al. formulated forming limit diagrams (FLDs) for AA5182-O, AA5754-O, and AZ31B magnesium alloy sheets through Marciniak and Limiting Dome Height (LDH) assessments. The findings validated that increased temperature significantly enhanced formability, however the LDH technique yielded more dependable FLD assessments [126]. In a similar vein, Shao et al. examined the AA5754 aluminium alloy at varying temperatures and forming velocities, revealing that elevated temperatures and reduced forming speeds enhanced forming limitations, while increasing speeds augmented thickness uniformity [52]. Similarly, Satish and Kumar investigated the warm

formability of AA6061 alloy and found that maximal formability occurred at elevated temperatures and minimal punch speeds. They additionally suggested a novel FLD_0 correlation that enhanced finite element failure forecasting by integrating the cumulative influences of temperature and strain rate. These investigations together illustrate that the temperature during warm forming, the rate of strain, and the speed of forming significantly affect strain hardening, strain-rate sensitivity, forming limits, and deformation characteristics. Consequently, the enhancement of warm forming parameters is crucial for optimizing formability, ensuring satisfactory mechanical properties, and refining the precision of formability forecasting models [53].

The enhancement of formability in warm forming is influenced by both material characteristics and processing variables, including forming temperature, strain rate, lubrication, blank holder force, and loading conditions. As a result, several research efforts have examined their impact on the deformation characteristics and mechanical properties of aluminium alloys. In this context, Venkateswarlu et al. examined the deep drawing characteristics of AA6061 and AA7075 alloys by DEFORM-2D finite element simulations throughout a temperature spectrum of 50–500 °C. The findings indicated ideal formability at temperatures ranging from 150 to 250 °C for AA6061 and from 400 to 500 °C for AA7075, highlighting the utility of finite element simulation in forecasting appropriate forming parameters [127]. In a similar vein, Mahabunphachai and Koç investigated the warm hydroforming of AA5052 and AA6061 alloys utilizing hydraulic bulging, tensile assessments, hydroforming trials, and finite element analysis. Elevated temperatures diminished flow stress and enhanced formability, whilst hydraulic bulge measurements yielded superior material characterization compared to traditional tensile data [128]. Similarly, Wang et al.

assessed the heated forming characteristics of AA7075 alloy by tensile tests, limiting drawing ratio (LDR), limiting dome height (LDH), hardness evaluations, and post-forming mechanical property analyses. The research indicated optimal deep drawability at around 180 °C, but temperatures beyond 220 °C diminished mechanical integrity [129]. Additionally, Sun et al. examined warm-formed AA5182 automobile parts and revealed enhanced energy absorption, satisfactory crash performance, and rigidity akin to steel frameworks [130]. In a similar, Takata examined warm forming technique for aluminium alloys, emphasizing that enhanced temperature, lubrication, blank holder force, and thermo-mechanical simulations markedly enhance deep drawability, dimensional precision, and springback management [131]. Similarly, Kumar et al. investigated the warm formability of AW-7020-T6 aluminium alloy within the temperature range of 150 to 250 °C. The findings indicated a notable enhancement in formability beyond 150 °C attributed to dynamic recovery and the coarsening of η′ precipitates, despite a reduction of around 30% in yield and tensile strengths, with temperatures between 200–250 °C offering the optimal compromise between formability and mechanical characteristics. These investigations collectively illustrate that the heated forming behavior is predominantly influenced by the interplay of forming temperature, strain rate, lubrication, material properties, precipitation development, and process variables. Consequently, meticulous adjustment of these variables is crucial for enhancing formability while preserving the mechanical integrity and dimensional precision of aluminium alloy components [132].

The utilization of warm forming on AA6082 aluminium alloys and custom welded blanks has attracted significant interest due to its capacity to enhance formability, weld quality, and dimensional precision. As a result, numerous scholars have examined the

synergistic impacts of post-weld heat treatment, warm forming, thermal distribution, and microstructural changes on the deformation characteristics of aluminium tailor-welded blanks. Gnibl and Merklein combined post-weld heat treatment (PWHT) with warm shaping for friction stir welded aluminium tailor welded blanks. Experimental studies and finite element assessments indicated that post-weld heat treatment at 250–300 °C, succeeded by warm forming at 150 °C, diminished the strength disparity between the weld and base material, augmented material flow, increased formability, and resulted in a more consistent thickness distribution [133]. In a similar vein, Liu et al. examined the hot stamping characteristics of friction stir welded AA6082 tailor welded blanks with varying thickness combinations through experimental methods and finite element simulations. The HFQ® technique effectively reinstated weld strength following artificial ageing, while the validated model precisely forecasted deformation characteristics and post-form hardness utilizing continuous cooling precipitation (CCP) diagrams [134]. Similarly, Panicker and Panda examined the warm formability of AA5754 and AA6082 sheets under both isothermal and non-isothermal conditions through stretch forming, deep drawing, and thermo-mechanical finite element analysis. The findings indicated that warm forming at 200 °C markedly enhanced the limiting dome height and forming limit diagrams, with non-isothermal forming utilizing a heated die and a cooled punch yielding the greatest drawability [54]. Additionally, Ye et al. examined the mechanical characteristics at increased temperatures and the microstructural changes of AA6082-T6 sheets. Tensile strength diminished as ductility augmented with temperature due to dynamic recrystallization and the coarsening of precipitates, while significant anisotropy at 200 °C was essentially eradicated at 400 °C via recrystallization. These investigations collectively

illustrate that warm forming, post-weld thermal treatment, thermal gradients, and microstructural changes collaboratively influence the deformation characteristics and formability of AA6082 alloys and customize welded blanks. Consequently, refining temperature distribution, heat treatment, and thermo-mechanical processing is crucial for augmenting weld integrity, minimizing strength discrepancies, boosting material flow, and optimizing TWB formability [135].

Recent studies have broadened the industrial relevance of warm forming by emphasizing component production, heat cycle enhancement, eco-friendly materials, and the performance of custom welded blanks in real-world processing scenarios. In this context, Polak et al. examined the heated forming of an automotive bracket utilizing AA7075-T6 at a temperature of 240 °C. The research indicated that components without defects were effectively manufactured, despite a fall in ultimate tensile strength by approximately 11% and a hardness of 165 HV, illustrating that heated forming presents a financially viable option when a moderate decrease in strength is permissible [55]. In a similar vein, Palumbo et al. investigated the heated forming of an AA5754-O railway component by material characterization and thermo-mechanical finite element simulations. Increased temperatures markedly enhanced formability, whereas elevated punch velocities encouraged fracturing; experimental verification established that 60 mm/min yielded flawless components, whereas 180 mm/min resulted in cracking [136]. Similarly, Behrens et al. examined the warm and hot forming of AA7022 and AA7075 alloys, revealing that higher temperatures significantly improved drawability and that the integration of artificial ageing with the paint-bake cycle diminished processing time by about 75% relative to traditional T6 treatment [137]. Moreover, Suresh et al. investigated the displacement of weld lines

during the warm formation of custom welded blanks via selective heating. The findings indicated that heating the more robust blank significantly reduced weld-line displacement, although the ratio of sheet thickness exerted a more substantial effect than the original weld-line location [138]. Moon and Welo conducted a comparison of the warm formability of primary and recycled AA6082 alloys, discovering that the recycled variant had similar drawability despite elevated impurity concentrations [139]. Furthermore, Simões et al. examined the effect of heat retention duration on the warm forming of AA6016 and AA6061 alloys. Extended holding durations facilitated artificial aging, enhancing strength and springback but diminishing ductility, underscoring the need of heat cycle regulation. These investigations together indicate that the effective industrial application of warm forming relies on the optimization of forming temperature, thermal cycles, forming velocity, heat treatment, weld-line management, and material state [140]. Nonetheless, scant research has thoroughly examined the synergistic impacts of laser welding parameters, annealing processes, thickness fluctuations, microstructural development, and warm formability of aluminium tailor welded blanks. Consequently, additional inquiry is necessary to ascertain these interconnections, thereby offering the scientific foundation and impetus for the current study.

2.7 Formability of TWBs

TWBs offer a proficient method for producing lightweight structural elements by amalgamating sheets of varying thicknesses, strengths, or material classifications prior to shaping. Nevertheless, the weld seam, variations in material properties, and discrepancies in thickness induce intricate deformation behavior, resulting in the

formability of TWB differing from that of homogeneous sheets. As a result, extensive studies have concentrated on comprehending TWB deformation and enhancing formability. In this context, Kinsey et al. presented a fabrication method that includes a uniquely engineered clamping apparatus along the weld joint. Numerical simulations conducted on Al 6111-T4 tailor-welded blanks indicated that the method diminished peak weld-line stress by approximately 20%, curtailed weld-line displacement, postponed fracture onset, and markedly enhanced drawability for intricate automobile parts [141]. Kridli et al. similarly examined the formability of gas tungsten arc welded (GTAW) AA5182-O custom welded blanks by Limiting Dome Height (LDH) assessments and finite element analysis. The results showed that weld orientation strongly influenced formability, with centrally located transverse welds exhibiting the lowest formability due to premature thinning of the thinner sheet, whereas inclined (45°) and offset transverse welds retained more than 80% of the formability of the corresponding base material. These investigations together illustrate that weld-line behavior, tooling arrangement, and weld orientation significantly influence the formability of custom welded blanks. Effective regulation of these parameters mitigates weld-line displacement, postpones fracture onset, and markedly improves the forming efficacy of aluminium tailor-welded blanks [142].

Among the elements influencing the formability of custom welded blanks, the ratio of sheet thickness, orientation of the weld, position of the weld, and movement of the weld line are the predominant geometric characteristics dictating deformation behavior. Discrepancies in thickness and strength among the constituent sheets lead to uneven plastic deformation, strain localization, weld-line displacement, and early fracture. As a result, a multitude of research endeavors have examined these impacts

through both experimental and computational methods. In this context, Chan et al. examined the effect of thickness ratio on the forming limit diagrams (FLDs) of tailor welded blanks made from Nd laser-welded SPCC steel. Tensile and Swift cup examinations indicated that augmenting the thickness ratio from 1.25 to 2.0 markedly diminished the forming limit curve and the minimum major strain, with the thinner sheet dictating the overall formability [143]. In a similar vein, Vijay Bhaskar and colleagues employed finite element simulations of tensile and Limiting Dome Height (LDH) tests to demonstrate that the thinner sheet dictated deformation, whereas thickness ratios beyond 1.3 resulted in the thicker sheet acting as a hard constraint, hence diminishing elongation and formability [144]. Similarly, Bhagwan et al. shown via LS-DYNA simulations that enhancing combinations of material strength minimized weld-line displacement, suggesting that formability is influenced by both gauge disparity and strength variation [145]. Chan et al. additionally validated that a heightened thickness ratio diminished forming limits, even though laser welding augmented fusion-zone hardness by approximately 60%, while the minimum main strain served as a dependable indicator of formability [146]. In a similar vein, Panda et al. indicated that discrepancies in thickness resulted in uneven strain distribution in the thinner sheet, while surface coatings hardly influenced deformation characteristics [147]. Similarly, Cheng et al. demonstrated that deformation was primarily localized in the thinner sheet and that discrepancies in thickness exerted a more significant effect on formability than the orientation of the weld [148]. Moreover, Panda et al. illustrated that an elevated strength ratio diminished formability and augmented weld-line displacement, with fractures invariably manifesting in the less robust sheet [149]. Riahi et al. discovered that decreasing the thickness ratio and relocating the weld line

towards the thicker sheet enhanced cup height and overall formability [150]. Abbasi et al. determined that geometric discontinuity was the principal factor affecting formability, while weld-zone characteristics accounted for about 6%, enabling simplified finite element modeling with minimal accuracy compromise [151]. Similarly, Korouyeh et al. introduced the Limit Thickness Ratio (LTR) as a significant factor for forecasting weld-line migration and deformation characteristics [152], whereas Kumar et al. demonstrated that shifting the initial weld line closer to the thinner sheet minimized weld-line displacement and enhanced hydroformed bulge uniformity by roughly 67–74%. These investigations collectively illustrate that the thickness ratio, weld orientation, weld position, strength mismatch, and weld-line movement collectively dictate the deformation characteristics and formability of custom welded blanks. Consequently, the refinement of these geometric parameters is crucial for reducing strain localization, inhibiting weld-line movement, postponing fracture onset, and enhancing TWB forming efficacy [153].

Precise forecasting of the deformation characteristics of custom welded blanks necessitates adequate characterization of the mechanical properties of the weld zone, along with dependable constitutive modeling of the heterogeneous blank. Due to the substantial differences in microstructure and mechanical properties between the weld region and the source materials, numerous researchers have devised sophisticated modeling techniques to enhance finite element simulations. In this context, Cheng et al. introduced an experimental technique to ascertain the authentic stress–strain characteristics of weldments in dissimilar stainless-steel tailor welded blanks. The research demonstrated that the weld zone exhibited the highest strength yet the lowest ductility, and integrating its specific characteristics into finite element analysis

markedly enhanced strain forecasting relative to uniform material models [154]. In a similar vein, Moayedi et al. examined the effect of weld orientation (0°, 45°, and 90°) on the forming limit diagrams of friction stir welded St14 steel tailor welded blanks by Nakazima testing and finite element analysis. The findings indicated that weld orientation influenced formability based on the strain path: the 90° orientation yielded the greatest formability in uniaxial tension, the 0° orientation excelled in plane strain, while weld orientation had a negligible impact during biaxial stretching. The research indicated that friction stir welding enhanced the grain structure and elevated the hardness of the weld zone, markedly affecting deformation characteristics [155]. Additionally, Kumar and Gautam examined recent developments in the formability of high-strength steel tailor welded blanks, highlighting the significance of TWB technology for lightweight vehicle construction, crash safety, and fuel economy. The assessment emphasized numerical modeling, laser welding parameters, sequential heating, and multiphase steel microstructures, while suggesting additional research on fiber laser defocus distance and Cold Metal Transfer (CMT) brazing for steel-aluminium tailored welded blanks. These investigations collectively illustrate that precise forecasting of TWB formability relies on authentic characterisation of weld-zone attributes, diverse constitutive modeling, and sophisticated finite element analyses. Integrating thorough material characterization with numerical analysis consequently gives a credible foundation for forecasting strain distribution, weld-line behaviour, and failure characteristics in custom welded blanks [156].

The welding technique employed in the production of custom welded blanks is vital for establishing weld integrity, microstructural development, mechanical characteristics, and finally the formability of the welded sheets. As a result, several

scholars have evaluated various welding procedures to determine appropriate joining approaches for creating high-performance TWBs. In this context, Kesharwani et al. produced tailor friction stir welded blanks (TFSWBs) from AA5754 and AA5052 alloys and refined the welding parameters by the Taguchi method and Grey relational analysis. The research indicated that TFSWBs demonstrated formability akin to the base materials, however a modified conical tractrix die (MCTD) enhanced the Limiting Drawing Ratio (LDR) by roughly 27% due to less punch force and wrinkling [157]. In a similar vein, Weckman and Moulton enhanced the formability of fusion-welded AA5182-O custom welded blanks with the application of double-sided arc welding (DSAW). By diminishing welding power and travel velocity, hydrogen and solidification porosity were eradicated, resulting in flawless welds with markedly enhanced ductility and fractures occurring in the thinner sheet instead of the weld [158]. Similarly, Bagheri et al. conducted a comparison of CO_2 laser welding, friction stir welding (FSW), and friction stir vibration welding (FSVW) for AA6061 custom welded blanks. The findings indicated that FSVW exhibited superior formability and mechanical characteristics due to its finer equiaxed grains and elevated dislocation density, which postponed crack start and enhanced forming limits [159]. Additionally, Acar et al. examined the uniaxial and biaxial deformation characteristics of friction stir welded AA7075-O joints at high temperatures by hydraulic bulge testing. The research revealed that high-temperature forming markedly enhanced plastic deformation and that the mechanical qualities of the weld zone had a substantial impact on overall formability [160]. In a similar vein, Abbasi et al. indicated that friction stir vibration welding markedly enhanced the formability of AA6061 tailor welded blanks through the refinement of stir-zone grains and the augmentation of dislocation density.

Taguchi and ANOVA assessments revealed welding speed as the predominant factor, whereas the fracture transitioned from the weld area to the thinner sheet, signifying enhanced joint integrity. These investigations together indicate that refining welding methods is crucial for improving the formability of aluminium tailor welded blanks. Enhanced weld integrity, grain refinement, diminished defects, and microstructural uniformity mitigate premature failure, augment deformation capacity, and markedly elevate the forming efficacy of welded aluminium sheets [161].

Recent studies have concentrated on enhancing the formability of dissimilar aluminium tailor welded blanks via process optimization, microstructural analysis, and post-weld thermal treatment. Significant focus has been directed into AA5083–AA6082 custom welded blanks due of their promise for lightweight automotive uses. Kumar and Sharma examined the effects of tool rotational velocity and pin diameter on the mechanical characteristics and formability of friction stir welded AA5083-O/AA6082-O tailor welded blanks. Response Surface Methodology (RSM) and Analysis of Variance (ANOVA) were employed to enhance Limiting Dome Height (LDH) and tensile strength. The findings indicated that optimal frictional heat production enhanced material flow and strain distribution, while regression analyses validated the significant impact of tool rotation and welding travel velocities on joint integrity and formability [162]. In a similar vein, Datta et al. investigated the association among microstructure, crystallographic texture, and the formability of friction stir welded AA5754 sheets by LDH testing, digital image correlation (DIC), and EBSD. The research indicated that the deterioration of the Goss texture component, along with fluctuations in grain misorientation and high-angle grain boundaries, diminished biaxial formability, so demonstrating a clear correlation

between crystallographic texture and forming limits [163]. Similarly, Konar and Gautam examined the influence of post-weld annealing on friction stir welded AA5083/AA6082 tailor welded blanks by LDH experiments and finite element analyses. Post-weld annealing enhanced formability by roughly 13% in both plane strain and biaxial stretching by augmenting stir-zone ductility and diminishing dislocation density, while reinstating ductility next to the weld/AA6082 interface. These investigations collectively indicate that the formability of dissimilar aluminium tailor welded blanks is influenced by welding conditions, microstructural changes, crystallographic orientation, and post-weld thermal treatment [164]. Nonetheless, few studies have thoroughly examined the formability of laser-welded aluminium tailor welded blanks under warm forming conditions while concurrently addressing welding parameter optimization, annealing treatment, thickness variation, microstructural evolution, and numerical simulation. Consequently, additional inquiry is necessary to ascertain these interconnections, thereby offering the scientific foundation and impetus for the current study.

2.8 Research Gaps

A thorough examination of the literature reveals that Aluminium alloys, tailor welded blanks (TWBs), laser welding, and hot shaping techniques have been intensively researched. Nevertheless, several critical scientific and technological questions persist unanswered, especially with laser-welded AA6082 tailor-welded blanks in heated forming settings.

The following research gaps have been identified:

1) There has been no extensive investigation into the warm forming characteristics of laser-welded tailor-welded blanks composed of similar AA6082 Aluminium alloy sheets with differing thicknesses.

2) The influence of tensile properties, microstructure, hardness, and anisotropy of parent sheets and tailor-welded blanks on their formability in heated forming conditions has not been thoroughly characterized.

3) The movement of weld lines during heated forming has not been extensively studied concerning process parameters, design specifications, sheet thickness ratios, and material characteristics.

4) The influence of punch velocity, forming temperature, sheet thickness, and the thickness ratio of tailor-welded blanks on the formability of Aluminium alloys in warm forming has been only slightly investigated.

5) The existing research does not comprehensively explore the application of finite element simulations for predicting the failure characteristics of parent sheets and tailor welded blanks in hot forming scenarios, nor does it include experimental validation to enhance formability evaluation.

2.9 Research Novelty and Contributions

In light of the recognized research deficiencies, this work examines the formability of laser-welded AA6082 tailor welded blanks in both ambient and elevated temperature forming scenarios. The key innovations and contributions of the current study are outlined as follows:

1) The forming characteristics of laser-welded AA6082 tailor welded blanks with varying thickness combinations, specifically 1.5-2.0 mm, 1.5-2.5 mm, and 1.5-3.0 mm, were methodically examined.

2) Integrated assessment of base sheets and TWBs: The mechanical and material properties pertinent to formability were analyzed via tensile testing, strain hardening behavior, normal anisotropy, microhardness, and microstructural examination of the base sheets and laser-welded TWBs.

3) Analysis of the weld zone: The tensile properties and strain hardening attributes of the weld area for various TWB thickness combinations were examined to supply material data for finite element simulations and enhance the depiction of failure behavior.

4) Evaluation of formability under ambient temperature and elevated temperature forming conditions: Forming Limit Curves (FLCs) were established for the base sheets and laser-welded Tailored Welded Blanks (TWB) under ambient and elevated temperature forming conditions, facilitating a comparative evaluation of their formability.

5) Experimental-numerical evaluation of failure characteristics: Finite element analyzes were conducted to forecast the failure characteristics of base sheets and laser-welded tailored blanks under various forming conditions, subsequently compared with experimental findings for numerical verification.

The research presents a comprehensive experimental and numerical analysis of the mechanical properties and formability of thickness-mismatched laser-welded AA6082

tailor welded blanks, focusing specifically on the effects of forming temperature and TWB arrangement.

2.10. Research Objectives

Based on the identified research gaps, the present investigation has been undertaken with the following objectives:

1) To select high strength AA6082 aluminium alloy sheets of different thicknesses and prepare tailor welded blanks (TWBs) using laser welding with different thickness ratios.

2) To characterize the hardness, tensile properties, strain hardening behaviour, and anisotropy of the parent sheets and laser welded tailor welded blanks at room temperature and warm forming temperature range.

3) To determine the tensile properties and strain hardening exponent of the weld zone in tailor welded blanks having different thickness ratios for incorporation into finite element simulations and improvement of failure prediction accuracy.

4) To develop the Forming Limit Curves (FLCs) of the parent sheets and laser welded tailor welded blanks under room temperature and warm forming conditions for the assessment of formability.

5) To predict the failure behaviour of parent sheets and tailor welded blanks using finite element simulations at room temperature and warm forming conditions and to validate the numerical predictions with experimental results.

CHAPTER 3

METHODOLOGY

The research process is depicted in Figure 3.1, encompassing material selection, annealing, laser welding of AA6082 tailor-welded blanks, mechanical and microstructural characterisation, formability evaluation, and finite element modeling at both ambient and increased temperatures. Three to five specimens were analyzed for each experimental condition to ensure repeatability, with consistent patterns observed in the repeated evaluations.

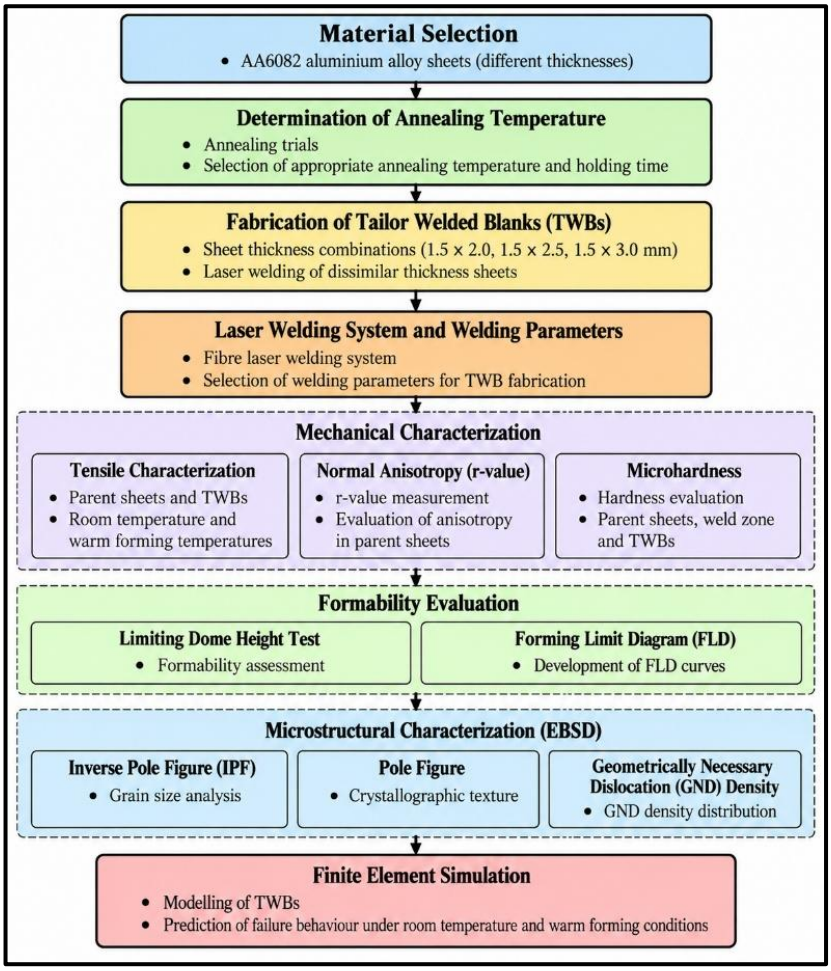


Figure 3.1 Schematic representation of the overall research methodology adopted in the present study.

3.1 Material Selection

AA6082 aluminium alloy sheets of four distinct thicknesses 1.5, 2.0, 2.5, and 3.0 mm were acquired in a tempered state from Mallinath Metal, Girgaon, Mumbai, Maharashtra, for this study. The chosen thicknesses were employed to produce laser-welded tailor welded blanks (TWBs) with various thickness combinations to examine their mechanical properties, microstructural attributes, and warm formability. AA6082 is an age-hardenable aluminium alloy including roughly 1 wt.% magnesium and silicon, with manganese as the primary alloying component. Due to its elevated specific strength, remarkable corrosion resistance, commendable weldability, and advantageous formability, AA6082 is widely utilized in structural applications including bridges, trusses, cranes, transports, automotive body frameworks, and various lightweight engineering elements. The elemental makeup of the acquired AA6082 sheets was ascertained by spark-based spectroscopy at Advance Inspection & Testing Lab, located in Mayapuri Industrial Area, New Delhi. The quantified chemical makeup of the alloy obtained from spectroscopy is given in Table 3.1.

Table 3.1 Chemical composition of AA 6082 aluminium alloy (in wt.%).

Alloy	Mg	Si	Mn	Sn	Cr	Ni	Fe	Al
AA 6082	0.91	1.06	0.55	0.06	0.21	0.04	0.24	97.02

3.2 Determination of Annealing Temperature of Parent Sheet

Initial annealing trials were conducted to ascertain the ideal annealing temperature for AA6082 aluminium alloy sheets before laser welding and warm formability assessments. The determination of the annealing temperature range for this study was

informed by previous research documented in the literature, which indicated that annealing treatment substantially affects the mechanical characteristics and microstructural development of aluminium alloys. Lee et al. and Changela et al. examined the influence of annealing processes across various temperature intervals on aluminium alloys, noting significant alterations in their mechanical properties and microstructure [165-166]. In light of these results, preliminary annealing trials were performed at six distinct temperatures: 150°C, 200°C, 250°C, 300°C, 350°C, and 400°C, utilizing a laboratory muffle furnace located at the Material Forming Laboratory, Department of Mechanical Engineering, Delhi Technological University, New Delhi. The AA6082 aluminium alloy sheets were elevated to the specified temperature and held for a soaking duration of 2 hours to guarantee consistent heat treatment across the material. Upon concluding the soaking duration, the specimens were let to cool slowly within the furnace and were extracted solely after the furnace temperature fell beneath 60°C. The annealed samples were then analyzed for their mechanical properties, and the ideal annealing temperature was determined from the experimental findings.

3.3 Fabrication of Tailor Welded Blanks

3.3.1 Laser Welding System and Fixture

Laser Beam welding (LBW) was chosen for the production of TWBs due to its elevated energy density, minimal heat input, restricted heat-affected zone (HAZ), rapid welding speed, superior dimensional precision, and straightforward automation, rendering it an optimal joining method for aluminium alloy TWBs [103-105]. The tailor welded blanks were produced with an industrial robotic fiber laser welding

apparatus combined with a six-axis ABB robotic arm positioned on a linear rail. The fiber laser apparatus possessed a peak power capability of 6000 W and ensured accurate alignment of the laser welding head throughout the welding operation. The industrial robotic fiber laser welding apparatus and the welding fixture employed for the production of tailor welded blanks are illustrated in Figure 3.2. All laser welding trials were conducted at Magod Fusion Technologies Pvt. Ltd., located in Pune, Maharashtra. Before welding, the annealed AA6082 aluminium alloy sheets were arranged in a butt-joint formation and securely fastened with a fixture to guarantee accurate alignment, inhibit relative motion during the welding operation, and reduce distortion during the welding procedure.

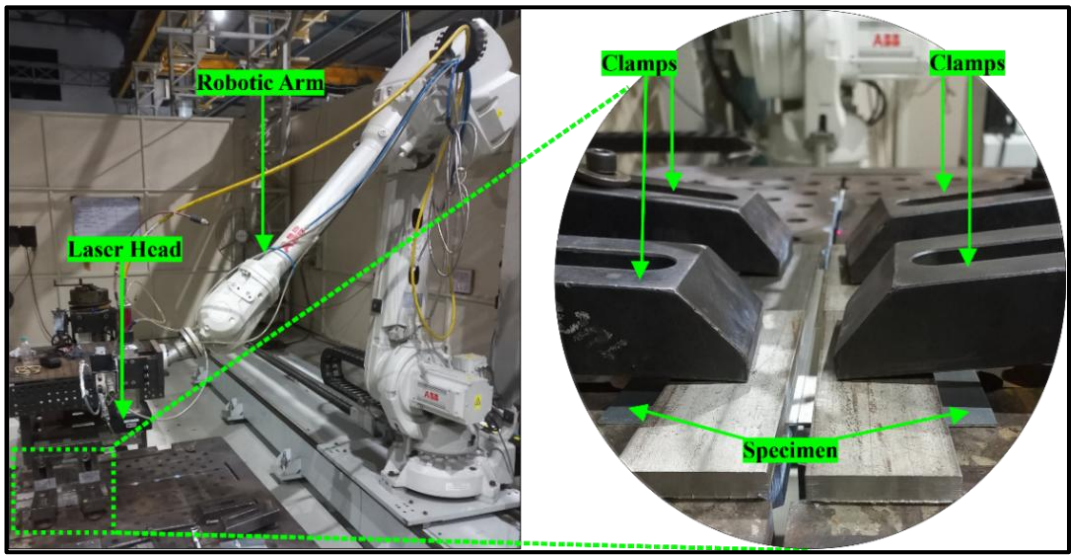
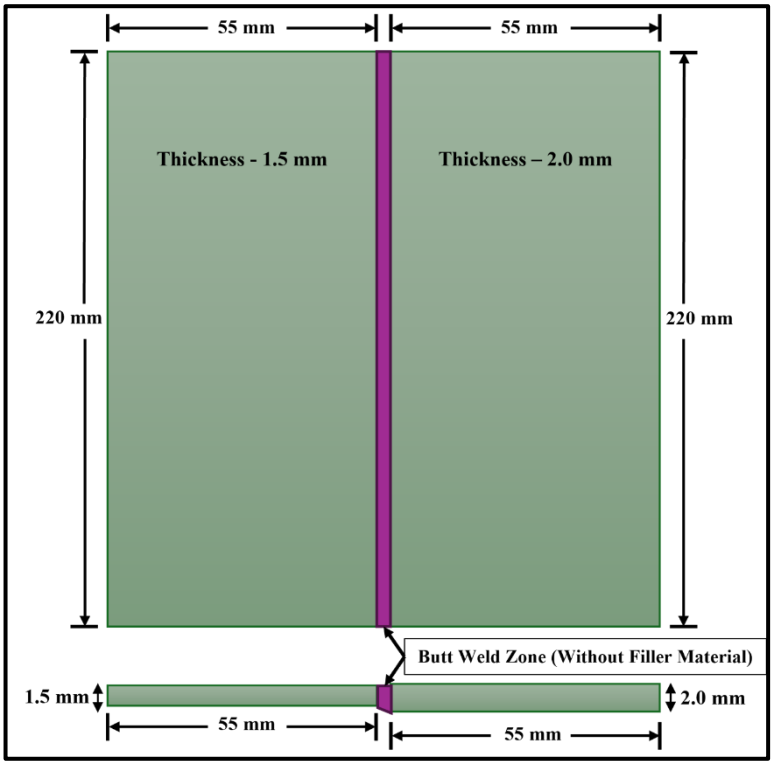


Figure 3.2 Experimental setup of the laser welding system and clamping fixture used for butt welding to fabricate TWBs.

3.3.2 Welding Parameters and TWB Combinations

The welding specifications utilized for the production of TWBs were determined following a sequence of initial welding experiments. In the preliminary experiments,

diminished laser power levels caused the tensile specimens to fracture at the weld bead, signifying insufficient weld integrity. Consequently, the welding parameters were systematically refined to provide robust welds with adequate joint integrity. The ultimate laser power (P) settings of 3700 W and 4000 W were chosen as the associated tensile samples broke from the thinner base material instead of the weld bead, signifying that the weld junction exhibited sufficient strength. Three tailor welded blank combinations were produced based on the chosen sheet thicknesses: 1.5 × 2.0 mm, 1.5 × 2.5 mm, and 1.5 × 3.0 mm. A laser output of 3700 W was utilized for the 1.5 × 2.0 mm TWB combination, while a laser output of 4000 W was applied for the 1.5 × 2.5 mm and 1.5 × 3.0 mm TWB combinations. For each of the three configurations, the welding velocity and operational distance were consistently set at 60 mm/s and 175 mm, respectively. A diagrammatic illustration of the tailor welded blank configurations utilized in the current study is depicted in Figure 3.3.



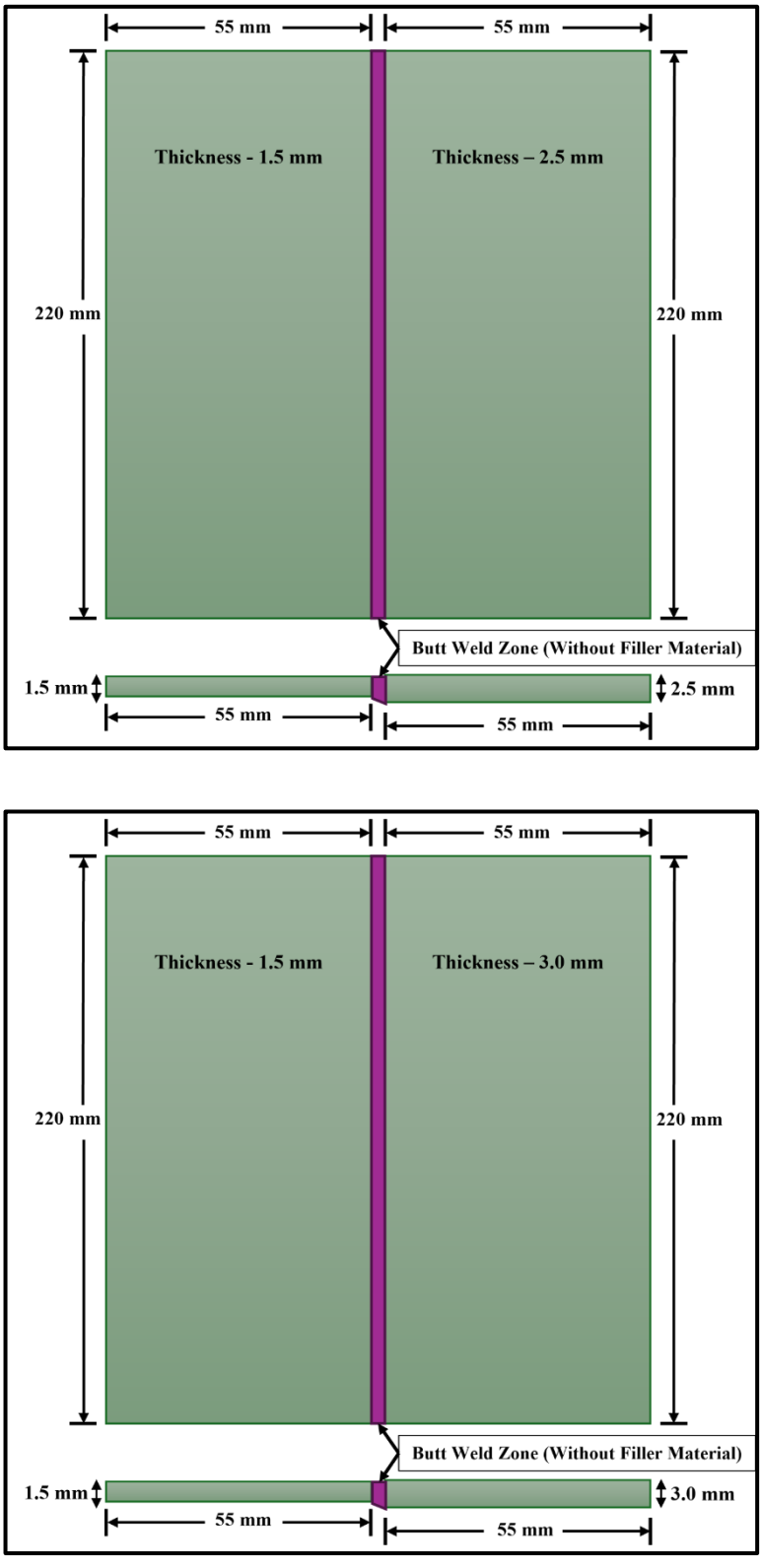


Figure 3.3 Schematic representation of the AA 6082 aluminium alloy TWB combinations.

3.4 Tensile Characterization

3.4.1 Tensile Specimen Preparation

The tensile specimens utilized for the mechanical evaluation of AA6082-O and laser welded tailor welded blanks were fabricated with a CO_2 laser cutting apparatus, adhering to the ASTM E8/E8M sub-size specimen standard. Laser cutting was utilized to create specimens with precise dimensions, superior edge quality, and excellent dimensional uniformity, while reducing edge distortion and burr development. The specimen preparation was conducted at Beacon Engineering Works, Haiderpur, Delhi. The shape and measurements of the ASTM E8/E8M sub-size tensile specimen used in this study are displayed in Figure 3.4.

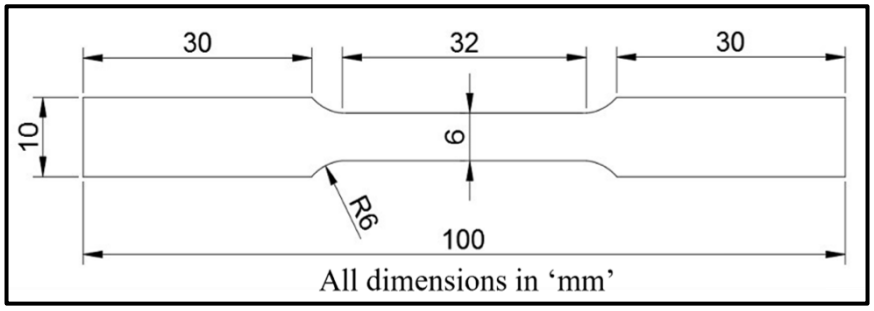


Figure 3.4 ASTM E8/E8M sub-size tensile specimen geometry and dimensions.

Various tensile specimen designs were created to fulfil the aims of the current study. Standard tensile specimens were fabricated from AA6082-O to assess mechanical characteristics and typical anisotropy. Furthermore, two distinct tensile specimen designs were fabricated from the laser welded tailor welded blanks to evaluate weld integrity (WI) and strength. The weld integrity specimens were created to assess the reliability of the welded joints by analyzing the fracture site in relation to the weld bead, while the weld strength (WS) specimens were utilized to examine the tensile

characteristics and mechanical efficacy of the welded junctions. The many laser-cut tensile specimens created for this study are depicted in Figure 3.5.

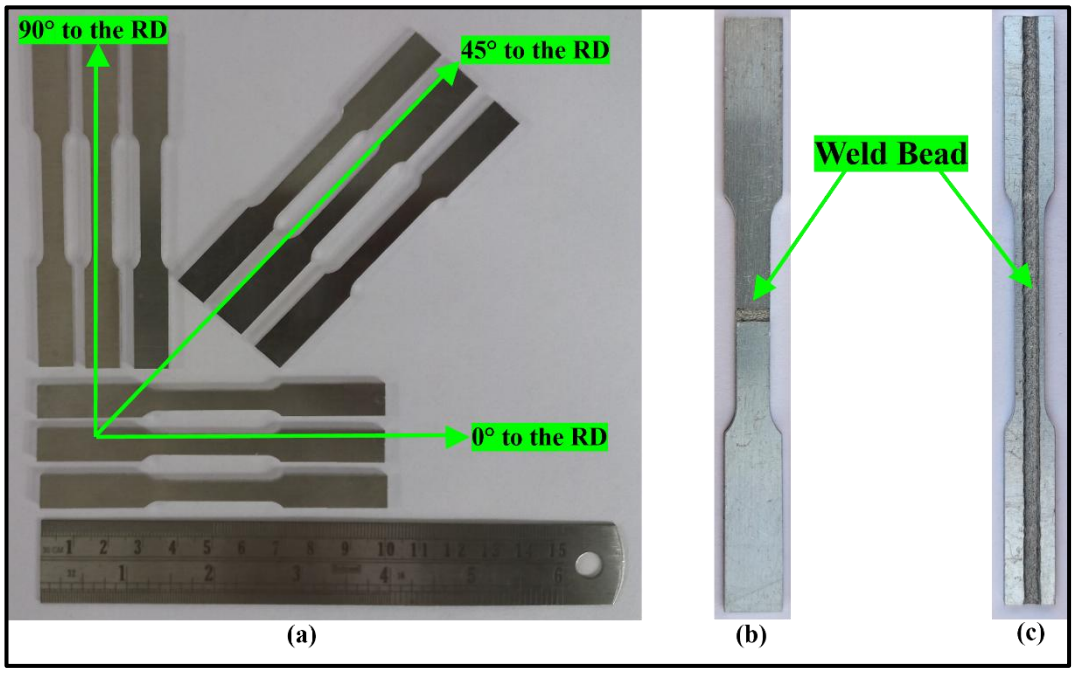


Figure 3.5 Laser-cut tensile specimens prepared for testing (a) anisotropy (b) weld integrity and (c) weld strength.

3.4.2 Tensile Testing of AA6082-O

The tensile characteristics of AA6082-O were assessed by examining specimens oriented in the rolling direction at ambient and higher temperatures. Tensile testing was performed with a Tinius Olsen H50KS bench-top universal testing apparatus fitted with a 50 kN load cell and an environmental chamber that functions within a temperature spectrum of −70°C to 300°C. The experimental configuration present at the Metal Forming Laboratory, Department of Mechanical Engineering, Delhi Technological University, New Delhi, is illustrated in Figure 3.6. All tensile examinations were conducted following the ASTM E8/E8M standard at a uniform

crosshead velocity of 2.5 mm/min, with load-displacement data being constantly recorded by Horizon software during the procedure.

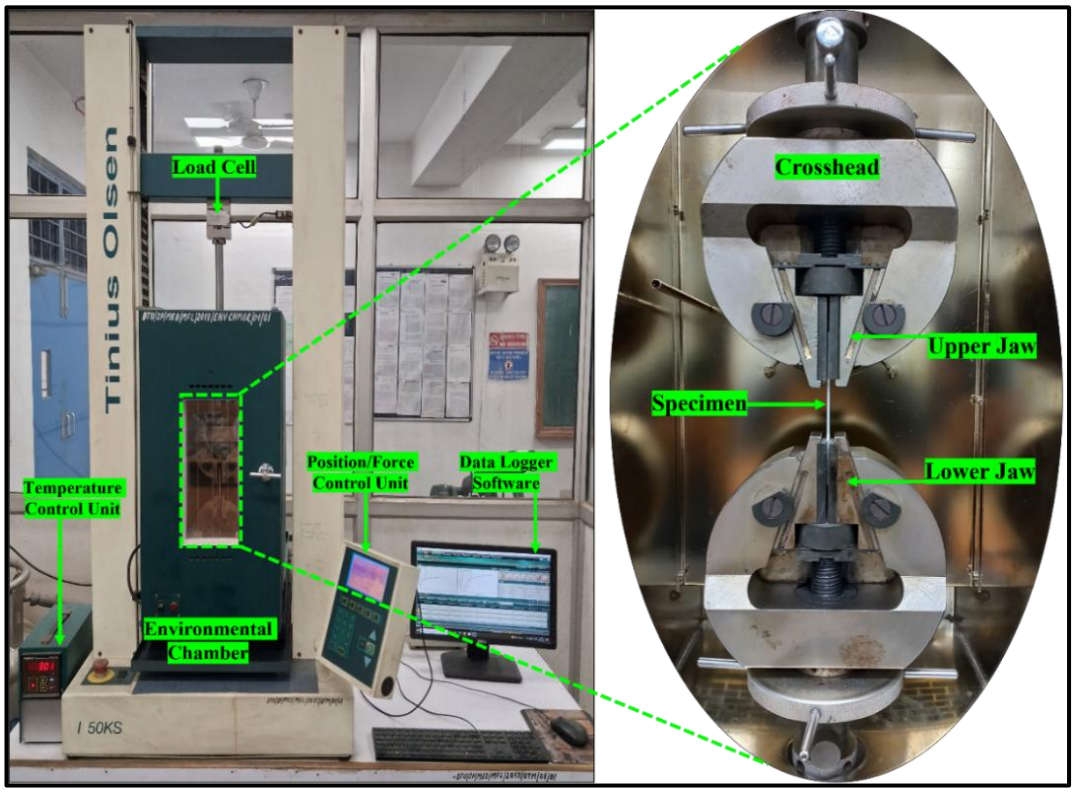


Figure 3.6 Tinius Olsen H50KS bench top universal tensile testing machine with environmental chamber.

To examine the effect of temperature on the tensile properties of AA6082-O, tensile experiments were performed at ambient temperature (RT), 180°C, 240°C, and 300°C. Before conducting high-temperature evaluations, the samples were situated within the environmental chamber and subjected to the necessary heating. Following the establishment of a consistent temperature over the gauge section, the tensile test was conducted under uniform loading circumstances. The tensile characteristics acquired at various temperatures were later contrasted to assess the influence of temperature on

the mechanical behavior of AA6082-O and to determine the suitable warm forming temperature for the ensuing formability studies.

The tensile tests provided engineering stress–strain curves that were utilized to ascertain the yield strength (YS), ultimate tensile strength (UTS), and percentage elongation of AA6082-O. Engineering stress (σ_e) and engineering strain (ε_e) were determined utilizing equations (3.1) and (3.2), correspondingly.

$$\sigma_e = \frac{P}{A_0} \qquad (3.1)$$

where P is the applied load and A_0 is the original cross-sectional area of the specimen.

$$\varepsilon_e = \frac{L - L_0}{L_0} \qquad (3.2)$$

where, L_0 is the original gauge length and L is the instantaneous gauge length during deformation.

The engineering stress-strain measurements were later transformed into true stress-true strain data to more precisely characterize the material's plastic deformation behavior. True stress (σ_t) and true strain (ε_t) were determined using Eqs. (3.3) and (3.4), respectively.

$$\sigma_t = \sigma_e(1 + \varepsilon_e) \qquad (3.3)$$

$$\varepsilon_t = \ln(1 + \varepsilon_e) \qquad (3.4)$$

The strain hardening characteristics of AA6082-O were defined utilizing the Hollomon equation, which connects actual stress to true plastic strain inside the uniform plastic deformation zone as follows:

$$\sigma_t = K\varepsilon_t^n \qquad (3.5)$$

where K is the strength coefficient and n is the strain hardening exponent.

The Hollomon equation was transformed into a linear form by applying the natural logarithm to both sides, resulting in:

$$\ln \sigma_t = \ln K + n \ln \varepsilon_t \qquad (3.6)$$

The strain hardening exponent n and strength coefficient K were ascertained using linear regression analysis of the true stress–true strain data in the uniform plastic deformation zone. The gradient of the linear correlation yielded the strain hardening exponent n, whereas the y-intercept represented $\ln K$, from which the strength coefficient K was derived. The tensile characteristics and strain hardening metrics acquired at various temperatures were later utilized to assess the effect of temperature on the mechanical behavior of AA6082-O and to determine the ideal warm forming temperature for ensuing formability investigations.

3.4.3 Normal Anisotropy (r-value) Measurement

The standard anisotropy (r-value) of AA6082-O was assessed to analyze the effect of the rolling direction on the material's plastic deformation characteristics and its appropriateness for sheet metal forming applications. The evaluations were conducted following ASTM E517 with tensile samples oriented at 0°, 45°, and 90° relative to the rolling direction. The specimen's width and gauge length were assessed prior to loading and following plastic deformation (up to UTS) during the tensile test. These measurements were utilized to ascertain the plastic strain ratio (r-value), which signifies the proportion of real width strain to true thickness strain during uniaxial tensile deformation.

The true width strain (ε_w) was calculated using Eq. (3.7):

$$\varepsilon_w = \ln\left(\frac{W}{W_0}\right) \qquad (3.7)$$

where W_0 and W are the initial and final specimen widths, respectively.

The true longitudinal strain (ε_l) was determined from Eq. (3.8):

$$\varepsilon_l = \ln\left(\frac{L}{L_0}\right) \qquad (3.8)$$

where L_0 and L denote the initial and final gauge lengths, respectively.

Assuming plastic incompressibility during deformation, the true thickness strain (ε_t) was obtained using Eq. (3.9):

$$\varepsilon_t = -(\varepsilon_l + \varepsilon_w) \qquad (3.9)$$

The plastic strain ratio (r-value) for each specimen orientation was then calculated using Eq. (3.10):

$$r = \frac{\varepsilon_w}{\varepsilon_t} \qquad (3.10)$$

The individual plastic strain ratios obtained along the 0°, 45°, and 90° directions with respect to the rolling direction were designated as r_0, r_{45}, and r_{90}, respectively. The average normal anisotropy ($\bar{r}$) was subsequently calculated using Eq. (3.11):

$$\bar{r} = \frac{r_0 + 2r_{45} + r_{90}}{4} \qquad (3.11)$$

The calculated average normal anisotropy was used to characterize the directional deformation behaviour of AA6082-O and to provide the material anisotropy data required for the formability.

3.4.4 Tensile Testing of Laser Welded Tailor Welded Blanks

The tensile properties of the laser welded tailor welded blanks (TWBs) were assessed through specimens designed for weld integrity and weld strength across all three TWB configurations (1.5 × 2.0 mm, 1.5 × 2.5 mm, and 1.5 × 3.0 mm). The weld integrity samples were evaluated to assess the robustness of the welded connections by determining the fracture site in relation to the weld bead and the surrounding base material. The fracture characteristics of all three TWB combinations were documented to evaluate the soundness of the laser welded connections. Consequently, the specimens for weld strength were examined to assess the tensile characteristics of the welded connections. The engineering stress-strain curves derived from the tensile tests were utilized to ascertain the ultimate tensile strength (UTS) and % elongation of the three TWB combinations. The tensile characteristics of the welded joints were subsequently analyzed to evaluate the effect of sheet thickness combinations on the mechanical performance of the laser welded tailor welded blanks.

3.5 Microhardness Measurement

The microhardness of the laser welded tailor welded blanks (TWBs) was assessed to determine the hardness variation throughout the welded joints for all three TWB configurations (1.5 × 2.0 mm, 1.5 × 2.5 mm, and 1.5 × 3.0 mm). Before testing, the samples were cut transversely to the weld bead, cold mounted, and processed according to conventional metallographic protocols. The specimens were progressively abraded using silicon carbide (SiC) abrasive sheets from 100 to 2500 grit, and subsequently wet polished with alumina suspension on a velvet fabric to provide a smooth, scratch-free surface appropriate for microhardness assessments.

The Vickers microhardness assessment was conducted utilizing a Struers DURAMIN 40 microhardness tester within the Metal Forming Laboratory of the Department of Mechanical Engineering at Delhi Technological University, New Delhi, as seen in Figure 3.7. The assessments were conducted following the ASTM E384 standard with a diamond pyramidal indenter with a force of 500 g (HV0.5) and a duration of 10 seconds. Hardness assessments for each TWB combination were conducted across the transverse cross-section of the welded joint, commencing from the thinner base metal, traversing the weld zone, and concluding at the thicker base metal. Fifteen indentation points were documented for each specimen to ascertain the hardness distribution throughout the welded joint. The assessed microhardness profiles were utilized to analyze the effect of laser welding on the hardness distribution within the welded joints and to relate the hardness fluctuations to the associated microstructural features and tensile properties of the various TWB combinations.

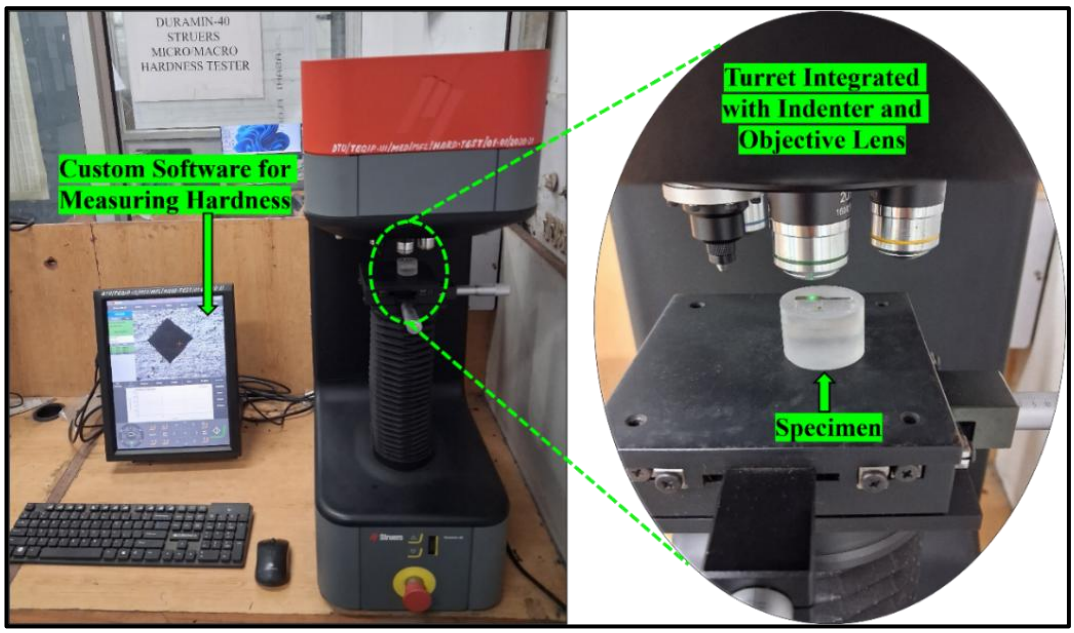


Figure 3.7 Struers DURAMIN 40 microhardness tester.

3.6 Formability Evaluation

The formability of laser welded tailor welded blanks (TWBs) was assessed by the Forming Limit Diagram (FLD) and Limit Dome Height (LDH) tests at ambient and elevated temperatures. The FLD was utilized to identify the critical strain combinations associated with the initiation of localized necking, whereas the LDH values were applied to evaluate the stretch formability of the laser welded TWBs. The FLD and LDH samples were fabricated by laser cutting, thereafter marked with a 2.5 mm diameter circular grid pattern on the surface to enable strain assessment post-deformation. The specimen preparation and laser labeling were conducted at Beacon Engineering Works in Haiderpur, Delhi. The experimental program encompassed laser welded tailor welded blanks (TWBs) with three thickness combinations (1.5 mm × 2.0 mm, 1.5 mm × 2.5 mm, and 1.5 mm × 3.0 mm) featuring both transverse and longitudinal weld bead orientations, as seen in Figure 3.8.

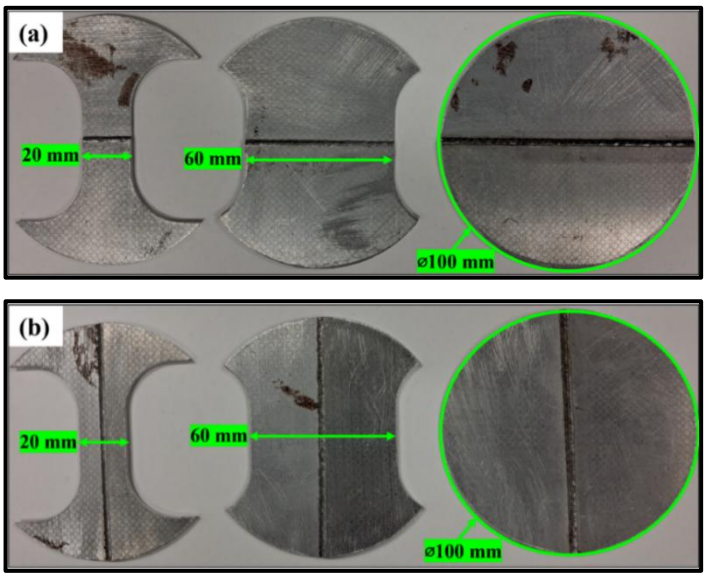


Figure 3.8 FLD specimens of laser welded tailor welded blanks showing (a) transverse and (b) longitudinal weld bead orientations.

The FLD and LDH assessments were performed utilizing a 50+50 tonne hydraulic press with a built-in heating mechanism in the Metal Forming Laboratory, Department of Mechanical Engineering, Delhi Technological University, New Delhi, as seen in Figure 3.9.

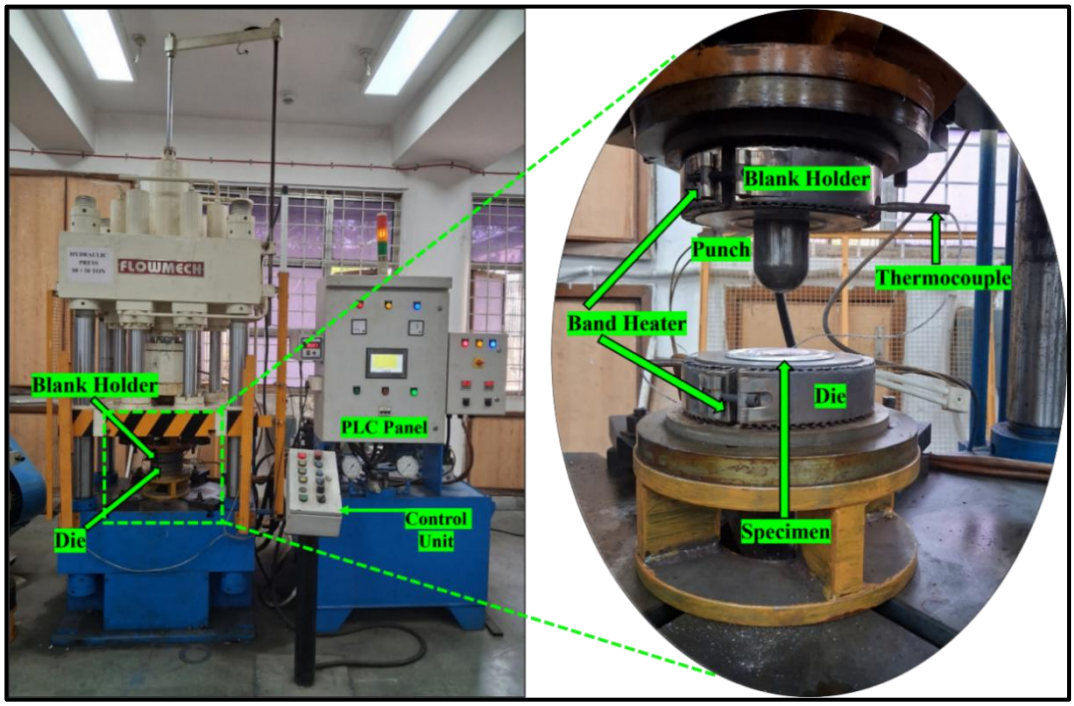


Figure 3.9 100 tonne hydraulic press with integrated heating system.

A hemispherical punch with a diameter of 50 mm was employed in all the experiments. For warm forming, the punch was heated with a cartridge heater, while band heaters encircled the die and blank holder to sustain the warm forming temperature. To reduce friction and facilitate seamless material movement during warm forming, molybdenum disulfide (MoS_2) was utilized as a high-temperature solid lubricant between the tooling surfaces and the specimens. For the TWB combinations of 1.5 × 2.0 mm, 1.5 × 2.5 mm, and 1.5 × 3.0 mm, pressure pad forces of 6 tonnes, 8 tonnes, and 10 tonnes were exerted, respectively.

The samples were distorted till the initiation of regional necking or rupture. Subsequent to testing, the distorted circular grids were assessed to ascertain the primary and secondary principle strains, which were later utilized to create the forming limit diagrams. The limit dome height (LDH) was assessed as the peak dome height of each specimen created to analyze the stretch formability of the laser welded tailor welded blanks under ambient and elevated temperature forming conditions.

3.7 Microstructural Characterization

Microstructural analysis was conducted to examine the influence of laser welding on the grain morphology and crystallographic properties of the welded junctions. Electron backscatter diffraction (EBSD) examination was conducted on the laser welded tailor welded blank measuring 1.5 mm × 3.0 mm to investigate the microstructural changes.

3.7.1 Sample Preparation

The samples for EBSD examination were cut perpendicular to the weld bead to reveal the cross-section of the welded connections. To reduce surface harm and distortion during sectioning, the specimens were meticulously sliced and then processed according to established metallographic protocols. The samples were systematically abraded with silicon carbide (SiC) abrasive sheets of ever finer grit sizes from 100 to 2500, and subsequently underwent wet polishing with alumina solution to achieve a polished surface. The ultimate surface preparation for EBSD investigation was performed through electropolishing with a Struers Lectropol-5 apparatus. The samples underwent electropolishing with an electrolyte composed of 20% perchloric acid in methanol, resulting in a surface devoid of deformation and scratches, ideal for electron backscatter diffraction investigation.

3.7.2 Electron Backscatter Diffraction (EBSD)

Electron backscatter diffraction (EBSD) assessment was conducted at the OIM and Texture Laboratory, Department of MEMS, Indian Institute of Technology Bombay, utilizing a TSL-EDAX Orientation Imaging Microscopy (OIM) apparatus linked to a scanning electron microscope (SEM). EBSD scans were obtained from the transverse cross-section of the welded joints at designated analysis sites, including base metals (1.5 and 3.0 mm), heat-affected zones, and the fusion zone. The obtained orientation data were examined utilizing EDAX/TSL OIM software, employing a grain tolerance angle of 5° and a step size of 1.5 μm. The EBSD examination was employed to delineate the weld microstructure through inverse pole figure (IPF) maps, grain dimensions, pole figures, and the distribution of geometrically required dislocations (GND). These microstructural parameters were later associated with the hardness distribution and tensile characteristics of the laser welded tailor welded blanks.

3.8 Finite Element Simulation

Finite element analyses were conducted utilizing ABAQUS/CAE to forecast the formability characteristics of laser welded tailor welded blanks (TWBs) under ambient and elevated temperature forming scenarios. The numerical calculations were conducted exclusively for the longitudinal direction of the weld bead, and the anticipated deformation characteristics and failure sites were juxtaposed with the relevant experimental findings. The TWB was represented as a three-dimensional flexible planar shell, whilst the punch, die, blank holder, and spacer were depicted as three-dimensional distinct hard entities. The partition function was utilized to segment the blank into various areas, allowing for the distinct assignment of mechanical

qualities to the thinner base material, weld bead, and thicker base material. The blank was modeled with S4R shell elements, while the punch, die, blank holder, and spacer were represented using R3D4 rigid elements. A Dynamic Explicit solver was employed to model the sheet making procedure. The shell segment was delineated employing the Simpson thickness integration method utilizing five thickness integration points. Contact interactions between the tooling components and the blank were designated as surface-to-surface. A friction coefficient of 0.05 was designated for the interaction between the punch and the blank, whereas a coefficient of 0.10 was allocated for the interface between the blank and the die. The boundary conditions were established by securing the die (ENCASTRE), imposing displacement on the punch (U2), restricting the blank (ENCASTRE), and applying the necessary displacement to the blank holder (U2) to replicate the experimental forming conditions.

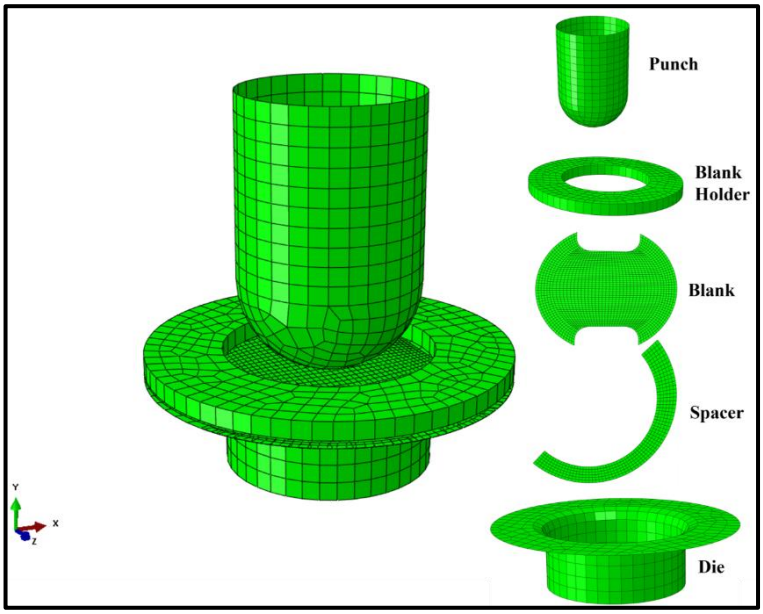


Figure 3.10 Finite element model of the blank, spacer, punch, die, and blank holder used for formability simulation in ABAQUS

The finite element analyzes were performed to forecast the deformation traits and failure sites of the laser-welded tailor-welded blanks. The simulation results were evaluated by the maximum in-plane primary strain contours, and the anticipated failure sites were juxtaposed with the experimental results to assess the numerical model. A conventional finite element model together with its associated simulation outcomes is depicted in Figure 3.10. The finite element model incorporates specific idealizations and assumptions, such as stiff forming tools, designated friction coefficients, simplified geometry and boundary conditions, together with empirically derived material attributes. These premises could create discrepancies between the numerical forecasts and the genuine forming behavior.

.

CHAPTER 4

RESULTS AND DISCUSSION

4.1 Optimization of Annealing Temperature

In order to determine an appropriate annealing condition for the forthcoming warm forming tests, the AA 6082 alloy sheets underwent annealing at temperatures varying from ambient temperature to 400°C. The effect of annealing temperature on the tensile strength, elongation, and Vickers hardness of the alloy was methodically examined [79-81]. The fluctuation of tensile strength in relation to annealing temperature is illustrated in Figure 4.1, while the associated changes in elongation and hardness are depicted in Figure 4.2 and Figure 4.3, respectively.

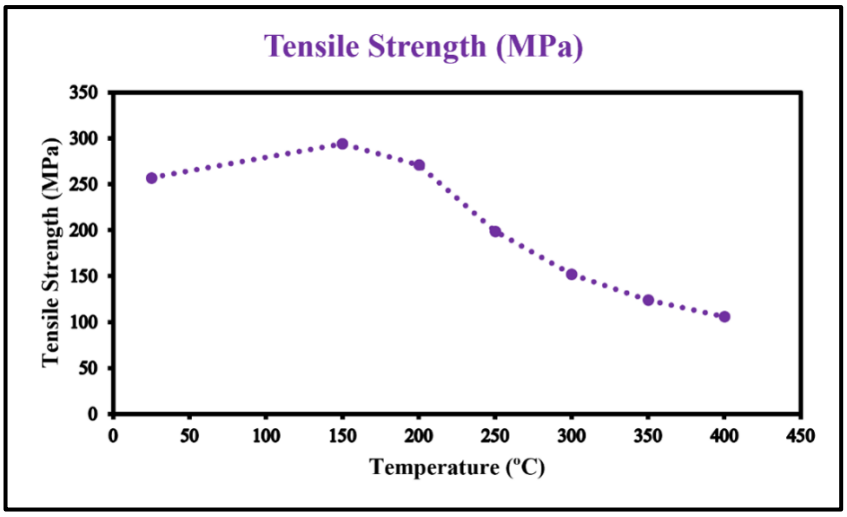


Figure 4.1 Effect of annealing temperature on the tensile strength of AA 6082.

As illustrated in Figure 4.1, both the yield strength and ultimate tensile strength exhibited an initial rise when the annealing temperature was elevated from ambient temperature to 150°C. The yield strength rose from 227 MPa to 254 MPa, while the ultimate tensile strength ascended from 257 MPa to 294 MPa. This preliminary

enhancement in strength is ascribed to the formation of fine strengthening phases during low-temperature annealing, which momentarily improved the resistance to dislocation movement. Nevertheless, as the annealing temperature continued to rise, both the yield strength and final tensile strength consistently diminished. The yield strength diminished from 239 MPa at 200°C to 166 MPa at 250°C, then declining to 122 MPa, 94 MPa, and 71 MPa at 300°C, 350°C, and 400°C, respectively. In a similar manner, the maximum tensile strength diminished from 271 MPa at 200°C to 199 MPa, 152 MPa, 124 MPa, and 106 MPa as the annealing temperature rose. The gradual decline in strength signifies that recovery and recrystallization became more prevalent at higher temperatures, leading to a persistent loss in the alloy's resistance to plastic deformation [82-83].

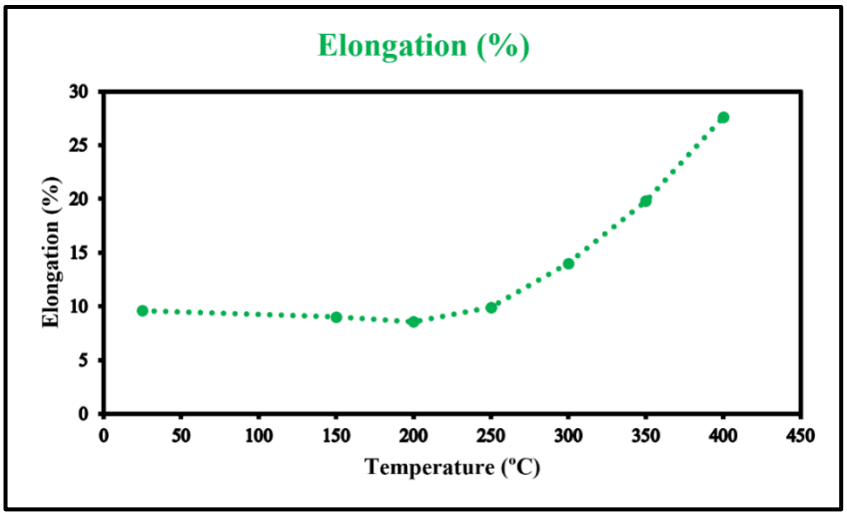


Figure 4.2 Effect of annealing temperature on the elongation of AA 6082.

The fluctuation in elongation corresponding to annealing temperature is depicted in Figure 4.2. The elongation exhibited minimal variation between ambient temperature and 250°C, fluctuating from 9.6% to 9.9%, suggesting that the material predominantly preserved its work-hardened microstructure during this temperature interval. A notable

enhancement in ductility was detected past 250°C, with elongation rising to 14% at 300°C, 19.8% at 350°C, and achieving a peak of 27.6% at 400°C. The significant rise in elongation at elevated annealing temperatures can be ascribed to the gradual recovery and recrystallization of the distorted microstructure. These procedures diminished the dislocation density and alleviated internal residual stresses, thereby facilitating the development of strain-free equiaxed grains that improved the alloy's plastic deformability [73-75].

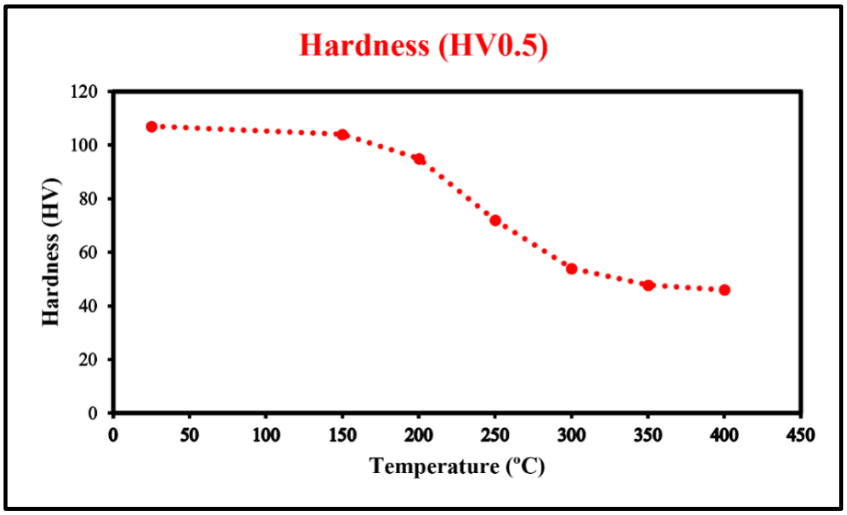


Figure 4.3 Effect of annealing temperature on the Vickers hardness of AA 6082.

The influence of annealing temperature on hardness is illustrated in Figure 4.3. The hardness demonstrated a slight decrease from 107 HV0.5 to 104 HV0.5 upon annealing at 150 °C, suggesting that minimal microstructural softening had taken place. With the escalation of the annealing temperature, the hardness consistently diminished to 95 HV0.5 at 200°C, 72 HV0.5 at 250°C, and 54 HV0.5 at 300°C. A subsequent decline to 47.8 HV0.5 was noted at 350°C, succeeded by a minimal drop to 46 HV0.5 at 400°C, indicating that most softening had likely occurred by 350°C. The ongoing decrease in hardness is directly related to the decline in tensile strength and is ascribed

to recovery, recrystallization, and the dissolution or coarsening of strengthening precipitates, which collectively diminish the alloy's resistance to localized plastic deformation.

Despite the fact that annealing at 400°C yielded the greatest elongation and minimal hardness, it concurrently caused a significant reduction in strength, with yield strength and ultimate tensile strength diminishing to 71 MPa and 106 MPa, respectively. Such significant softening could negatively impact the material's load-bearing capacity in future forming processes. Conversely, annealing at 350°C yielded a more favorable equilibrium between strength and ductility, exhibiting a yield strength of 94 MPa, an ultimate tensile strength of 124 MPa, an elongation of 19.8%, and a hardness of 47.8 HV0.5. Furthermore, the hardness remained constant above 350°C, whereas both the yield strength and ultimate tensile strength persisted in their decrease. Consequently, subsequent annealing at 400°C provided minimal more softening while causing a considerable reduction in mechanical strength. As a result, 350°C was determined to be the ideal annealing temperature for all following laser welding, warm forming, and microstructural studies.

4.2 Tensile Properties of AA 6082-O

After optimizing the annealing temperature, the tensile properties of the annealed AA 6082-O alloy were assessed at ambient and increased temperatures (180°C, 240°C, and 300°C) to evaluate its deformation traits under warm forming conditions. The tensile characteristics of the annealed material at room temperature are encapsulated in Table 4.1, whereas the engineering and real stress-strain graphs acquired at various testing temperatures are illustrated in Figure 4.4 (a) and Figure 4.4 (b), respectively.

These findings elucidate the impact of forming temperature on the alloy's strength, ductility, and strain-hardening characteristics, which are crucial for determining suitable heated forming parameters.

Table 4.1 Mechanical properties of annealed AA 6082-O at room temperature.

Yield Strength (MPa)	94±1.59
Ultimate Tensile Strength (MPa)	124±1.19
Elongation (%)	19.8±1.24
Strain Hardening Exponent, n	0.1
Strength Coefficient, K (MPa)	176
Normal Anisotropy ($\bar{r}$)	0.649

The tensile characteristics of the annealed AA 6082-O at ambient temperature reveal a yield strength of 94 ± 1.59 MPa, an ultimate tensile strength of 124 ± 1.19 MPa, and an elongation of 19.8 ± 1.24%, as shown in Table 4.1. The strain hardening exponent (n) and strength coefficient (K) were found to be 0.10 and 176 MPa, respectively, with the normal anisotropy value ($\bar{r}$) at 0.649. The mechanical characteristics suggest that the alloy exhibits comparatively low strength and notable ductility post-annealing, rendering it appropriate for subsequent warm forming processes necessitating more plastic deformation.

The engineering stress-strain graphs depicted in Figure 4.4 (a) demonstrate a considerable effect of testing temperature on the tensile behavior of the annealed alloy. As the testing temperature rose from ambient conditions to 180°C, the yield strength diminished from 94 MPa to 75.4 MPa, and the ultimate tensile strength fell from 124

MPa to 107 MPa. The elongation, meanwhile, stayed almost constant at 20.1%, suggesting that the deformation at this temperature resulted in only a slight enhancement in ductility. The diminishment in strength can be ascribed to the heightened mobility of dislocations at elevated temperatures, which diminishes the resistance to plastic deformation. At a testing temperature of 240°C, the material demonstrated a yield strength of 103 MPa and an ultimate tensile strength of 131 MPa, surpassing the values recorded at 180°C, with elongation rising to 24.3%. This conduct indicates that the alloy maintained enough load-bearing strength while also demonstrating enhanced plastic deformation. The rise in elongation signifies improved deformation uniformity, while the slight enhancement in strength could be linked to the intricate interplay of thermal softening and precipitation phenomena within this intermediate temperature spectrum. An additional rise in testing temperature to 300°C led to a significant decline in strength, with yield strength and ultimate tensile strength diminishing to 81 MPa and 93.1 MPa, respectively. Conversely, the elongation rose markedly to 28.2%, indicating the greatest ductility across all tested temperatures. The stress-strain diagrams indicate that the alloy exhibited reduced flow stresses while enduring greater plastic strains before to failure, validating the advantageous impact of heated deformation on formability. At this temperature, recovery mechanisms are accentuated, promoting dislocation reorganization and diminishing strain concentration during tensile deformation [51-53].

The authentic stress-strain graphs depicted in Figure 4.4 (b) further demonstrate the effect of temperature on the strain-hardening characteristics of AA 6082-O. The strain hardening exponent (n) diminished marginally from 0.10 at ambient temperature to 0.07 and 0.08 at 180°C and 240°C, respectively, signifying a constrained strain-

hardening potential within this thermal spectrum. At 300°C, the strain hardening exponent significantly rose to 0.18, indicating an enhanced capacity of the material to endure homogeneous plastic deformation prior to necking. An elevated n-value postpones localized deformation by facilitating a more homogeneous strain distribution across the specimen, therefore enhancing the alloy's overall formability during warm forming processes.

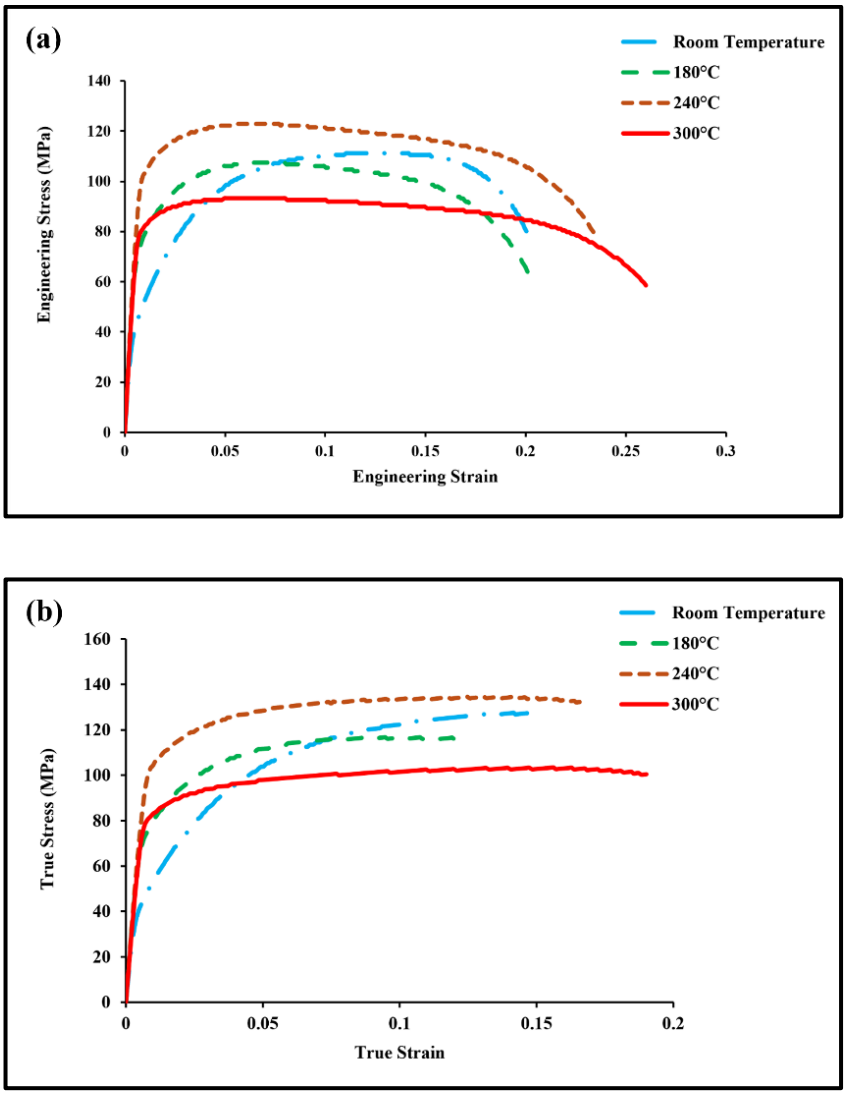


Figure 4.4 (a) Engineering and (b) true stress–strain curves of annealed AA 6082-O tested at room temperature, 180°C, 240°C, and 300°C.

In general, the tensile characteristics indicate that elevating the testing temperature gradually diminishes the flow stress while enhancing the ductility of the annealed AA 6082-O alloy. Despite the alloy demonstrating relatively greater strength at 240°C, the peak elongation and the highest strain-hardening exponent were recorded at 300°C, suggesting improved resistance to strain localization and augmented deformability. These traits are especially beneficial for heated sheet metal forming, where elevated ductility paired with enhanced strain hardening is crucial for attaining superior formability and postponing early failure during deformation.

4.3 Laser Weld Quality

The caliber of laser-welded tailor welded blanks (TWBs) is important in assessing their appropriateness for ensuing warm forming processes. A superior weld must demonstrate robust metallurgical adhesion, appropriate mechanical integrity, and acceptable resistance to early failure under tensile stress. Consequently, the constructed TWBs underwent evaluations of weld integrity and weld strength to ascertain the dependability of the welded connections prior to additional mechanical characterization and formability analyses.

4.3.1 Weld Integrity

The structural integrity of the manufactured custom welded blanks was assessed via room-temperature tensile testing to determine the quality and continuity of the laser-welded connections. The engineering stress-strain curves acquired from the weld integrity assessments are illustrated in Figure 4.5, whereas the associated cracked tensile specimens post-testing are depicted in Figure 4.6.

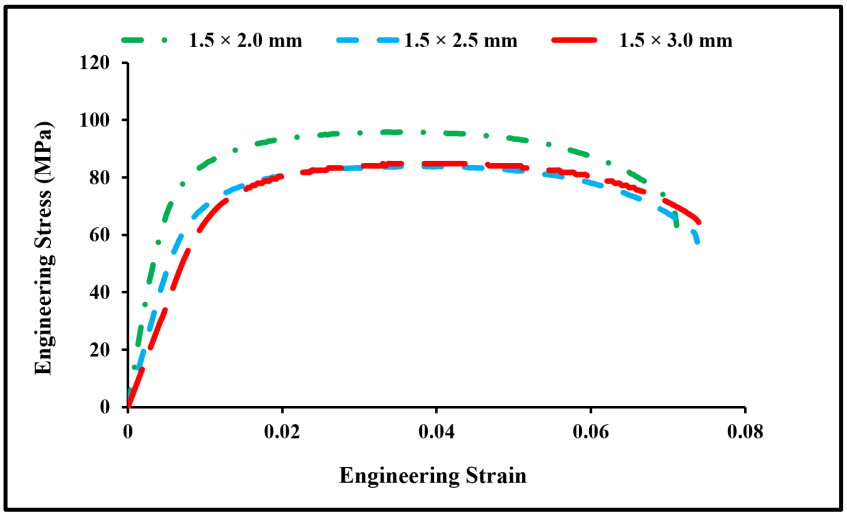


Figure 4.5 Engineering stress–strain curves of laser-welded tailor welded blanks for weld integrity evaluation.

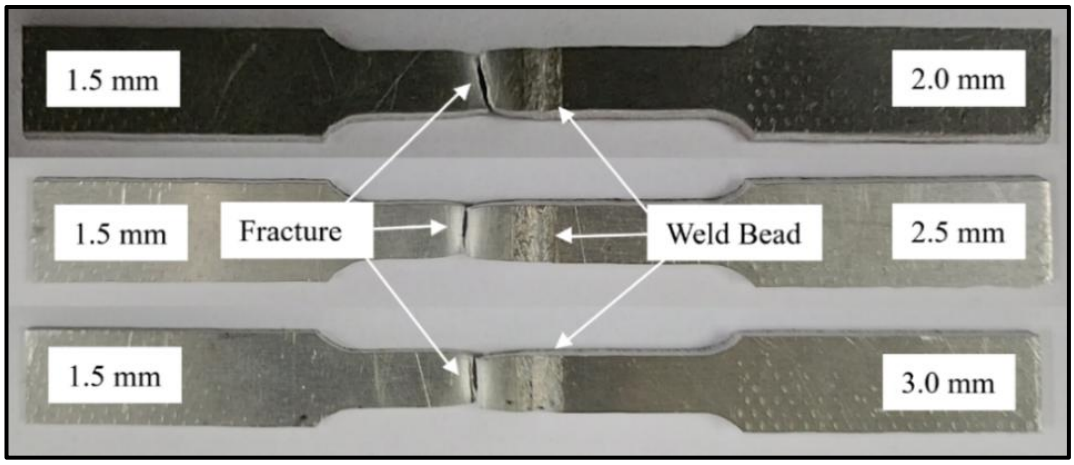


Figure 4.6 Tensile-tested laser-welded tailor welded blank specimens used for weld integrity evaluation.

The engineering stress-strain curves illustrated in Figure 4.5 demonstrate consistent deformation characteristics for all three-tailor welded blank configurations throughout the tensile test, with no early failure occurring in the elastic and plastic deformation phases. The seamless and uninterrupted stress-strain behavior signifies that effective metallurgical bonding was accomplished during laser welding, implying the lack of

significant welding flaws such fusion deficiencies, extensive porosity, or weld interruptions.

The tensile characteristics indicated that the 1.5 × 2.0 mm TWB demonstrated superior mechanical capabilities, featuring a yield strength of 79.8 MPa, an ultimate tensile strength of 95.8 MPa, and an elongation of 7.08%. The 1.5 × 2.5 mm TWB demonstrated a yield strength of 69.7 MPa, an ultimate tensile strength of 83.6 MPa, and an elongation of 7.38%, while the 1.5 × 3.0 mm TWB displayed a yield strength of 71.6 MPa, an ultimate tensile strength of 84.9 MPa, and an elongation of 7.40%. Despite the yield strength and ultimate tensile strength of the 1.5 × 2.5 mm and 1.5 × 3.0 mm TWBs being relatively inferior to that of the 1.5 × 2.0 mm TWB, all three welded joints demonstrated nearly uniform elongation values, signifying consistent ductility regardless of the sheet thickness combination. The diminished strength noted in the 1.5 × 2.5 mm and 1.5 × 3.0 mm TWBs could be linked to variations in the welding heat input due to the increased laser power utilized during production. The augmented thermal input may have facilitated enhanced softening in the fusion zone and surrounding heat-affected area, thereby diminishing the load-bearing capability of the welded connections. Nonetheless, the analogous elongation metrics suggest that the general deformation characteristics of the welded connections were mainly unchanged.

The broken tensile specimens illustrated in Figure 4.6 indicate that tensile failure invariably originated from the 1.5 mm (thinner) base sheet across all three-tailor welded blank configurations, with no fractures detected within the laser weld. The lack of fractures in the weld area indicates that the welded junction exhibited superior

mechanical strength compared to the thinner base material and was devoid of significant welding flaws that might lead to early failure. The identified failure mechanism is advantageous for custom welded blanks as it indicates that the welded connection has the strength to endure the imposed tensile load without emerging as the preferred fracture site. The persistent fracture site suggests that the welded connection was not the most vulnerable part of the specimen; rather, the failure was dictated by the diminished load-bearing ability of the thinner sheet, which endures greater stress owing to its reduced cross-sectional area under tensile loading. This analysis offers compelling proof that the chosen laser welding parameters resulted in flawless joints with robust metallurgical adhesion and enough weld integrity, rendering the manufactured TWBs appropriate for future warm forming studies.

4.3.2 Weld Strength

Subsequent to the successful validation of weld integrity, tensile assessments were conducted to determine the mechanical robustness of the enhanced laser-welded tailor welded blanks. The engineering stress-strain graphs acquired during the assessment of weld strength are illustrated in Figure 4.7. The engineering stress-strain graphs depicted in Figure 4.7 illustrate a notable enhancement in the tensile behavior of the welded joints following the optimization of laser welding parameters. In contrast to the assessment of weld integrity, the optimized welds demonstrated superior yield strength, ultimate tensile strength, and increased deformation characteristics, signifying greater metallurgical bonding and more effective load distribution at the welded junction. Among the combinations examined, the 1.5 × 2.0 mm TWB demonstrated a yield strength of 115 MPa, an ultimate tensile strength of 158 MPa,

and an elongation of 4.84%. The 1.5 × 2.5 mm TWB exhibited a peak yield strength of 142 MPa, an ultimate tensile strength of 176 MPa, and an elongation of 7.41%. Correspondingly, the 1.5 × 3.0 mm TWB had a yield strength of 115 MPa, an ultimate tensile strength of 176 MPa, and the greatest elongation of 8.11% among all examined combinations. The equivalent ultimate tensile strength achieved for the 1.5 × 2.5 mm and 1.5 × 3.0 mm TWBs suggests that both welded connections exhibited similar load-bearing abilities following the refinement of the laser welding settings. The increased elongation demonstrated by the 1.5 × 3.0 mm TWB signifies its enhanced capacity to endure plastic deformation before failure. The amalgamation of elevated tensile strength and enhanced ductility is especially beneficial for warm sheet metal forming, as it postpones strain localization and diminishes the chances of early failure during deformation.

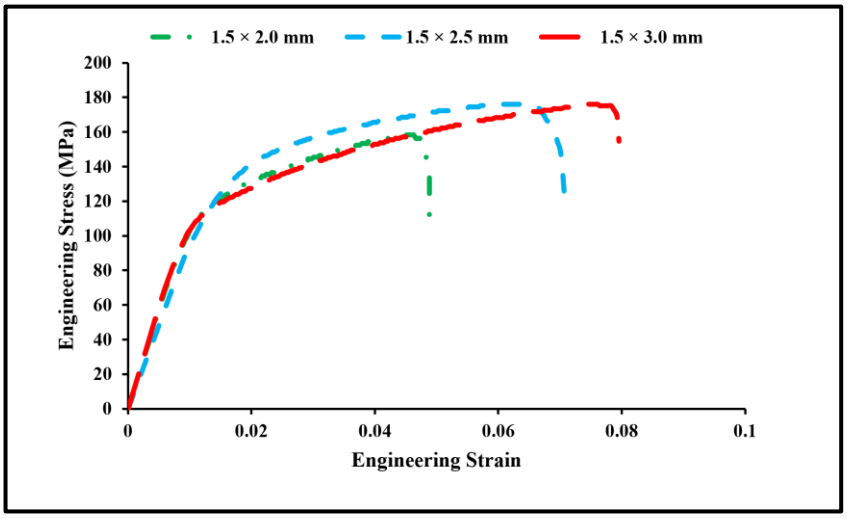


Figure 4.7 Engineering stress–strain curves of laser-welded tailor welded blanks for weld strength evaluation.

The assessment of weld strength indicates that the refinement of laser welding parameters significantly enhanced the mechanical properties of the custom welded

blanks. Of the three configurations examined, the 1.5 × 3.0 mm TWB demonstrated the most advantageous balance of tensile strength and ductility. Consequently, this TWB configuration was chosen for the ensuing hardness, formability assessment, microstructural examination, and finite element simulations.

4.4 Hardness Distribution

The hardness variation throughout the laser-welded tailor welded blanks was assessed to investigate the differences in localized mechanical properties within the welded junction [15]. The Vickers hardness profiles recorded throughout the weld area for the 1.5 × 2.0 mm, 1.5 × 2.5 mm, and 1.5 × 3.0 mm TWBs are illustrated in Figure 4.8.

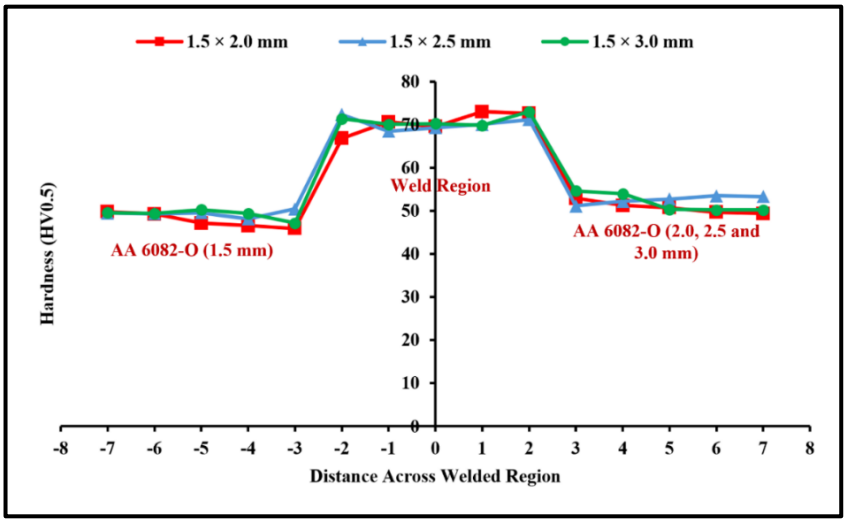


Figure 4.8 Vickers hardness distribution across the weld region of laser-welded tailor welded blanks with different thickness combinations.

The hardness profiles illustrated in Figure 4.8 display a comparable pattern across all three custom welded blank configurations. The hardness exhibited a consistent pattern within the base materials adjacent to the weld, then experienced a significant rise in the weld area before declining once more towards the opposing base material. This

distinctive hardness profile suggests that laser welding markedly affected the local mechanical characteristics solely in the area surrounding the welded junction, whilst the foundation materials on both sides maintained almost consistent hardness.

For the 1.5 × 2.0 mm TWB, the hardness of the 1.5 mm substrate fluctuated between 45.89 and 49.77. As one nears the weld area, the hardness escalates swiftly to 66.83, attaining a peak of 73.02 before slowly diminishing to around 49–53 within the 2.0 mm base material. A comparable hardness distribution was noted for the 1.5 × 2.5 mm TWB, with hardness escalating from around 48–50 in the thinner sheet to a maximum of 72.35 in the weld area, before declining to roughly 51–53 in the 2.5 mm base material. Similarly, the 1.5 × 3.0 mm TWB demonstrated hardness measurements varying from roughly 47–50 in the thinner section to a peak of 73.01 in the weld area, thereafter declining to about 50–54 in the 3.0 mm base material.

For all three combinations of tailor welded blanks, the highest hardness was uniformly noted at the weld area, whereas the surrounding base materials exhibited relatively decreased hardness levels. The maximum hardness measurements exhibited minimal variation across the three combinations, consistently falling within a tight band of about 72–73 HV0.5, suggesting that comparable welding properties were attained regardless of the thickness combination. Moreover, the hardness values recorded in both base materials were rather stable, indicating that the influence of laser welding was predominantly limited and did not substantially modify the mechanical properties beyond the welded junction.

The increased hardness noted in the weld area signifies that this region provides enhanced resistance to localized plastic deformation compared to the adjacent base

materials. As a result, the welded connection is anticipated to demonstrate distinct deformation characteristics under tensile stress and sheet forming due to the differences in local hardness throughout the weld. The analogous hardness distributions achieved for all three tailor-welded blank combinations further illustrate the reliability and reproducibility of the chosen laser welding parameters in generating welds with comparable mechanical properties.

4.5 Formability (Limit Dome Height)

The stretch formability of the laser-welded tailor welded blanks (TWBs) was assessed utilizing the Limit Dome Height (LDH) test in a plane strain scenario. The LDH test offers a direct evaluation of the malleability of sheet materials by measuring the peak dome height reached before rupture [38-42]. The impact of sheet thickness variation, weld bead alignment, and forming temperature on the deformation characteristics of the produced TWBs was examined. The findings from the experiments conducted on the 1.5 × 2.0 mm, 1.5 × 2.5 mm, and 1.5 × 3.0 mm tailor welded blanks are illustrated in Figures 4.9-4.11.

The LDH findings for the 1.5 × 2.0 mm TWB indicate that the orientation of the weld bead and the forming temperature significantly affected the stretch formability of the welded blank. As illustrated in Figure 4.9 (a), the orientation of the transverse weld bead had a dome height of 14 mm at ambient temperature, which diminished to 11.8 mm at 300°C, suggesting that heated forming did not enhance the stretch formability in the transverse orientation. This decrease indicates that the transverse weld arrangement was more prone to localized distortion during the forming process. Conversely, the orientation of the longitudinal weld bead demonstrated a contrary

tendency, as depicted in Figure 4.9 (b). The dome elevation rose from 13 mm at ambient temperature to 15.5 mm at 300°C, indicating an enhancement of roughly 19.2%. The increased dome height indicates that positioning the weld bead parallel to the primary deformation direction facilitated more consistent deformation and postponed fracture, therefore enhancing the stretch formability of the welded blank.

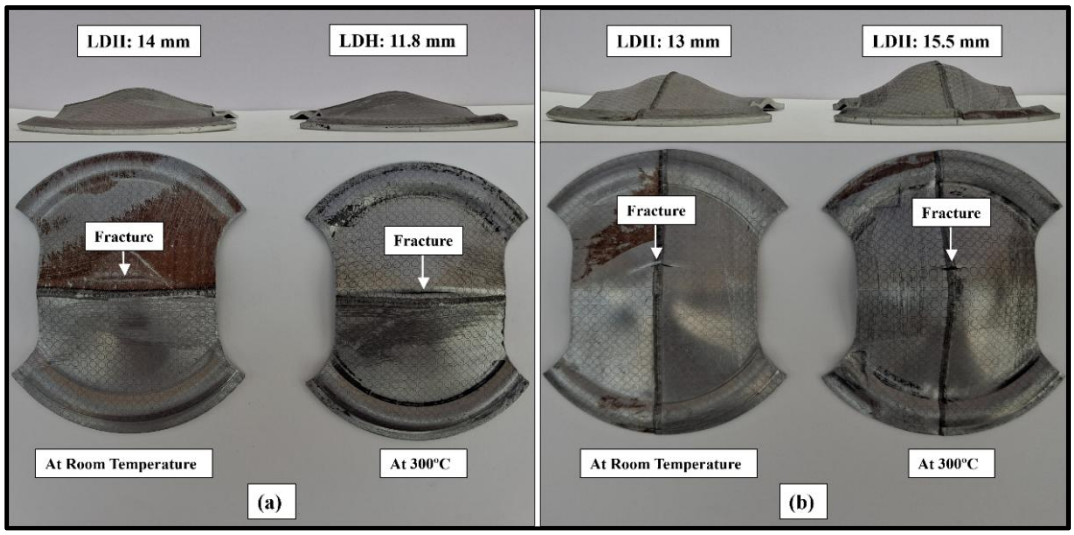


Figure 4.9 LDH specimens of the 1.5 × 2.0 mm TWB under (a) transverse and (b) longitudinal weld bead orientation.

The LDH findings for the 1.5 x 2.5 mm TWB are illustrated in Figure 4.10. In the transverse weld bead orientation (Figure 4.10 (a)), the dome height consistently measured 12 mm at both ambient temperature and 300°C, suggesting that elevating the forming temperature had minimal impact on the stretch formability of the transverse weld arrangement. Nonetheless, a significant enhancement was noted in the direction of the longitudinal weld bead, as illustrated in Figure 4.10 (b). The dome elevation rose from 12 mm at ambient temperature to 16.5 mm at 300°C, reflecting an enhancement of roughly 37.5%. The notable rise in dome height suggests that the

longitudinal weld alignment was markedly superior in facilitating plastic deformation during warm forming compared to the transverse alignment.

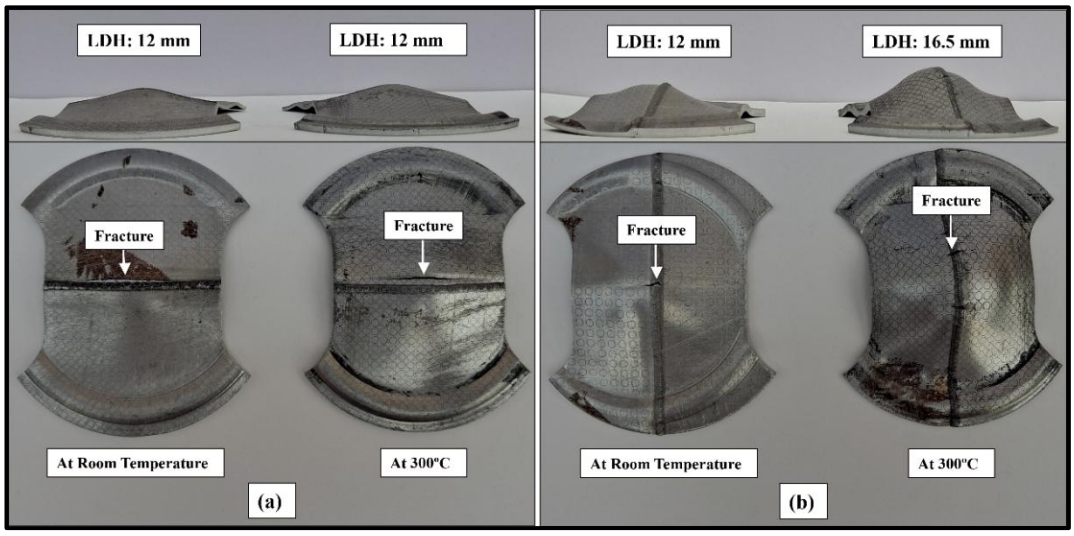


Figure 4.10 LDH specimens of the 1.5 × 2.5 mm TWB under (a) transverse and (b) longitudinal weld bead orientation.

The LDH outcomes for the 1.5 × 3.0 mm TWB are illustrated in Figure 4.11. In a manner akin to the other thickness combinations, the orientation of the transverse weld bead (Figure 4.11 (a)) demonstrated relatively diminished formability. The height of the dome diminished marginally from 13 mm at ambient temperature to 12.4 mm at 300°C, suggesting that warm forming did not substantially enhance the deformation capacity of the transverse weld arrangement. Conversely, the longitudinal weld bead alignment (Figure 4.11 (b)) demonstrated the greatest formability across all examined custom welded blank configurations. The height of the dome rose significantly from 11.7 mm at ambient temperature to 17.5 mm at 300°C, indicating an enhancement of roughly 49.6%. The significant elevation in dome height illustrates the advantageous impact of warm forming when the weld bead is oriented parallel to the direction of

deformation. Under these circumstances, the welded blank demonstrated a markedly enhanced capacity for plastic deformation prior to fracture, signifying exceptional stretch formability.

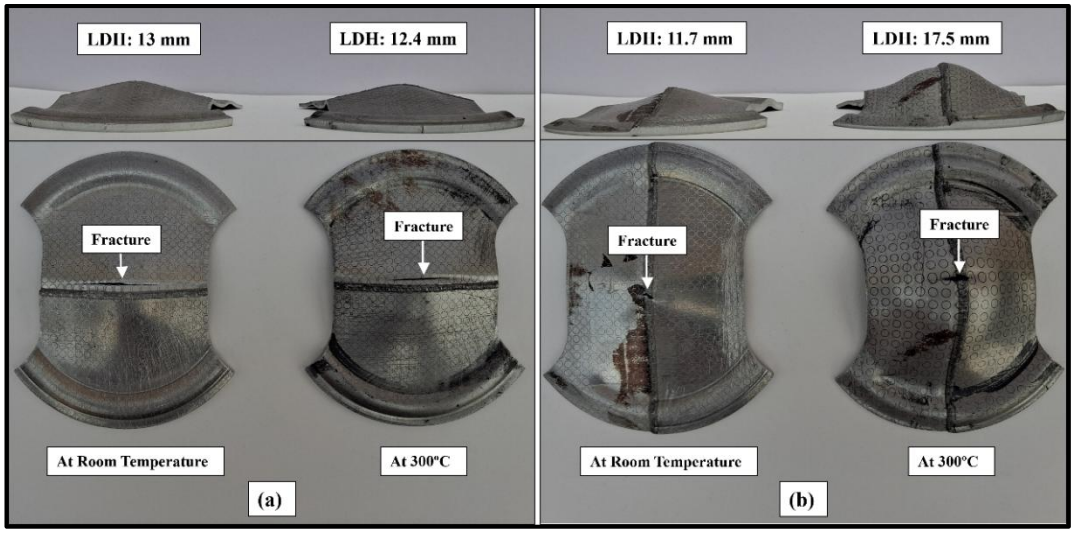


Figure 4.11 LDH specimens of the 1.5 × 3.0 mm TWB under (a) transverse and (b) longitudinal weld bead orientation.

The LDH findings unequivocally indicate that the orientation of the weld bead significantly influences the stretch formability of laser-welded tailor welded blanks. Under elevated forming temperatures, the orientation of the longitudinal weld bead consistently demonstrated greater dome heights compared to the transverse weld bead orientation across all three thickness combinations. Conversely, the transverse weld bead alignment exhibited either no enhancement or a marginal decrease in dome height at 300°C, suggesting that high temperature alone is not suffice to enhance stretch formability when the weld is positioned perpendicular to the direction of deformation. The differing LDH behavior noted between the transverse and longitudinal weld bead orientations suggests that weld orientation has a greater impact on the stretch

formability of tailor welded blanks than the forming temperature by itself [153-154]. Warm forming at 300°C diminished the flow stress and increased the ductility of the annealed AA 6082-O alloy; nevertheless, the orientation of the transverse weld bead showed minimal or no enhancement in dome height. This behavior can be ascribed to the deformation trajectory being orthogonal to the weld interface, where the disparity in thickness and mechanical characteristics of the welded sheets fosters uneven strain distribution and localized deformation. As a result, strain localization manifests at an earlier phase, constraining the enhancement of formability despite the increased forming temperature. Conversely, when the weld bead was aligned parallel to the primary deformation direction, the distortion was more evenly distributed across the welded joint, which diminished strain concentration and postponed the initiation of localized necking. Consequently, the material could endure more extensive plastic deformation prior to rupture, resulting in a significant enhancement in the limit dome height during warm forming processes. These findings indicate that the advantageous impact of heated forming was completely achieved just with the longitudinal weld bead alignment, leading to a notable enhancement in LDH across all three tailor-welded blank configurations.

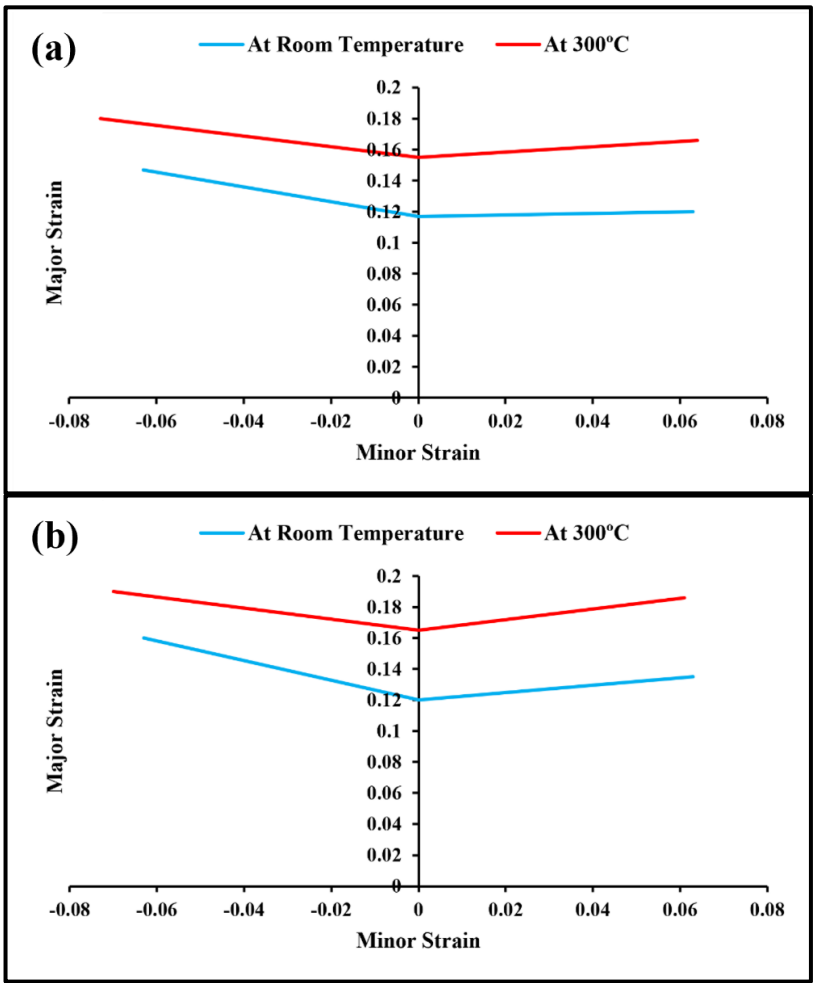
Among the analyzed tailor welded blanks, the 1.5 × 3.0 mm TWB demonstrated the greatest dome height of 17.5 mm, succeeded by the 1.5 × 2.5 mm TWB at 16.5 mm and the 1.5 × 2.0 mm TWB at 15.5 mm, all tested under the longitudinal weld bead orientation at 300°C. The findings suggest that augmenting the thickness ratio of the welded sheets, in conjunction with the orientation of the longitudinal weld bead, markedly improves the stretch formability of tailor welded blanks [150-152]. As a result, the 1.5 × 3.0 mm TWB demonstrated the superior forming capabilities

compared to all other thickness combinations examined, leading to its selection for further in-depth microstructural analysis and finite element validation.

4.6 Forming Limit Diagram

The formability of the laser-welded tailor welded blanks having a longitudinal weld bead orientation was additionally assessed utilizing the Forming Limit Diagram (FLD). The FLD delineates the restrictive strain combinations for tension-compression, plane strain, and biaxial deformation scenarios, thereby delivering an exhaustive evaluation of the deformation potential of the welded blanks [1-4]. The experimentally obtained FLDs for the longitudinal weld bead alignment of the 1.5 × 2.0 mm, 1.5 × 2.5 mm, and 1.5 × 3.0 mm tailor welded blanks at ambient temperature and 300°C are illustrated in Figure 4.12. The forming limit diagram for the 1.5 × 2.0 mm TWB is illustrated in Figure 4.12 (a). The FLD measured at 300°C consistently surpasses the room-temperature FLD over the examined strain spectrum, signifying a general enhancement in formability during hotter forming processes. The enhancement in the forming limit is apparent under tension-compression, plane strain, and biaxial deformation scenarios, indicating that the material can endure greater main strains prior to the initiation of localized necking. The elevation of the FLD indicates that warm forming improved the deformation potential of the welded blank by augmenting its resistance to early failure during stretching. The FLD of the 1.5 x 2.5 mm TWB is depicted in Figure 4.12 (b). Analogous to the earlier thickness configuration, the forming limit curve acquired at 300°C is situated above the one obtained at ambient temperature across the complete deformation spectrum. The enhancement is noted in tension-compression, plane strain, and biaxial loading scenarios, suggesting that

increased temperature allowed the welded blank to endure greater plastic deformations before to failure. The elevated forming limit indicates that warm forming significantly enhanced the stretch formability of this TWB structure. The FLD of the 1.5 × 3.0 mm TWB is seen in Figure 4.12 (c). Of all the examined thickness combinations, this TWB had the greatest forming limit under warm forming conditions. The FLD recorded at 300°C is uniformly elevated compared to the room-temperature curve over the whole strain trajectory, signifying a significant enhancement in formability. The enhancement in the forming limit under tension-compression, plane strain, and biaxial deformation circumstances illustrates the exceptional deformation capacity of the 1.5 × 3.0 mm TWB prior to the onset of localized necking.



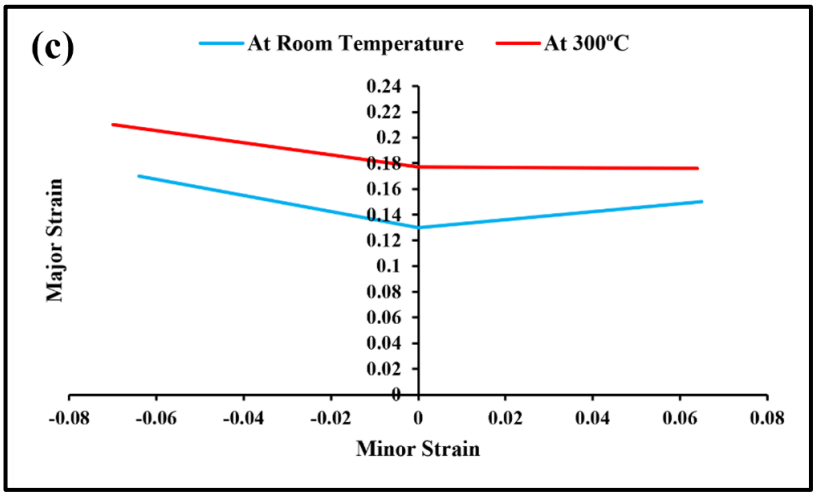


Figure 4.12 Forming limit diagrams of the (a) 1.5 × 2.0 mm, (b) 1.5 × 2.5 mm and (c) 1.5 × 3.0 mm TWB.

The FLD outcomes for the longitudinal weld bead orientation unequivocally indicate that warm forming at 300°C consistently enhanced the forming limits of all examined tailor welded blanks. For every thickness combination, the forming limit diagram (FLD) acquired at the increased temperature consistently surpassed the related room-temperature curve across the examined strain spectrum, validating that the longitudinal weld bead alignment permitted the welded blanks to endure greater major strains prior to the initiation of localized necking. These findings align with the LDH data, indicating that the longitudinal weld bead orientation demonstrated enhanced stretch formability during heated forming circumstances. Of the three configurations examined, the 1.5 × 3.0 mm TWB had the greatest forming limit, succeeded by the 1.5 × 2.5 mm and 1.5 × 2.0 mm TWBs. The exceptional FLD of the 1.5 × 3.0 mm TWB under uniaxial, plane strain, and biaxial deformation scenarios illustrates its better capacity to endure plastic deformation prior to localized necking. This finding aligns remarkably well with the LDH results, as the identical TWB combination

demonstrated the greatest dome height, thereby affirming that the 1.5 × 3.0 mm tailor welded blank exhibits the most advantageous formability among the examined thickness combinations.

4.7 Microstructural Characterization

Subsequent to the mechanical characterization and assessment of formability, an exhaustive microstructural analysis was conducted to elucidate the correlation between the microstructure and the documented mechanical and forming characteristics of the laser-welded tailor welded blanks. According to the tensile, LDH, and FLD findings, the 1.5 × 3.0 mm TWB demonstrated the optimal balance of strength and formability, leading to its selection for comprehensive microstructural analysis. Electron Backscatter Diffraction (EBSD) research was conducted to investigate the crystallographic properties of the welded joint, encompassing grain shape, crystallographic orientation, and the distribution of geometrically necessary dislocations (GND) [16]. The microstructural analysis was conducted in various areas of the welded joint, specifically the 1.5 mm base metal, 3.0 mm base metal, heat-affected zone (HAZ) next to the 1.5 mm sheet, heat-affected zone (HAZ) next to the 3.0 mm sheet, and the fusion zone (weld zone). The integrated analysis of the IPF maps, pole figures, GND distribution maps, and GND density plots offer an extensive insight into the microstructural development within the welded joint and its impact on the mechanical characteristics and formability of the examined tailor welded blank.

4.7.1 Base Metals

The microstructural properties of the 1.5 mm base metal of the 1.5 × 3.0 mm tailor welded blank were examined by Electron Backscatter Diffraction (EBSD). The

relevant inverse pole figure (IPF) map, pole figures, GND distribution map, and GND density distribution are illustrated in Figure 4.13 (a–d).

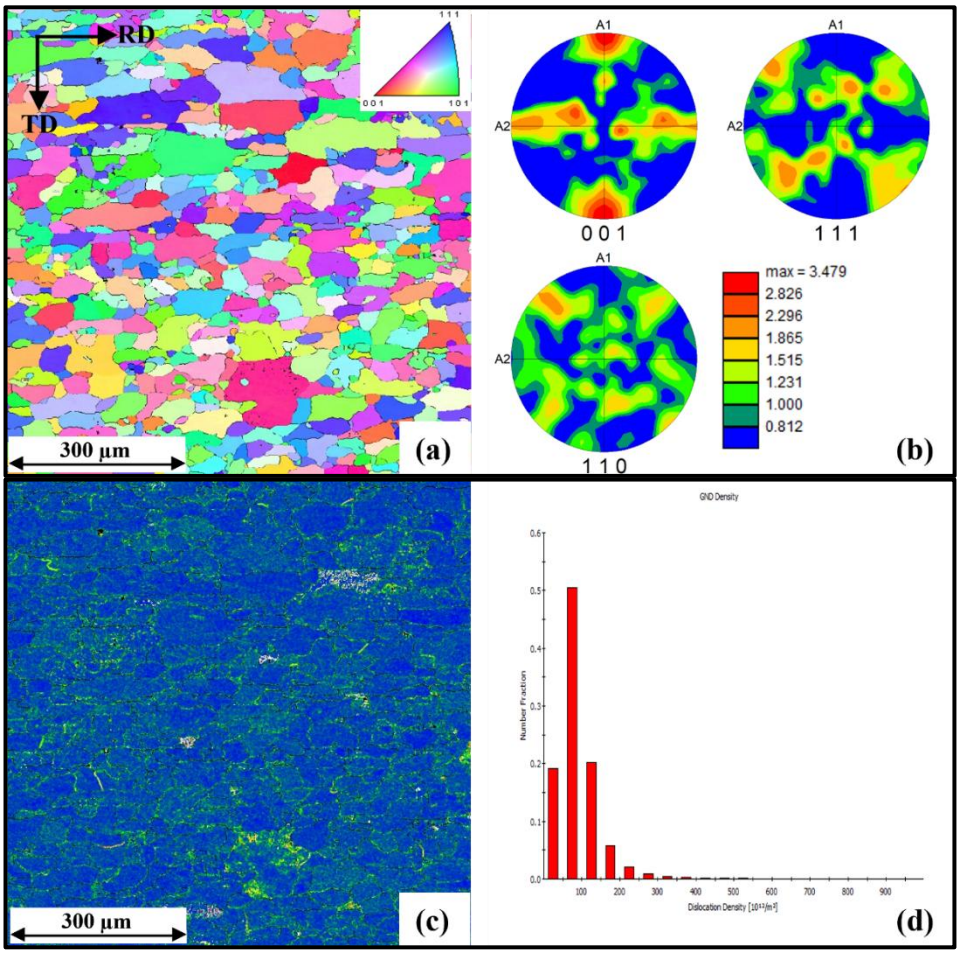
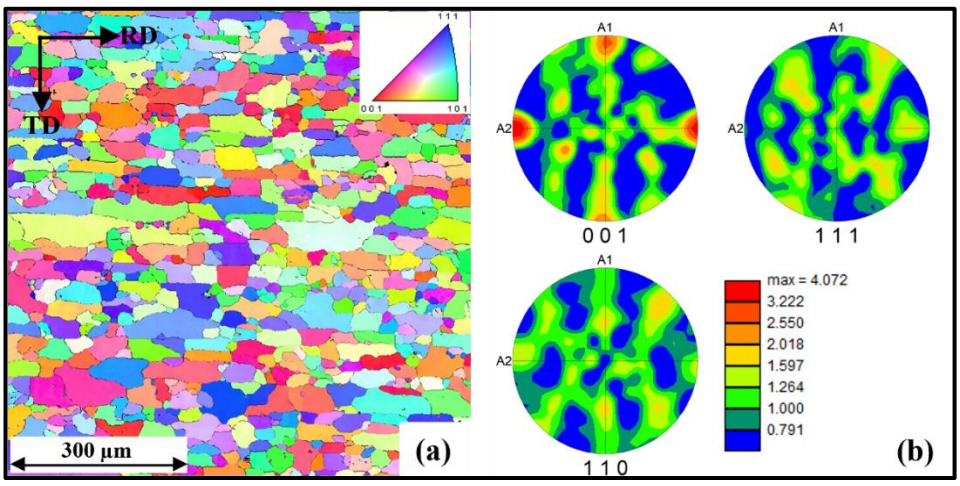


Figure 4.13 EBSD characterization of the 1.5 mm base metal: (a) inverse pole figure (IPF) map, (b) pole figures, (c) geometrically necessary dislocation (GND) distribution map, and (d) GND density distribution.

The inverse pole figure (IPF) map illustrated in Figure 4.13 (a) displays a largely equiaxed grain morphology, with grains demonstrating a diverse array of crystallographic orientations, as evidenced by the color variation. In the annealed state, the mean grain size of the 1.5 mm base metal was found to be 21.43 µm. The pole figures in Figure 4.13 (b) depict the crystallographic texture. The {001}, {111}, and

{110} pole figures display concentrated intensity peaks, signifying a favored crystallographic alignment. The peak texture intensity was recorded at 3.479 MRD (multiples of random distribution), indicating a moderate crystallographic texture. The GND distribution map illustrated in Figure 4.13 (c) reveals that elevated dislocation densities are predominantly located along grain borders, whilst the interiors of the grains exhibit significantly lower dislocation densities. The GND density distribution illustrated in Figure 4.13 (d) displays a significant peak at reduced dislocation densities, with frequency diminishing steadily as GND density escalates. The mean GND density was recorded at 91.30 × 10^{12} m^{-2}, accompanied by a standard deviation of 64.61 × 10^{12} m^{-2}, suggesting that the majority of the examined area exhibits a relatively low dislocation density with minimal localized lattice distortion.

The microstructural properties of the 3.0 mm base metal in the 1.5 × 3.0 mm tailor welded blank were examined by Electron Backscatter Diffraction (EBSD). The associated inverse pole figure (IPF) map, pole figures, GND distribution map, and GND density distribution are illustrated in Figure 4.14 (a–d).



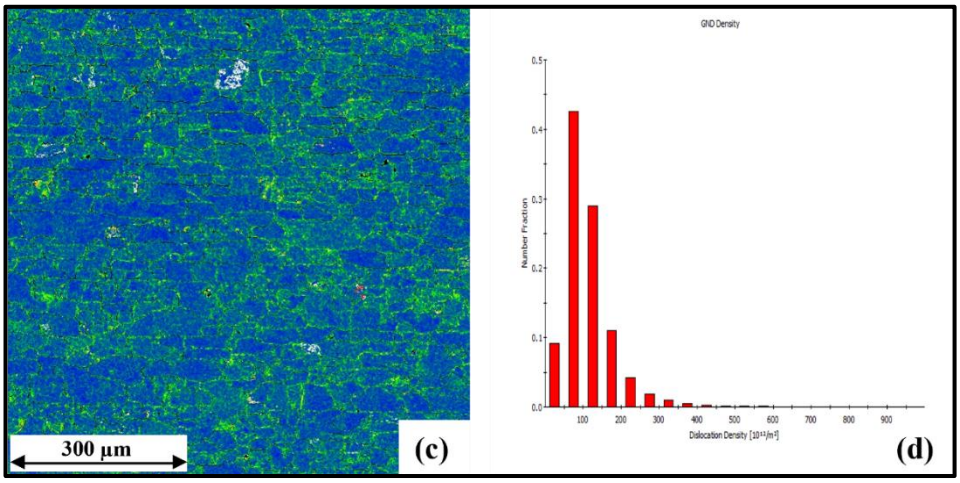


Figure 4.14 EBSD characterization of the 3.0 mm base metal: (a) inverse pole figure (IPF) map, (b) pole figures, (c) geometrically necessary dislocation (GND) distribution map, and (d) GND density distribution.

The inverse pole figure (IPF) map illustrated in Figure 4.14 (a) displays a largely equiaxed grain morphology, with grains demonstrating diverse crystallographic orientations, as evidenced by the color variation. In the annealed state, the mean grain size of the 3.0 mm base metal was found to be 22.58 µm, which was marginally larger than the 1.5 mm base metal. The pole images in Figure 4.14 (b) depict the crystallographic texture. The {001}, {111}, and {110} pole figures display concentrated intensity peaks, signifying a favored crystallographic alignment. The peak texture intensity recorded was 4.072 MRD, signifying a moderately robust crystallographic texture, marginally exceeding that noted for the 1.5 mm base metal. The GND distribution map illustrated in Figure 4.14 (c) reveals that elevated dislocation densities are predominantly located along the grain borders, whereas the interiors of the grains have significantly lower dislocation densities. The GND density distribution depicted in Figure 4.14 (d) exhibits a significant peak at reduced

dislocation densities, with the frequency progressively diminishing as the GND density escalates. The mean GND density was recorded at 113.91 × 10^{12} m^{-2}, accompanied by a standard deviation of 72.01 × 10^{12} m^{-2}, suggesting that while most of the examined area exhibits modest dislocation density, there are some zones with elevated lattice distortion.

4.7.2 Heat Affected Zones (HAZs)

The microstructural properties of the heat-affected zone (HAZ) next to the 1.5 mm sheet of the 1.5 × 3.0 mm tailor welded blank were examined by Electron Backscatter Diffraction (EBSD). The relevant inverse pole figure (IPF) map, pole figures, GND distribution map, and GND density distribution are depicted in Figure 4.15 (a–d). The inverse pole figure (IPF) map illustrated in Figure 4.15 (a) displays a primarily equiaxed grain morphology, with grains demonstrating varied crystallographic orientations across the examined area. In comparison to the equivalent base metals, the mean grain size of the heat-affected zone next to the 1.5 mm sheet was found to be 16.98 μm. The pole images in Figure 4.15 (b) depict the crystallographic texture. The {001}, {111}, and {110} pole figures display more significant intensity peaks, suggesting a heightened preferred crystallographic alignment. The peak texture intensity was recorded at 5.929 MRD, indicating a robust crystallographic texture. The GND distribution map illustrated in Figure 4.15 (c) reveals a heightened concentration of elevated dislocation densities along the grain borders and in various localized areas inside the grains relative to the base metal. The GND density distribution depicted in Figure 4.15 (d) demonstrates a more extensive dispersion, reaching towards elevated dislocation densities. The mean GND density was recorded at 172.63 × 10^{12} m^{-2},

accompanied by a standard deviation of 129.46 × 10^{12} m^{-2}, signifying a considerable rise in lattice distortion and dislocation buildup in the HAZ due to the welding thermal cycle.

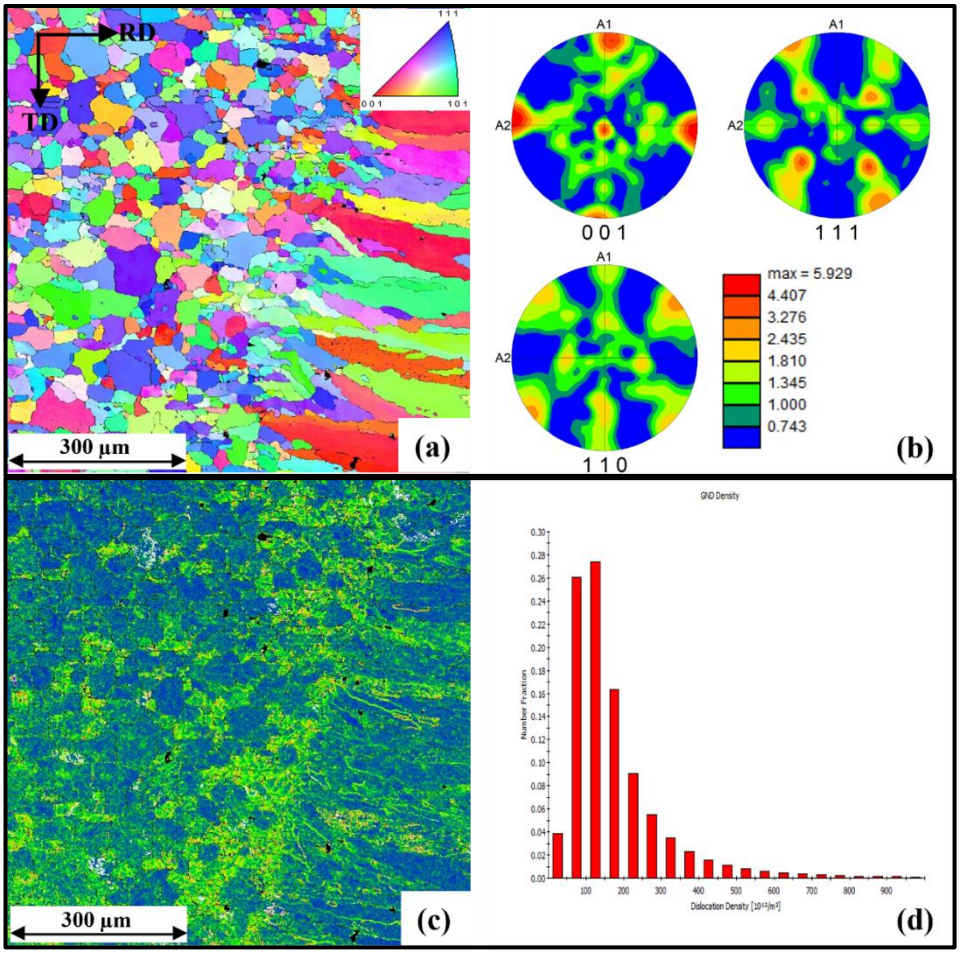


Figure 4.15 EBSD characterization of the heat-affected zone (HAZ) adjacent to the 1.5 mm sheet: (a) inverse pole figure (IPF) map, (b) pole figures, (c) geometrically necessary dislocation (GND) distribution map, and (d) GND density distribution.

The microstructural features of the heat-affected zone (HAZ) next to the 3.0 mm sheet of the 1.5 × 3.0 mm tailor welded blank were examined utilizing Electron Backscatter Diffraction (EBSD). The related inverse pole figure (IPF) map, pole figures, GND distribution map, and GND density distribution are illustrated in Figure 4.16 (a–d).

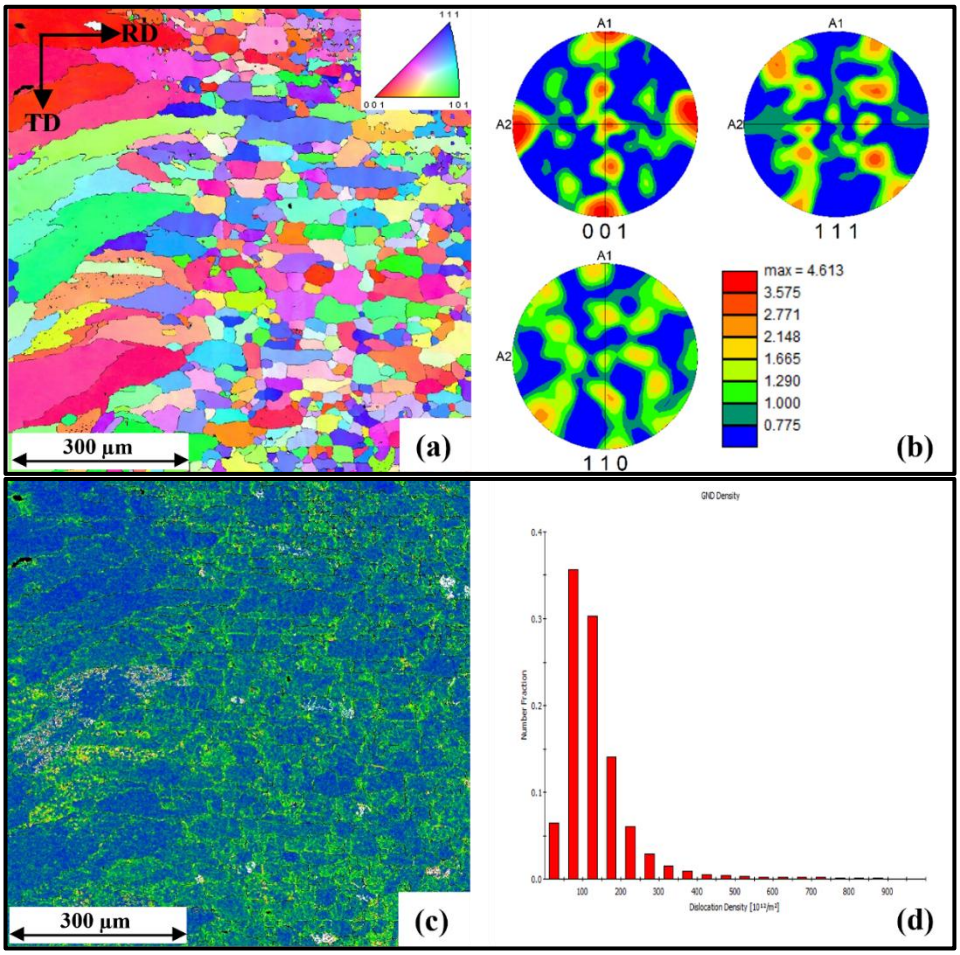


Figure 4.16 EBSD characterization of the heat-affected zone (HAZ) adjacent to the 3.0 mm sheet: (a) inverse pole figure (IPF) map, (b) pole figures, (c) geometrically necessary dislocation (GND) distribution map, and (d) GND density distribution.

The inverse pole figure (IPF) map illustrated in Figure 4.16 (a) demonstrates a largely equiaxed grain morphology, with grains displaying various crystallographic orientations across the examined area. The heat-affected zone next to the 3.0 mm sheet had a mean grain size of 18.41 µm, which was less than the equivalent base metals. The pole images in Figure 4.16 (b) depict the crystallographic texture. The {001}, {111}, and {110} pole figures display concentrated intensity peaks, signifying a favored crystallographic alignment. The peak texture intensity was recorded at 4.613

MRD, indicating a moderately robust crystallographic texture. The GND distribution map presented in Figure 4.16 (c) reveals that dislocation densities are predominantly higher along the grain boundaries, with several localized areas demonstrating significant dislocation aggregation. The GND density distribution depicted in Figure 4.16 (d) displays a wide range that extends into elevated dislocation densities. The mean GND density was recorded at 133.78 × 10^{12} m^{-2}, accompanied by a standard deviation of 96.07 × 10^{12} m^{-2}, suggesting that the HAZ exhibits a greater dislocation density and increased lattice distortion compared to the base metal, yet remains inferior to that found in the HAZ near the 1.5 mm sheet.

4.7.3 Fusion Zone (Weld Zone)

The microstructural properties of the fusion zone (weld zone) of the 1.5 × 3.0 mm tailor welded blank were examined utilizing Electron Backscatter Diffraction (EBSD). The relevant inverse pole figure (IPF) map, pole figures, GND distribution map, and GND density distribution are illustrated in Figure 4.17 (a–d). The inverse pole figure (IPF) map illustrated in Figure 4.17 (a) displays a largely coarse equiaxed grain morphology, with grains demonstrating varied crystallographic orientations across the examined area. The mean grain dimension of the fusion zone was recorded at 29.25 μm, signifying considerable grain enlargement due to the melting and solidification involved in the laser welding procedure. The pole images in Figure 4.17 (b) depict the crystallographic texture. The {001}, {111}, and {110} pole figures display concentrated intensity peaks, signifying a favored crystallographic alignment. The peak texture intensity was recorded at 4.091 MRD, indicating a moderately robust crystallographic texture.

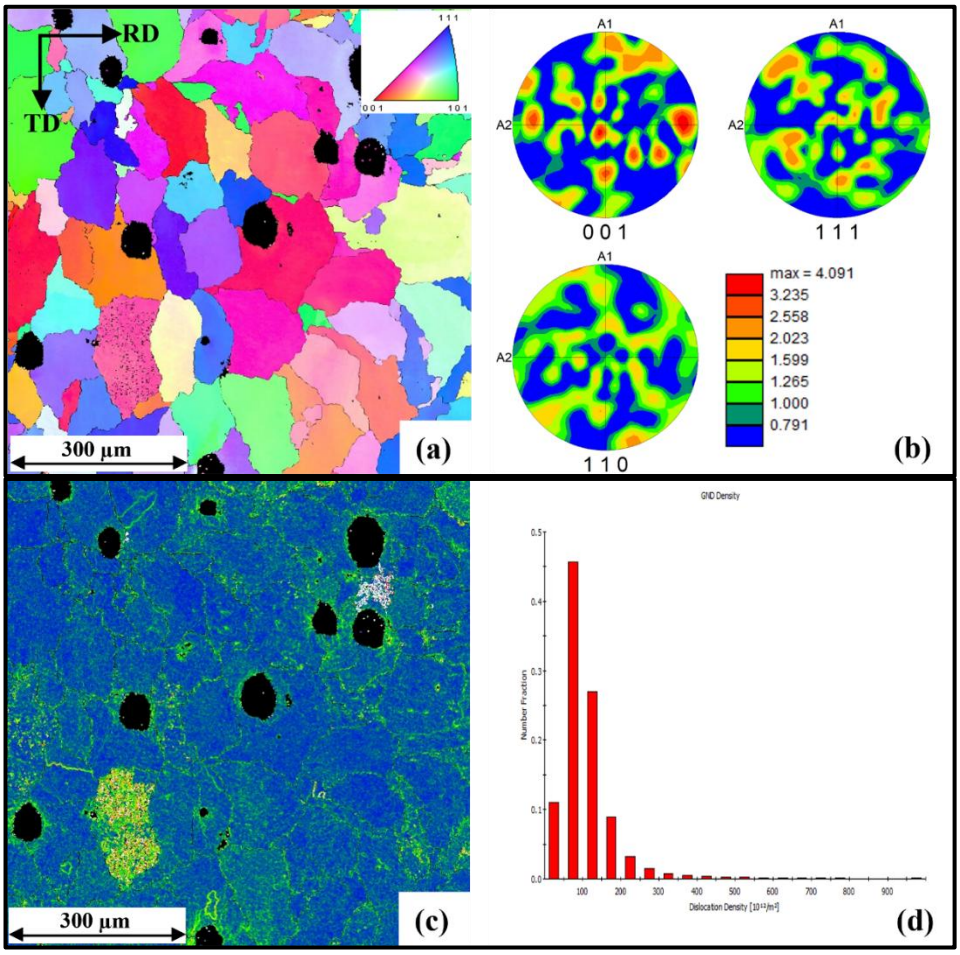


Figure 4.17 EBSD characterization of the fusion zone (weld zone): (a) inverse pole figure (IPF) map, (b) pole figures, (c) geometrically necessary dislocation (GND) distribution map, and (d) GND density distribution.

The GND distribution map illustrated in Figure 4.17 (c) reveals that elevated dislocation densities are predominantly found along the grain borders, whilst the grain interiors have significantly lower dislocation densities. The GND density distribution illustrated in Figure 4.17 (d) displays a significant peak at reduced dislocation densities, with the frequency progressively diminishing as the GND density escalates. The mean GND density was recorded at 111.23 × 10^{12} m^{-2}, along by a standard deviation of 85.18 × 10^{12} m^{-2}, suggesting that the fusion zone possesses a moderate

dislocation density while also showcasing the largest grain size among the examined areas.

An analysis of the EBSD findings indicated notable microstructural differences among the base metals, heat-affected zones (HAZs), and fusion zone of the 1.5 × 3.0 mm tailor welded blank. The fusion zone, heat-affected zones (HAZs), and base metals all have different mean grain sizes. The mean grain size of the 1.5 mm base metal was 21.43 μm, but the 3.0 mm base metal had a significantly higher value of 22.58 μm. The mean grain sizes of the HAZ next to the 1.5 mm and 3.0 mm sheets were 16.98 μm and 18.41 μm, respectively, which were smaller than those of the comparable base metals. Compared to the base metals and HAZs, the fusion zone had the greatest mean grain size (29.25 μm), suggesting a coarser granular structure. The pole figure analysis indicated discrepancies in crystallographic texture, with the heat-affected zone next to the 1.5 mm sheet displaying the peak texture intensity of 5.929 MRD, whereas other areas presented moderate texture intensities between 3.479 and 4.613 MRD. The 1.5 mm base metal demonstrated the least hardness and tensile strength, which might be associated with its somewhat diminished crystallographic texture intensity (3.479 MRD) and the lowest mean GND density (91.30×10^{12} m^{-2}) [63-66]. The comparatively low GND density suggests a reduced number of geometrically essential dislocations that hinder dislocation movement during plastic deformation, whilst the diminished texture intensity signifies a less pronounced preferred crystallographic orientation. Conversely, the 3.0 mm base metal, together with both heat-affected zones and the fusion zone, demonstrated elevated MRD values and/or GND densities, resulting in enhanced resistance to dislocation movement and, thus, superior hardness compared to the 1.5 mm base metal. Moreover, the EBSD analysis offers a

microstructural rationale for the tensile characteristics of the 1.5 × 3.0 mm custom welded blank. Notwithstanding the welding temperature cycle, the fusion zone preserved a modest crystalline structure and GND density, while demonstrating increased hardness compared to the surrounding base metals, signifying that the welded junction sustained sufficient mechanical integrity. As a result, tensile failure invariably transpired in the 1.5 mm base metal instead of the fusion zone, validating that the weld was not the mechanically weakest area of the custom welded blank. These findings align with the integrity of the weld and the distribution of hardness, indicating that the refined laser welding settings resulted in a robust welded junction with enhanced mechanical properties.

4.8 Finite Element Analysis (FEA)

Finite element analyses were conducted to examine the deformation characteristics of longitudinal tailor welded blanks with thickness variations of 1.5 × 2.0 mm, 1.5 × 2.5 mm, and 1.5 × 3.0 mm under ambient and warm-forming (300°C) conditions. The deformation characteristics were assessed by the maximum in-plane principal strain (PE, Max. In-Plane Principal) contours derived from Abaqus/Explicit [50], [127]. The simulated strain distributions for the three tailored welded blank configurations are illustrated in Figures 4.18–4.20. The contours of the highest in-plane primary strain for the 1.5 × 2.0 mm longitudinal tailor welded blank at ambient temperature and 300 °C are illustrated in Figure 4.18 (a–b). At ambient temperature (Figure 4.18 (a)), the peak primary strain attained roughly 0.53, with strain concentration observed in the center area of the longitudinal weld bead. In warm-forming conditions (Figure 4.18 (b)), the peak primary strain rose to around 1.08, and the high-strain area became more

evenly distributed. This signifies that the material endured more extensive plastic deformation prior to localized necking. The concentration of strain localization persisted in the identical center area of the longitudinal weld bead across both forming circumstances, signifying that the deformation mechanism remained consistent. Moreover, the anticipated strain localization aligns closely with the experimentally identified fracture site of the longitudinal LDH specimen, validating that the established finite element model effectively forecasts the deformation characteristics and failure site of the 1.5 × 2.0 mm tailor welded blank.

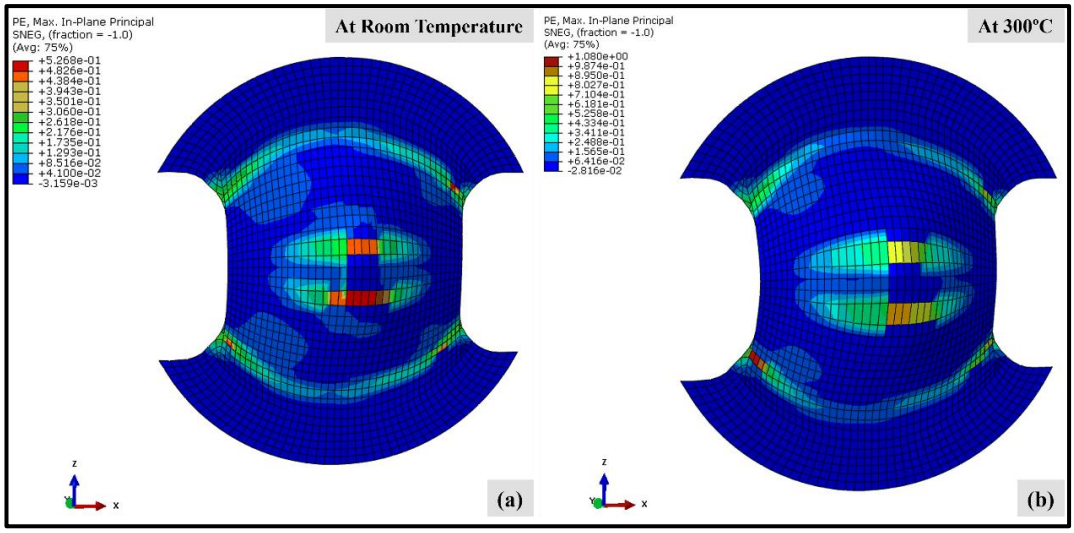


Figure 4.18 Maximum in-plane principal strain distribution predicted by FEA for the 1.5 × 2.0 mm tailor welded blank at (a) room temperature and (b) 300°C.

The contours of the highest in-plane primary strain for the 1.5 × 2.5 mm longitudinal tailor welded blank at ambient temperature and 300°C are illustrated in Figure 4.19 (a–b). At ambient temperature (Figure 4.19 (a)), the peak primary strain attained roughly 0.42, with strain localization focused in the center area of the longitudinal weld bead. In warm-forming conditions (Figure 4.19 (b)), the peak primary strain rose

markedly to around 1.17, and the high-strain area expanded and became more uniformly distributed. This suggests that the material underwent significantly more plastic deformation prior to localized necking. The concentration of strain localization persisted in the identical center area of the longitudinal weld bead across both forming circumstances, suggesting that the manner of deformation remained constant. Moreover, the anticipated strain localization aligns closely with the experimentally identified fracture site of the longitudinal LDH specimen, validating that the established finite element model effectively forecasts the deformation characteristics and failure position of the 1.5 × 2.5 mm tailor welded blank.

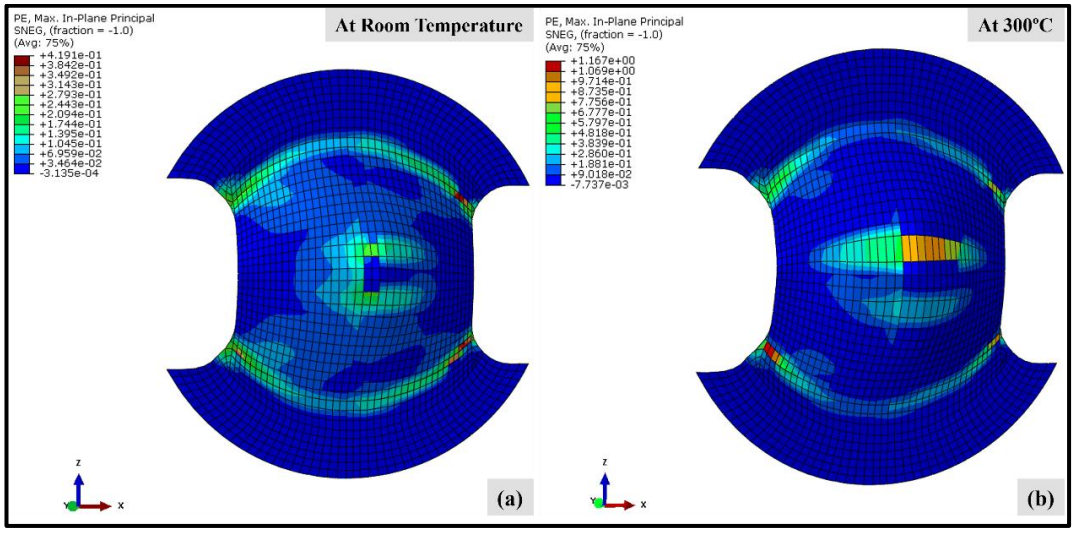


Figure 4.19 Maximum in-plane principal strain distribution predicted by FEA for the 1.5 × 2.5 mm tailor welded blank at (a) room temperature and (b) 300°C.

The contours of the highest in-plane primary strain for the 1.5 × 3.0 mm longitudinal tailor welded blank at ambient temperature and 300°C are illustrated in Figure 4.20 (a–b). At ambient temperature (Figure 4.20 (a)), the peak primary strain attained roughly 2.13, with strain localization primarily occurring in the center area of the

longitudinal weld bead. In warm-forming conditions (Figure 4.20 (b)), the peak principal strain remained relatively constant at about 2.11, while the high-strain area became more evenly dispersed around the core deformation zone. This suggests that heated forming facilitated a more uniform plastic deformation while maintaining the overall deformation mechanism. The concentration of strain localization persisted in the identical center area of the longitudinal weld bead across both forming circumstances, signifying that the deformation pattern remained consistent. Moreover, the anticipated strain localization aligns closely with the experimentally identified fracture site of the longitudinal LDH specimen, validating that the established finite element model effectively forecasts the deformation characteristics and failure site of the 1.5 × 3.0 mm tailor welded blank.

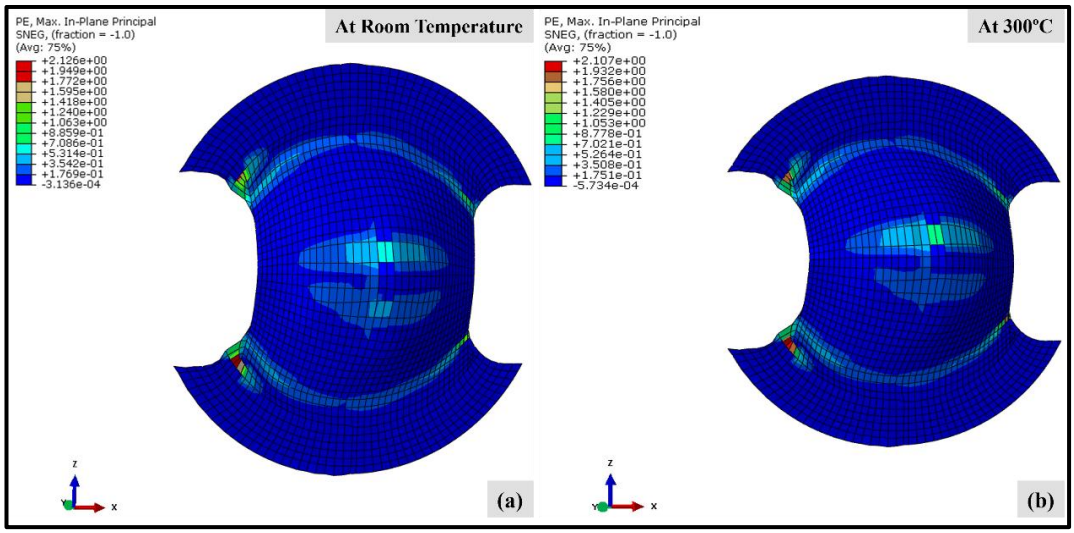


Figure 4.20 Maximum in-plane principal strain distribution predicted by FEA for the 1.5 × 3.0 mm tailor welded blank at (a) room temperature and (b) 300°C.

The finite element study revealed that the deformation characteristics of the longitudinal tailor welded blanks were significantly affected by the combination of

thickness and forming temperature [31-33]. For all three TWBs, the anticipated strain localization persisted in the middle area of the longitudinal weld bead, aligning with the experimentally identified fracture site of the longitudinal LDH specimens, hence validating the accuracy of the established numerical model. At 300°C, the strain patterns exhibited a more uniform distribution compared to ambient temperature, signifying enhanced plastic deformation in warm-forming scenarios. The 1.5 × 2.0 mm TWB displayed a peak in-plane primary strain of around 1.08, while the 1.5 × 2.5 mm and 1.5 × 3.0 mm TWBs reached significantly elevated strain values of about 2.11, indicating their enhanced deformation potential. Furthermore, the 1.5 × 3.0 mm TWB exhibited the most consistent strain distribution, with less strain concentration in the dome area, signifying superior strain accommodation and greater deformation stability. These computational findings align well with the experimental LDH and FLD outcomes, validating that the 1.5 × 3.0 mm longitudinal tailor welded blank had superior warm-forming capabilities among the thickness combinations examined.

4.9 Summary

This chapter provided an extensive assessment of the mechanical properties, weld integrity, formability, microstructural changes, and finite element analysis of laser-welded AA6082 tailor welded blanks under ambient and elevated temperature forming circumstances. The annealing characteristics of AA6082 alloy were first examined within the temperature range of room temperature to 400°C. The findings indicated that 350°C offered the ideal equilibrium between strength and ductility, hence it was chosen as the annealing temperature for further studies. The laser-welded tailor welded blanks demonstrated excellent weld integrity, with tensile failures routinely occurring

beyond the weld area, validating the absence of defects and ensuring adequate metallurgical bonding. The enhancement of laser welding parameters markedly elevated the tensile characteristics, whilst hardness assessments indicated localized hardening in the weld area and a practically consistent hardness in the base materials. Among the thickness combinations analyzed, the 1.5 × 3.0 mm TWB demonstrated the most advantageous balance of strength and ductility, leading to its selection for additional formability, microstructural, and numerical studies. The LDH and FLD findings indicated that both the direction of the weld bead and the forming temperature significantly affected the formability of the tailor welded blanks. In the transverse weld bead alignment, warm forming yielded minimal enhancement in formability, but the longitudinal orientation markedly improved deformation potential at 300°C. The longitudinal TWB measuring 1.5 × 3.0 mm demonstrated the most elevated LDH and FLD metrics, validating its exceptional resistance to localized necking and overall formability.

Comprehensive EBSD analysis of the refined 1.5 x 3.0 mm TWB disclosed microstructural differences throughout the base metals, heat-affected regions, and fusion zone. The fusion zone displayed fine grains alongside the greatest GND density, suggesting that dislocation strengthening surpassed the influence of grain size and enhanced the mechanical properties of the welded joint. Finite element calculations corroborated the experimental findings, indicating strain localization in the identical center area of the longitudinal weld bead where breakage was observed experimentally. Warm forming resulted in elevated maximum primary strain together with a more consistent strain distribution, signifying enhanced plastic deformation prior to localized necking. The strong correlation between the experimental and

numerical findings validates the dependability of the established finite element model and illustrates that the 1.5 × 3.0 mm longitudinal tailor welded blank, formed at 300°C, offers the ideal amalgamation of weld integrity, mechanical properties, microstructural traits, and warm-forming performance.

CHAPTER 5

CONCLUSIONS AND FUTURE RESEARCH SCOPE

5.1 Conclusions

The current research offers a methodical examination of the mechanical properties, weld quality, hardness traits, microstructural changes, and warm-forming features of laser-welded AA6082 tailor welded blanks (TWBs). The inquiry encompassed the enhancement of pre-welding annealing processes and laser welding settings, succeeded by assessments of tensile strength and hardness, evaluations of limiting dome height (LDH) and forming limit diagram (FLD), EBSD-driven microstructural examination, and finite element modeling. The subsequent conclusions are derived from the experimental observations and computational outcomes:

1. Annealing experiments conducted from room temperature to 400°C determined that 350°C is the ideal pre-welding heat-treatment temperature for AA6082 alloy. Under these circumstances, the material demonstrated a yield strength of 94 MPa, an ultimate tensile strength of 124 MPa, an elongation of 19.8%, and a hardness of 47.8 HV0.5. Despite the elevation to 400°C resulting in an elongation of 27.6%, it concurrently diminished the yield strength and ultimate tensile strength to 71 MPa and 106 MPa, respectively. Consequently, 350°C ensured enough ductility for shaping while maintaining appropriate load-bearing strength.

2. The tensile properties of annealed AA6082-O exhibited significant dependence on temperature. Elevating the temperature to 300°C diminished the yield strength and ultimate tensile strength from 94 MPa and 124 MPa to 81 MPa

and 93.1 MPa, correspondingly, while elongation rose from 19.8% to 28.2%. The strain-hardening exponent rose from 0.10 to 0.18, signifying enhanced uniform plastic deformation and postponed strain localization. Consequently, 300°C was chosen as the optimal temperature for warm formation.

3. The refinement of laser welding settings, employing 3700 W for the 1.5 × 2.0 mm TWB and 4000 W for the 1.5 × 2.5 mm and 1.5 × 3.0 mm TWBs, produced robust welded connections. Weld-integrity tensile assessments revealed ultimate tensile strength (UTS) measurements of 95.8, 83.6, and 84.9 MPa, with elongation ranging from about 7.1% to 7.4%. Fractures regularly manifested in the 1.5 mm thinner base sheet instead of the weld area, affirming sufficient metallurgical bonding and indicating that the weld was not the most vulnerable zone.

4. The tensile behavior fluctuated based on the TWB thickness configuration. The 1.5 × 2.0 mm TWB demonstrated a UTS of 158 MPa, whilst the 1.5 × 2.5 mm and 1.5 × 3.0 mm TWBs reached 176 MPa. The 1.5 × 3.0 mm TWB exhibited the greatest elongation at 8.11%, in contrast to the 7.41% of the 1.5 × 2.5 mm TWB, signifying enhanced ductility and deformation potential.

5. All three TWBs demonstrated increased toughness in the weld area compared to the surrounding base materials. The maximum hardness reached was 72–73 HV0.5, in contrast to 47–54 HV0.5 in the foundational materials. This localized strengthening reflects the impact of the welding thermal cycle and swift solidification, whereas the analogous hardness profiles illustrate the uniformity of the chosen welding parameters.

6. LDH tests revealed that the direction of the weld significantly impacted formability more than the forming temperature by itself. In the transverse alignment, the 1.5 x 2.0 mm TWB diminished from 14.0 mm at ambient temperature to 11.8 mm at 300°C. Conversely, the longitudinal alignment augmented its dome height from 13.0 mm to 15.5 mm, illustrating the advantageous impact of orienting the weld with the primary direction of deformation.

7. The integration of longitudinal weld alignment with warm forming yielded the greatest stretch formability for the 1.5 × 3.0 mm TWB, with LDH rising from 11.7 mm at ambient temperature to 17.5 mm at 300°C, representing an enhancement of almost 49.6%. The relative enhancements for the 1.5 × 2.0 mm and 1.5 × 2.5 mm TWBs were 19.2% and 37.5%, correspondingly. Consequently, the increased thickness ratio in the longitudinal direction facilitated more consistent strain distribution and postponed localized necking.

8. FLD findings validated that heated forming at 300°C improved the deformability of all longitudinally welded tailor-welded blanks. The 300°C FLD curves consistently exceeded the room-temperature curves during tension–compression, plane-strain, and biaxial deformation, signifying enhanced limiting strains and superior resistance to localized necking. The 1.5 × 3.0 mm TWB demonstrated the greatest forming limits, aligning with its LDH efficacy.

9. The 1.5 × 3.0 mm TWB's EBSD analysis showed microstructural variations in the base metals, fusion zone, and heat-affected zones (HAZs). The comparable

HAZs showed smaller mean grain sizes of 16.98 μm and 18.41 μm, while the mean grain sizes of the 1.5 mm and 3.0 mm base metals were 21.43 μm and 22.58 μm, respectively. Compared to the base metals and HAZs, the fusion zone had the greatest mean grain size (29.25 μm), suggesting a coarser granular structure. The microstructural alterations linked to the laser welding heat cycle are reflected in these fluctuations, which show the variations in grain size throughout the welded regions.

10. EBSD examination revealed discrepancies in crystallographic texture and GND density throughout the welded junction. The heat-affected zone (HAZ) next to the 1.5 mm sheet displayed the peak texture intensity of 5.929 MRD and a GND density of 172.63×10^{12} m^{-2}, in contrast to the 3.479 MRD and 91.30×10^{12} m^{-2} seen in the 1.5 mm base metal. An elevated GND density signifies increased lattice distortion and dislocation build-up resulting from the welding thermal cycle, leading to enhanced resistance to plastic deformation and revealing the tendency for failure in the thinner base material.

11. Finite element analysis effectively replicated the deformation properties of the longitudinal TWBs at ambient temperature and 300°C. For the 1.5 × 2.0 mm and 1.5 × 2.5 mm TWBs, the peak in-plane primary strain rose from around 0.53 to 1.08 and from 0.42 to 1.17, correspondingly, exhibiting a more uniform strain distribution at 300°C. For the 1.5 × 3.0 mm TWB, the peak strain persisted at roughly 2.1, although its distribution became increasingly uniform. The anticipated strain concentration closely aligned with the observed fracture area, validating the dependability of the computational model.

5.2 Future Research Scope

In light of the recognized research deficiencies and the outcomes of this study, the subsequent domains are recommended for further exploration:

1. Investigation of Dissimilar TWBs: Future research may investigate the heated forming characteristics of tailor welded blanks (TWB) produced by fusing AA6082 with other aluminium alloys (such as AA5083 or AA7075) to assess the implications of significant material disparity.

2. Weld Line Movement Analysis: A methodical investigation of weld line displacement in warm forming, especially its correlation with punch velocity, sheet thickness ratios, and material flow, would yield significant insights for industrial die fabrication.

3. Advanced Numerical Modeling: To improve forecast precision, further studies ought to integrate Barlat 2005 yield criteria and temperature-sensitive anisotropic constitutive laws into the finite element analyses.

4. Alternative Heat Treatments: Exploring multi-step annealing processes or solution treatment succeeded by aging may enhance formability above the thresholds defined in this research.

5. Complex Industrial Forming: The existing research on basic stretching can be extended to more intricate loading trajectories, including warm hydroforming, incremental sheet forming (ISF), and multi-stage deep drawing.

6. Extended Temperature Ranges: Evaluating the mechanical robustness and malleability of AA6082 TWBs in cryogenic conditions or temperatures over

300°C may assist in establishing the definitive operational boundaries of the alloy.

7. Tribological Optimization: Investigating the application of nano-lubricants or sophisticated die coatings (such as laser texturing) may further diminish friction and enhance surface quality in high-temperature forming processes.

REFERENCES

[1] Smith, P. E., & Lee, D. (1998). *Determination of forming limits for Aluminium alloys* (No. 982375). SAE Technical Paper.

[2] Ungureanu, C. A., Das, S., & Jawahir, I. S. (2007). Life-cycle cost analysis: Aluminium versus steel in passenger cars. *TMS (the minerals, metals & materials society)*, *1*, 11-24.

[3] Mordike, B. L., & Ebert, T. J. M. S. (2001). Magnesium: properties-applications-potential. *Materials Science and Engineering: A*, *302*(1), 37-45.

[4] Miller, W. S., Zhuang, L., Bottema, J., Wittebrood, A., De Smet, P., Haszler, A., & Vieregge, A. J. M. S. (2000). Recent development in aluminium alloys for the automotive industry. *Materials Science and Engineering: A*, *280*(1), 37-49.

[5] Cole, G. S., & Sherman, A. M. (1995). Light weight materials for automotive applications. *Materials characterization*, *35*(1), 3-9.

[6] Roth, R., Clark, J., & Kelkar, A. (2001). Automobile bodies: can Aluminium be an economical alternative to steel?. *Jom*, *53*(8), 28-32.

[7] http://www.Aluminiumintransportation.org/research-resources/2014-duckerworldwide-survey-of-automakers accessed on 21-01-2023

[8] https://european-aluminium.eu/wp-content/uploads/2023/05/2023_04_Aluminium-Content_Ducker-Study_EA-Public-Summary_190423.pdf accessed on 14-12-2025

[9] Hirsch, J. (2014). Recent development in aluminium for automotive applications. *Transactions of Nonferrous Metals Society of China*, *24*(7), 1995-2002.

[10] Hayashi, H., & Nakagawa, T. (1994). Recent trends in sheet metals and their formability in manufacturing automotive panels. *Journal of Materials Processing Technology*, *46*(3-4), 455-487.

[11] Davies, R. W., Oliver, H. E., Smith, M. T., & Grant, G. J. (1999). Characterizing Al tailor-welded blanks for automotive applications. *JOM*, *51*(11), 46-50.

[12] Shakeri, H. R., Buste, A., Worswick, M. J., Clarke, J. A., Feng, F., Jain, M., & Finn, M. (2002). Study of damage initiation and fracture in Aluminium tailor welded blanks made via different welding techniques. *Journal of Light Metals*, *2*(2), 95-110.

[13] Babu, K. V., Narayanan, R. G., & Kumar, G. S. (2009). An expert system based on artificial neural network for predicting the tensile behavior of tailor welded blanks. *Expert Systems with Applications*, *36*(7), 10683-10695.

[14] Merklein, M., Johannes, M., Lechner, M., & Kuppert, A. (2014). A review on tailored blanks—Production, applications and evaluation. *Journal of Materials Processing Technology*, *214*(2), 151-164.

[15] Costa, M. I., Rodrigues, D. M., & Leitão, C. (2015). Analysis of AA 6082-T6 welds strength mismatch: stress versus hardness relationships. *The International Journal of Advanced Manufacturing Technology*, *79*(5), 719-727.

[16] Wang, B., Lei, B. B., Zhu, J. X., Feng, Q., Wang, L., & Wu, D. (2015). EBSD study on microstructure and texture of friction stir welded AA5052-O and AA6061-T6 dissimilar joint. *Materials & Design*, *87*, 593-599.

[17] Liu, J., Wang, L. L., Lee, J., Chen, R., El-Fakir, O., Chen, L., ... & Dean, T. A. (2015). Size-dependent mechanical properties in AA6082 tailor welded specimens. *Journal of Materials Processing Technology*, *224*, 169-180.

[18] Jula, M., Dehmolaei, R., & Ranjbar, K. (2023). Softening, hardening, and precipitation evolution of the AA6082-T651 heat-affected zone caused by thermal cycles during and after welding. *Metals and Materials International*, *29*(12), 3664-3678.

[19] Gautam, V., & Kumar, D. R. (2018). Experimental and numerical investigations on springback in V-bending of tailor-welded blanks of interstitial free steel. *Proceedings of the Institution of Mechanical Engineers, Part B: Journal of Engineering Manufacture*, *232*(12), 2178-2191.

[20] Koli, Y., Yuvaraj, N., Vipin, & Aravindan, S. (2019). Investigations on weld bead geometry and microstructure in CMT, MIG pulse synergic and MIG welding of AA6061-T6. *Materials Research Express*, *6*(12), 1265e5.

[21] Svoboda, H. G., Tufaro, L. N., & Varela, F. J. B. (2019). Residual stresses in similar and dissimilar friction stir welds of AA5083 and AA6061. *Key Engineering Materials*, *813*, 147-152.

[22] Koli, Y., Yuvaraj, N., Aravindan, S., & Vipin. (2021). CMT joining of AA6061-T6 and AA6082-T6 and examining mechanical properties and microstructural characterization. *Transactions of the Indian Institute of Metals*, *74*(2), 313-329.

[23] Koli, Y., Yuvaraj, N., Aravindan, S., & Vipin. (2021). Enhancement of mechanical properties of 6061/6082 dissimilar aluminium alloys through ultrasonic-assisted cold metal transfer welding. *Arabian Journal for Science and Engineering*, *46*(12), 12089-12104.

[24] Katayama, S. (Ed.). (2013). *Handbook of laser welding technologies*. Elsevier.

[25] Katayama, S., Kawahito, Y., & Mizutani, M. (2012). Latest progress in performance and understanding of laser welding. *Physics Procedia*, *39*, 8-16.

[26] Srinivas, B., Sivaprasad, K., Babu, N. K., Muthupandi, V., & Susila, P. (2013). Studies on dissimilar welding of AA5083 and AA6061 alloys by laser beam welding. *Advanced Materials Research*, *626*, 701-705.

[27] Alfieria, V., Caiazzoa, F., & Sergi, V. (2015). Autogenous laser welding of AA 2024 aluminium alloy: process issues and bead features. *Procedia Cirp*, *33*, 406-411.

[28] Wang, L., Gao, M., Zhang, C., & Zeng, X. (2016). Effect of beam oscillating pattern on weld characterization of laser welding of AA6061-T6 Aluminium alloy. *Materials & Design*, *108*, 707-717.

[29] Dhanaraj, P. S., & Rathinasuriyan, C. (2022). Optimization of fiber laser welding parameters for high strength aluminium alloy AA7075-T6. *Materials Today: Proceedings*, *52*, 283-289.

[30] Hong, K. M., & Shin, Y. C. (2017). Prospects of laser welding technology in the automotive industry: A review. *Journal of Materials Processing Technology*, *245*, 46-69.

[31] Stavridis, J., Papacharalampopoulos, A., & Stavropoulos, P. (2018). Quality assessment in laser welding: a critical review. *The International Journal of Advanced Manufacturing Technology*, *94*(5), 1825-1847.

[32] He, X. (2012). Finite element analysis of laser welding: a state of art review. *Materials and Manufacturing Processes*, *27*(12), 1354-1365.

[33] Merklein, M., & Herrmann, J. (2016). Effect of a local laser heat treatment on the formability of multi-layered 6000 series Aluminium alloys. *Physics Procedia*, *83*, 560-567.

[34] Maciolek, A., Jöckel, A., Völkers, S., Hatzky, M., Suckow, T., Schell, L., ... & Niendorf, T. (2024). Influence of Short-Time Post-Weld heat treatment on the performance of friction stir welded AA7075 Aluminium sheets. *International Journal of Fatigue*, *178*, 107998.

[35] Vedani, M. (2025). Plastic Deformation of Metals. In *Metal Science in Modern Manufacturing Technologies* (pp. 35-56). Cham: Springer Nature Switzerland.

[36] Schuler. (1998). *Metal forming handbook*. Springer Science & Business Media.

[37] Kleiner, M., Geiger, M., & Klaus, A. (2003). Manufacturing of lightweight components by metal forming. *CIRP annals*, *52*(2), 521-542.

[38] Hosford, W. F., & Caddell, R. M. (2011). *Metal forming: mechanics and metallurgy*. Cambridge university press.

[39] Erichsen, A. (1914). A new test for thin sheets. *Stahl und Eisen*, *34*, 879-882.

[40] Sorce, F. S., Ngo, S., Lowe, C., & Taylor, A. C. (2019). Quantification of coating surface strains in Erichsen cupping tests. *Journal of Materials Science*, *54*(10), 7997-8009.

[41] Hecker, S. S. (1974). A cup test for assessing stretchability.

[42] Duncan, J. L., Kolodziejski, J., & Glover, G. (1976). BULGE TESTING AS AN AID TO FORMABILITY ASSESSMENT.

[43] Altan, T., & Tekkaya, A. E. (Eds.). (2012). *Sheet metal forming: fundamentals*. Asm International.

[44] Swift, H. W. (1954). The mechanism of a simple deep-drawing operation. *Sheet Met Ind*, *31*(330), 817-828.

[45] Semiatin, S. L., Marquard, E., & Lampman, H. (2006). Metalworking: Sheet Forming, vol. 14B. *ASM International, Materials Park, Ohio, USA*.

[46] Li, D., & Ghosh, A. (2003). Tensile deformation behavior of Aluminium alloys at warm forming temperatures. *Materials Science and Engineering: A*, *352*(1-2), 279-286.

[47] Li, D., & Ghosh, A. K. (2004). Biaxial warm forming behavior of Aluminium sheet alloys. *Journal of Materials Processing Technology*, *145*(3), 281-293.

[48] Toros, S., Ozturk, F., & Kacar, I. (2008). Review of warm forming of Aluminium–magnesium alloys. *Journal of materials processing technology*, *207*(1-3), 1-12.

[49] Abedrabbo, N., Pourboghrat, F., & Carsley, J. (2006). Forming of Aluminium alloys at elevated temperatures–Part 1: Material characterization. *International Journal of plasticity*, *22*(2), 314-341.

[50] Abedrabbo, N., Pourboghrat, F., & Carsley, J. (2006). Forming of Aluminium alloys at elevated temperatures–Part 2: Numerical modeling and experimental verification. *International Journal of Plasticity*, *22*(2), 342-373.

[51] Panicker, S. S., & Panda, S. K. (2015). Formability analysis of AA5754 alloy at warm condition: appraisal of strain rate sensitive index. *Materials Today: Proceedings*, *2*(4-5), 1996-2004.

[52] Shao, Z., Bai, Q., Li, N., Lin, J., Shi, Z., Stanton, M., ... & Dean, T. (2018). Experimental investigation of forming limit curves and deformation features in warm forming of an aluminium alloy. *Proceedings of the Institution of Mechanical Engineers, Part B: Journal of Engineering Manufacture*, *232*(3), 465-474.

[53] Raja Satish, D., & Ravi Kumar, D. (2019). Formability of AA6061 alloy sheets in warm forming temperature range. *Proceedings of the Institution of*

Mechanical Engineers, Part L: Journal of Materials: Design and Applications, *233*(3), 413-425.

[54] Panicker, S. S., & Panda, S. K. (2019). Investigations into improvement in formability of AA5754 and AA6082 sheets at elevated temperatures. *Journal of Materials Engineering and Performance*, *28*(5), 2967-2982.

[55] Polak, S., Kaczyński, P., Gronostajski, Z., Jaskiewicz, K., Krawczyk, J., Skwarski, M., ... & Chorzępa, W. (2017). Warm forming of 7075 Aluminium alloys. *Procedia engineering*, *207*, 2399-2404.

[56] El Fakir, O., Wang, L., Balint, D., Dear, J. P., Lin, J., & Dean, T. A. (2014). Numerical study of the solution heat treatment, forming, and in-die quenching (HFQ) process on AA5754. *International Journal of Machine Tools and Manufacture*, *87*, 39-48.

[57] Den Uijl, N. J., & Carless, L. J. (2012). Advanced metal-forming technologies for automotive applications. In *Advanced materials in automotive engineering* (pp. 28-56). Woodhead Publishing.

[58] Holmberg, S., Enquist, B., & Thilderkvist, P. (2004). Evaluation of sheet metal formability by tensile tests. *Journal of materials processing technology*, *145*(1), 72-83.

[59] Kalpakjian, S., & Schmid, S. R. (2006). Machining Engineering and Technology.

[60] Narayanasamy, R., Ponalagusamy, R., & Raghuraman, S. (2008). The effect of strain rate sensitivity on theoretical prediction of limiting draw ratio for cylindrical cup drawing process. *Materials & Design*, *29*(4), 884-890.

[61] Stachowicz, F. (1986). Formability of aluminium-alloy sheets. *Journal of Mechanical Working Technology*, *13*(2), 229-235.

[62] Lahaye, C., Hirsch, J., Bassan, D., Criqui, B., Sahr, C., Goede, M., & Volkswagen, A. G. (2008). Contribution of aluminium to the multimaterial light-weight BIW design of superlight-car [C]. In *Proceedings of the 11th International Conference on Aluminium Alloys. Weinheim: Wiley-VCH Verlag GmbH & Co. KGaA* (pp. 2363-2373).

[63] Hirsch, J. (2011). Aluminium in innovative light-weight car design. *Materials transactions*, *52*(5), 818-824.

[64] Mukhopadhyay, P. (2012). Alloy designation, processing, and use of AA6XXX series aluminium alloys. *International Scholarly Research Notices*, *2012*(1), 165082.

[65] Singh, R. K., Singh, A. K., & Prasad, N. E. (2000). Texture and mechanical property anisotropy in an Al–Mg–Si–Cu alloy. *Materials Science and Engineering: A*, *277*(1-2), 114-122.

[66] Tajally, M., & Emadoddin, E. (2011). Mechanical and anisotropic behaviors of 7075 Aluminium alloy sheets. *Materials & Design*, *32*(3), 1594-1599.

[67] Kumar, N., Goel, S., Jayaganthan, R., & Brokmeier, H. G. (2017). Effect of grain boundary misorientaton, deformation temperature and AlFeMnSi-phase on fatigue life of 6082 Al alloy. *Materials Characterization*, *124*, 229-240.

[68] Lodh, A., Tak, T. N., Prakash, A., Guruprasad, P. J., Hutchinson, C., & Samajdar, I. (2017). Relating residual stress and substructural evolution during tensile deformation of an Aluminium-manganese alloy. *Metallurgical and Materials Transactions A*, *48*(11), 5317-5331.

[69] Tomstad, A. J., Thomesen, S., Børvik, T., & Hopperstad, O. S. (2021). Effects of constituent particle content on ductile fracture in isotropic and anisotropic 6000-series aluminium alloys. *Materials Science and Engineering: A*, *820*, 141420.

[70] Bhargava, M., Tewari, A., & Mishra, S. (2013). Strain path diagram simulation of AA 5182 Aluminium alloy. *Procedia Engineering*, *64*, 1252-1258.

[71] Kumar, R., & Gautam, V. (2025). Influence of Magnesium Content on Tensile Properties and Deformation Behaviour of Al–Mg–Si Alloy Sheets. *Transactions of the Indian Institute of Metals*, *78*(2), 51.

[72] Baig, M., Khan, A. S., Choi, S. H., & Lee, E. (2015). Effect of manufacturing processes and welding type on quasi-static and dynamic responses of Aluminium alloys: experiments and modeling. *Journal of Dynamic Behavior of Materials*, *1*(3), 299-314.

[73] Sheikhi, M., Malek Ghaini, F., & Assadi, H. (2014). Solidification crack initiation and propagation in pulsed laser welding of wrought heat treatable aluminium alloy. *Science and Technology of Welding and Joining*, *19*(3), 250-255.

[74] Drysdale, R. J., & Bahrani, A. S. (1985). The effect of annealing processes on the limit strains of an aluminium alloy. *Journal of mechanical working technology*, *11*(1), 105-114.

[75] Poole, W. J., Militzer, M., & Wells, M. A. (2003). Modelling recovery and recrystallisation during annealing of AA 5754 aluminium alloy. *Materials science and technology*, *19*(10), 1361-1368.

[76] Narayanasamy, R., Ravindran, R., Manonmani, K., & Satheesh, J. (2009). A crystallographic texture perspective formability investigation of aluminium

5052 alloy sheets at various annealing temperatures. *Materials & Design*, *30*(5), 1804-1817.

[77] Lin, S., Nie, Z., Huang, H., & Li, B. (2010). Annealing behavior of a modified 5083 Aluminium alloy. *Materials & Design*, *31*(3), 1607-1612.

[78] Rao, P. N., Singh, D., & Jayaganthan, R. (2013). Effect of annealing on microstructure and mechanical properties of Al 6061 alloy processed by cryorolling. *Materials Science and Technology*, *29*(1), 76-82.

[79] Kumar, N., Rao, P. N., Jayaganthan, R., & Brokmeier, H. G. (2015). Effect of cryorolling and annealing on recovery, recrystallisation, grain growth and their influence on mechanical and corrosion behaviour of 6082 Al alloy. *Materials Chemistry and Physics*, *165*, 177-187.

[80] Fröck, H., Milkereit, B., Wiechmann, P., Springer, A., Sander, M., Kessler, O., & Reich, M. (2018). Influence of solution-annealing parameters on the continuous cooling precipitation of Aluminium alloy 6082. *Metals*, *8*(4), 265.

[81] Kumar, N., Owolabi, G. M., Jayaganthan, R., & Warner, G. (2019). Effect of annealing on mechanical properties and metallurgical factors of ultrafine-grained 6082 Al alloy. *Transactions of the Indian Institute of Metals*, *72*(9), 2523-2531.

[82] Zhao, Y., Li, L., Lu, Z., Teng, G., Liu, S., Hu, Z., & He, A. (2021). The effect of annealing temperature on the recrystallization and mechanical properties of severe plastic deformed commercial pure aluminium during ultra-fast annealing. *Materials Research Express*, *8*(4), 046515.

[83] Abdullah, K., Wild, P. M., Jeswiet, J. J., & Ghasempoor, A. (2001). Tensile testing for weld deformation properties in similar gage tailor welded blanks

using the rule of mixtures. *Journal of Materials Processing Technology*, *112*(1), 91-97.

[84] Shi, Y., Lin, Z., Zhu, P., & Han, S. (2008). Impact modeling of the weld line of tailor-welded blank. *Materials & Design*, *29*(1), 232-238.

[85] Huntington, C.A., & Eagar, T.W. (1982). Laser Welding of Aluminium and Aluminium Alloys. *Welding Research Supplement*, 61(4), pp.105s–107s.

[86] Katayama, S., Kawahito, Y., & Mizutani, M. (2010). Elucidation of laser welding phenomena and factors affecting weld penetration and welding defects. *Physics procedia*, *5*, 9-17.

[87] Katayama, S. (2013). Introduction: fundamentals of laser welding. In *Handbook of laser welding technologies* (pp. 3-16). Woodhead Publishing.

[88] Quintino, L., Miranda, R., Dilthey, U., Iordachescu, D., Banasik, M., & Stano, S. (2011). Laser welding of structural aluminium. In *Structural connections for lightweight metallic structures* (pp. 33-57). Berlin, Heidelberg: Springer Berlin Heidelberg.

[89] Zhao, H., White, D. R., & DebRoy, T. (1999). Current issues and problems in laser welding of automotive aluminium alloys. *International materials reviews*, *44*(6), 238-266.

[90] Cao, X., Wallace, W., Poon, C., & Immarigeon, J. P. (2003). Research and progress in laser welding of wrought Aluminium alloys. I. Laser welding processes. *Materials and Manufacturing Processes*, *18*(1), 1-22.

[91] Cao, X., Wallace, W., Immarigeon, J. P., & Poon, C. (2003). Research and progress in laser welding of wrought Aluminium alloys. II. Metallurgical

microstructures, defects, and mechanical properties. *Materials and manufacturing processes*, *18*(1), 23-49.

[92] Matsunawa, A. (2001). Problems and solutions in deep penetration laser welding. *Science and Technology of welding and Joining*, *6*(6), 351-354.

[93] Haboudou, A., Peyre, P., Vannes, A. B., & Peix, G. (2003). Reduction of porosity content generated during Nd: YAG laser welding of A356 and AA5083 aluminium alloys. *Materials Science and Engineering: A*, *363*(1-2), 40-52.

[94] Hu, B., & Richardson, I. M. (2006). Mechanism and possible solution for transverse solidification cracking in laser welding of high strength aluminium alloys. *Materials Science and Engineering: A*, *429*(1-2), 287-294.

[95] Katayama, S., Nagayama, H., Mizutani, M., & Kawahito, Y. (2009). Fibre laser welding of aluminium alloy. *Welding International*, *23*(10), 744-752.

[96] El-Batahgy, A., & Kutsuna, M. (2009). Laser beam welding of AA5052, AA5083, and AA6061 Aluminium alloys. *Advances in Materials Science and Engineering*, *2009*(1), 974182.

[97] Zhang, R., Tang, X., Xu, L., Lu, F., & Cui, H. (2020). Study of molten pool dynamics and porosity formation mechanism in full penetration fiber laser welding of Al-alloy. *International Journal of Heat and Mass Transfer*, *148*, 119089.

[98] Braun, R., Donne, C. D., & Staniek, G. (2000). Laser beam welding and friction stir welding of 6013-T6 aluminium alloy sheet. *Materialwissenschaft und Werkstofftechnik: Materials Science and Engineering Technology*, *31*(12), 1017-1026.

[99] Sánchez-Amaya, J. M., Delgado, T., González-Rovira, L., & Botana, F. J. (2009). Laser welding of aluminium alloys 5083 and 6082 under conduction regime. *Applied Surface Science*, *255*(23), 9512-9521.

[100] Zhou, H., Fu, F., Dai, Z., Qiao, Y., Chen, J., & Liu, W. (2020). Effect of laser power on microstructure and micro-galvanic corrosion behavior of a 6061-T6 Aluminium alloy welding joints. *Metals*, *11*(1), 3.

[101] Enz, J., Riekehr, S., Ventzke, V., Sotirov, N., & Kashaev, N. (2014). Laser welding of high-strength aluminium alloys for the sheet metal forming process. *Procedia Cirp*, *18*, 203-208.

[102] Enz, J., Kumar, M., Riekehr, S., Ventzke, V., Huber, N., & Kashaev, N. (2017). Mechanical properties of laser beam welded similar and dissimilar Aluminium alloys. *Journal of Manufacturing Processes*, *29*, 272-280.

[103] Park, Y. W., Yu, J., & Rhee, S. (2010). A study on the weld characteristics of 5182 Aluminium alloy by Nd: YAG laser welding with filler wire for car bodies. *International Journal of Automotive Technology*, *11*(5), 729-736.

[104] Sathish, T., Sevvel, P., Sudharsan, P., & Vijayan, V. (2021). Investigation and optimization of laser welding process parameters for AA7068 aluminium alloy butt joint. *Materials Today: Proceedings*, *37*, 1672-1677.

[105] Qi, S., Wang, C., Liu, Y., Liu, A., Bai, Z., Peng, Z., ... & Wang, D. (2025). Process parameter optimization of laser welding for dissimilar Aluminium alloys 4047 and 6061 using response surface methodology: Microstructure and mechanical properties. *Optics & Laser Technology*, *190*, 113198.

[106] Sibillano, T., Ancona, A., Berardi, V., Schingaro, E., Parente, P., & Lugara, P. M. (2006). Correlation spectroscopy as a tool for detecting losses of ligand

elements in laser welding of aluminium alloys. *Optics and lasers in engineering*, *44*(12), 1324-1335.

[107] Tušek, J., Kampuš, Z., & Suban, M. (2001). Welding of tailored blanks of different materials. *Journal of materials processing technology*, *119*(1-3), 180-184.

[108] Wu, Q., Gong, J., Chen, G., & Xu, L. (2008). Research on laser welding of vehicle body. *Optics & Laser Technology*, *40*(2), 420-426.

[109] Rajesham, S., Reddy, A. C. S., Reddy, P. R., & Umamaheswar, A. C. (2020). Formability: A review on different sheet metal tests for formability. In *International Conference on Multifunctional Materials (ICMM-2019)*.

[110] Ahmadi, S., Eivani, A. R., & Akbarzadeh, A. (2009). Experimental and analytical studies on the prediction of forming limit diagrams. *Computational materials science*, *44*(4), 1252-1257.

[111] Mishra, S. K., Desai, S. G., Pant, P., Narasimhan, K., & Samajdar, I. (2009). Improved predictability of forming limit curves through microstructural inputs. *International Journal of Material Forming*, *2*(1), 59-67.

[112] Abspoel, M., Scholting, M. E., & Droog, J. M. (2013). A new method for predicting forming limit curves from mechanical properties. *Journal of Materials Processing Technology*, *213*(5), 759-769.

[113] Habibi, M., Ghazanfari, A., Assempour, A., Naghdabadi, R., & Hashemi, R. (2017). Determination of forming limit diagram using two modified finite element models. *Mech Eng*, *48*(4), 141-144.

[114] Simoncini, M., Cabibbo, M., & Forcellese, A. (2016). Development of double-side friction stir welding to improve post-welding formability of joints in

AA6082 aluminium alloy. *Proceedings of the Institution of Mechanical Engineers, Part B: Journal of Engineering Manufacture*, *230*(5), 807-817.

[115] Nghishiyeleke, E. T., Mashingaidze, M. M., & Ogunmokun, A. A. (2018). Formability characterization of aluminium AA6082-O sheet metal by uniaxial tension and Erichsen cupping tests. *Int J Eng Technol*, *7*, 6768-6777.

[116] Çavuşoğlu, O., Sürücü, H. İ., Toros, S., & Alkan, M. (2020). Thickness dependent yielding behavior and formability of AA6082-T6 alloy: experimental observation and modeling. *The International Journal of Advanced Manufacturing Technology*, *106*(9), 4083-4091.

[117] Simoncini, M., Forcellese, A., Mancini, E., Chiappini, G., & Sasso, M. (2021). Experimental and numerical investigation on forming limit curves of AA6082 Aluminium alloy at high strain rates. *The International Journal of Advanced Manufacturing Technology*, *112*(7), 1973-1991.

[118] Pranavi, U., Ramulu, P. J., Chandramouli, C., Govardhan, D., & Prasad, P. R. (2016). Formability analysis of Aluminium alloys through deep drawing process. In *IOP Conference Series: Materials Science and Engineering* (Vol. 149, No. 1, p. 012025). IOP Publishing.

[119] Gautam, V., & Konar, S. (2018). Material selection for a fuel tank and its FE simulation in deep drawing. *Int J Adv Prod Ind Eng*, *3*, 1-4.

[120] Ramulu, P. J. (2020). Aluminium alloys behavior during forming. *Aluminium Alloys and Composites*, 695-728.

[121] He, H., Yang, T., Ren, Y., Peng, Y., Song, X., & Zheng, L. (2022). Experimental investigation on the formability of Al-Mg alloy 5052 sheet by tensile and cupping test. *Materials*, *15*(24), 8949.

[122] Hodžić, E., Domitner, J., Thum, A., Sabet, A. S., Müllner, N., Fragner, W., & Sommitsch, C. (2023). Influence of alloy composition and lubrication on the formability of Al-Mg-Si alloy blanks. *Journal of Manufacturing Processes*, *85*, 109-121.

[123] Bolt, P. J., Lamboo, N. A. P. M., & Rozier, P. J. C. M. (2001). Feasibility of warm drawing of aluminium products. *Journal of Materials Processing Technology*, *115*(1), 118-121.

[124] Tebbe, P. A., & Kridli, G. T. (2004). Warm forming of aluminium alloys: an overview and future directions. *International Journal of Materials and Product Technology*, *21*(1-3), 24-40.

[125] Naka, T., Torikai, G., Hino, R., & Yoshida, F. (2001). The effects of temperature and forming speed on the forming limit diagram for type 5083 Aluminium–magnesium alloy sheet. *Journal of Materials Processing Technology*, *113*(1-3), 648-653.

[126] Hsu, E., Carsley, J. E., & Verma, R. (2008). Development of forming limit diagrams of Aluminium and magnesium sheet alloys at elevated temperatures. *Journal of materials engineering and performance*, *17*(3), 288-296.

[127] Venkateswarlu, G., Davidson, M. J., & Tagore, G. R. N. (2010). Finite element simulation of deep drawing of aluminium alloy sheets at elevated temperatures. *ARPN journal of Engineering and APplied Sciences*, *5*(7), 93-98.

[128] Mahabunphachai, S., & Koç, M. (2010). Investigations on forming of Aluminium 5052 and 6061 sheet alloys at warm temperatures. *Materials & Design (1980-2015)*, *31*(5), 2422-2434.

[129] Hui, W. A. N. G., FRIEDMAN, P., & Lin, G. A. O. (2012). Warm forming behavior of high strength Aluminium alloy AA7075. *Transactions of Nonferrous Metals Society of China*, *22*(1), 1-7.

[130] Sun, H. T., Wang, J., Shen, G. Z., & Hu, P. (2013). Application of warm forming Aluminium alloy parts for automotive body based on impact. *International Journal of Automotive Technology*, *14*(4), 605-610.

[131] Takata, K. (2013). Warm forming of Aluminium alloys. *Nippon Steel Technical Report*, *103*.

[132] Kumar, M., Sotirov, N., & Chimani, C. M. (2014). Investigations on warm forming of AW-7020-T6 alloy sheet. *Journal of Materials Processing Technology*, *214*(8), 1769-1776.

[133] Gnibl, T., & Merklein, M. (2016). Material flow control in tailor welded blanks by a combination of heat treatment and warm forming. *CIRP Annals*, *65*(1), 305-308.

[134] Liu, J., Wang, A., Zheng, Y., Liu, X., Gandra, J., Beamish, K., ... & Wang, L. L. (2017). Hot stamping of AA6082 tailor welded blanks for automotive applications. *Procedia Engineering*, *207*, 729-734.

[135] Ye, T., Xia, E., Qiu, S., Wang, Y., Yue, H., Liu, J., & Wu, Y. (2023). High-temperature tensile mechanical properties and microstructure of rolled 6082-T6 Aluminium alloy sheets. *Materials*, *16*(21), 7019.

[136] Palumbo, G., Piccininni, A., Guglielmi, P., Spina, R., Tricarico, L., Sorgente, D., ... & Franco, A. L. (2017). Warm forming of an AA5754 component for railway vehicle applications. *Procedia Engineering*, *183*, 351-356.

[137] Behrens, B. A., Hübner, S., & Vogt, H. (2018). Formability of 7000 Aluminium alloys in warm and hot forming condition. In *IOP Conference Series: Materials Science and Engineering* (Vol. 418, No. 1, p. 012027). IOP Publishing.

[138] Satya Suresh, V. V. N., Regalla, S. P., & Gupta, A. K. (2018). Optimum parameters to minimize weld line movement in the warm forming of tailor-welded blanks. *Journal of the Brazilian Society of Mechanical Sciences and Engineering*, *40*(4), 234.

[139] Moon, C., & Welo, T. (2026). Formability comparison of recycled and primary AA6082 alloy exposed to different heat treatments. *Advances in Mechanical Engineering*, *18*(4), 16878132261444894.

[140] Simões, V., Oliveira, M., Laurent, H., & Menezes, L. (2026). The Influence of Heat and Holding Time on the Warm Forming of Al–Mg–Si Alloys. *Journal of Manufacturing and Materials Processing*, *10*(3), 94.

[141] Kinsey, B., Liu, Z., & Cao, J. (2000). A novel forming technology for tailor-welded blanks. *Journal of Materials Processing Technology*, *99*(1-3), 145-153.

[142] Kridli, G. T., Friedman, P. A., & Sherman, A. M. (2000). *Formability of Aluminium tailor-welded blanks* (No. 2000-01-0772). SAE Technical Paper.

[143] Chan, S. M., Chan, L. C., & Lee, T. C. (2003). Tailor-welded blanks of different thickness ratios effects on forming limit diagrams. *Journal of Materials Processing Technology*, *132*(1-3), 95-101.

[144] Bhaskar, V. V., Narayanan, R. G., & Narasimhan, K. (2004). Effect of thickness ratio on formability of tailor welded blanks (TWB). In *AIP Conference Proceedings* (Vol. 712, No. 1, pp. 863-868). American Institute of Physics.

[145] Bhagwan, A. V., Kridli, G. T., & Friedman, P. A. (2004). Formability improvement in Aluminium tailor-welded blanks via material combinations. *Journal of manufacturing processes*, *6*(2), 134-140.

[146] Chan, L. C., Chan, S. M., Cheng, C. H., & Lee, T. C. (2005). Formability and weld zone analysis of tailor-welded blanks for various thickness ratios. *J. Eng. Mater. Technol.*, *127*(2), 179-185.

[147] Panda, S. K., Kumar, D. R., Kumar, H., & Nath, A. K. (2007). Characterization of tensile properties of tailor welded IF steel sheets and their formability in stretch forming. *Journal of Materials Processing Technology*, *183*(2-3), 321-332.

[148] Cheng, C. H., Chan, L. C., & Chow, C. L. (2007). Weldment properties evaluation and formability study of tailor-welded blanks of different thickness combinations and welding orientations. *Journal of Materials Science*, *42*(15), 5982-5990.

[149] Panda, S. K., Baltazar Hernandez, V. H., Kuntz, M. L., & Zhou, Y. (2009). Formability analysis of diode-laser-welded tailored blanks of advanced high-strength steel sheets. *Metallurgical and Materials Transactions A*, *40*(8), 1955-1967.

[150] Riahi, M., Amini, A., Sabbaghzadeh, J., & Torkamany, M. J. (2012). Analysis of weld location effect and thickness ratio on formability of tailor welded blank. *Science and Technology of Welding and Joining*, *17*(4), 282-287.

[151] Abbasi, M., Ketabchi, M., Ramazani, A., Abbasi, M., & Prahl, U. (2012). Investigation into the effects of weld zone and geometric discontinuity on the

formability reduction of tailor welded blanks. *Computational Materials Science*, *59*, 158-164.

[152] Korouyeh, R. S., Naeini, H. M., Torkamany, M. J., & Liaghat, G. H. (2013). Experimental and theoretical investigation of thickness ratio effect on the formability of tailor welded blank. *Optics & Laser Technology*, *51*, 24-31.

[153] Kumar, A., Gautam, V., & Kumar, D. R. (2018). Maximum bulge height and weld line displacement in hydroforming of tailor welded blanks. *Journal of Manufacturing Science and Engineering*, *140*(3), 031005.

[154] Cheng, C. H., Jie, M., Chan, L. C., & Chow, C. L. (2007). True stress–strain analysis on weldment of heterogeneous tailor-welded blanks—a novel approach for forming simulation. *International Journal of Mechanical Sciences*, *49*(2), 217-229.

[155] Moayedi, H., Darabi, R., Ghabussi, A., Habibi, M., & Foong, L. K. (2020). Weld orientation effects on the formability of tailor welded thin steel sheets. *Thin-Walled Structures*, *149*, 106669.

[156] Kumar, A., & Gautam, V. (2021). Formability of tailor welded blanks of high strength steel: A review. *Materials Today: Proceedings*, *46*, 6547-6551.

[157] Kesharwani, R. K., Panda, S. K., & Pal, S. K. (2015). Experimental investigations on formability of Aluminium tailor friction stir welded blanks in deep drawing process. *Journal of Materials Engineering and Performance*, *24*(2), 1038-1049.

[158] Weckman, D. C., & Moulton, J. A. (2017). Improved formability of fusion welded AA5182-O Aluminium tailor welded blanks. *Wekding J*, *96*, 319s-333s.

[159] Bagheri, B., Abbasi, M., & Hamzeloo, R. (2021). Comparison of different welding methods on mechanical properties and formability behaviors of tailor welded blanks (TWB) made from AA6061 alloys. *Proceedings of the Institution of Mechanical Engineers, Part C: Journal of Mechanical Engineering Science*, *235*(12), 2225-2237.

[160] Acar, D., Karalı, M., Cora, Ö. N., Burford, D., & Koç, M. (2020). Uniaxial and biaxial deformation characteristics of AA7075-O friction stir welded joints. *Welding in the World*, *64*(9), 1553-1564.

[161] Abbasi, M., Bagheri, B., Abdollahzadeh, A., & Moghaddam, A. O. (2021). A different attempt to improve the formability of Aluminium tailor welded blanks (TWB) produced by the FSW. *International Journal of Material Forming*, *14*(5), 1189-1208.

[162] Kumar, P., & Sharma, S. (2022). Effect of high tool rotational speed and pin diameter on mechanical properties, microstructure and formability of friction stir tailor welded blanks. *Advances in Materials and Processing Technologies*, *8*(4), 4613-4641.

[163] Datta, R., Raja, D., & Bhargava, M. (2025). Microstructure and texture correlation with mechanical properties and formability of friction stir-welded AA5754 sheets. *Journal of Materials Engineering and Performance*, *34*(1), 151-172.

[164] Priyadarshini, A., Sancheti, C. I., & Dwarka, S. S. (2015). Comparative Study of Forgeability of as Extrude AA6082 and as Cast AA6082 Alloy. *ISME J. Manuf. Sci., 6*(1), 1-8.

[165] Lee, Y. B., Shin, D. H., Park, K. T., & Nam, W. J. (2004). Effect of annealing temperature on microstructures and mechanical properties of a 5083 Al alloy deformed at cryogenic temperature. *Scripta materialia*, *51*(4), 355-359.

[166] Changela, K., Krishnaswamy, H., & Digavalli, R. K. (2020). Mechanical behavior and deformation kinetics of Aluminium alloys processed through cryorolling and subsequent annealing. *Metallurgical and Materials Transactions A*, *51*(2), 648-666.

PLAGIARISM REPORT

DELHI TECHNOLOGICAL UNIVERSITY

(Formerly Delhi College of Engineering)
Shahbad Daulatpur, Main Bawana Road, Delhi-42

PLAGIARISM VERIFICATION

Title of the Thesis "**Investigations on Formability of Tailor Welded Blanks of Aluminium Alloy in Warm Working"**

Total Pages: **199**

Name of the Scholar: **Mr. Rakesh Kumar**

Supervisor: **Prof. Vijay Gautam**

Department of Mechanical Engineering

This is to report that the above thesis was scanned for similarity detection. Process and outcome is given below:

Software used: **Turnitin**

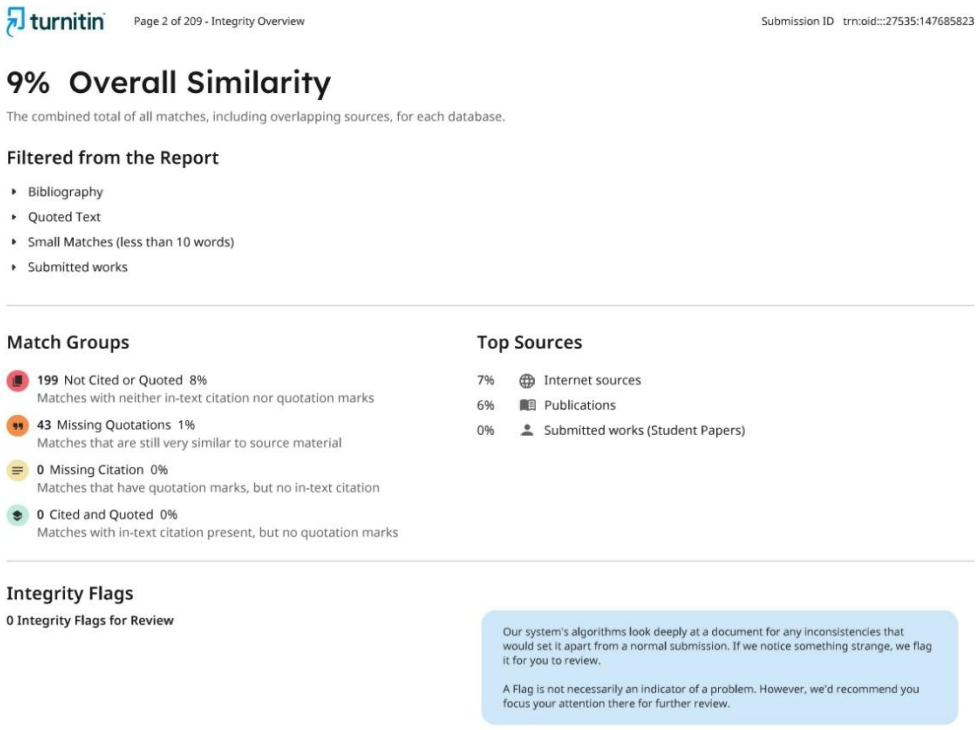
Similarity Index: **9%**

Total Word Count: **39,907**

Date: _____

Candidate's Signature **Signature of Supervisor**

PLAGIARISM REPORT



turnitin Page 2 of 209 - Integrity Overview Submission ID trn:oid:::27535:147685823

9% Overall Similarity

The combined total of all matches, including overlapping sources, for each database.

Filtered from the Report

- Bibliography
- Quoted Text
- Small Matches (less than 10 words)
- Submitted works

Match Groups

199 Not Cited or Quoted 8%
Matches with neither in-text citation nor quotation marks

43 Missing Quotations 1%
Matches that are still very similar to source material

0 Missing Citation 0%
Matches that have quotation marks, but no in-text citation

0 Cited and Quoted 0%
Matches with in-text citation present, but no quotation marks

Top Sources

7% Internet sources
6% Publications
0% Submitted works (Student Papers)

Integrity Flags

0 Integrity Flags for Review

Our system's algorithms look deeply at a document for any inconsistencies that would set it apart from a normal submission. If we notice something strange, we flag it for you to review.

A Flag is not necessarily an indicator of a problem. However, we'd recommend you focus your attention there for further review.

turnitin Page 2 of 209 - Integrity Overview Submission ID trn:oid:::27535:147685823

PUBLICATIONS BASED ON THE RESEARCH WORK

The followings are the publications in journals and conferences based on the present work.

International Journals:

1. **Rakesh Kumar** and Vijay Gautam (2025). Influence of Magnesium Content on Tensile Properties and Deformation Behaviour of Al–Mg–Si Alloy Sheets. Transactions of the Indian Institute of Metals, 78:51. [Springer: IF 1.6, SCIE]

2. **Rakesh Kumar** and Vijay Gautam (2026). Optimization of Laser Butt Welding Parameters for Al-3Mg-Si Aluminium Alloy Sheets Using Response Surface Methodology. International Journal of Maritime Engineering. [Univ Buckingham Press: IF 0.6, SCIE] [Accepted]

International Conferences:

1. **Rakesh Kumar** and Vijay Gautam "Design Consideration of Laser Power Source for Welding Aluminium Alloy Sheet Metal: A Review." Recent Advances in Materials, Manufacturing and Thermal Engineering (RAMMTE-2022) held at Delhi Technological University, New Delhi, India during July 08-09, 2022.

2. **Rakesh Kumar** and Vijay Gautam "The Effect of Magnesium Content on th Microstructure and Mechanical Properties of Al-Mg-Si Alloys." International conference on Optimization Techniques in Engineering and Technology (ICOTET-2024) held at Dronacharya Group of Institution, Greater Noida, U.P, India during June 14-15, 2024.

PROOF OF PUBLICATIONS

Trans Indian Inst Met (2025) 78:51
https://doi.org/10.1007/s12666-024-03543-1

ORIGINAL ARTICLE

Influence of Magnesium Content on Tensile Properties and Deformation Behaviour of Al–Mg–Si Alloy Sheets

Rakesh Kumar[1] · **Vijay Gautam**[1]

Received: 16 November 2024 / Accepted: 17 December 2024
© The Indian Institute of Metals - IIM 2024

Abstract The present study is based on the measurement and effect of Mg content on the tensile behaviour, formability and microstructural characteristics of two different sheets of Al–0.9 Mg–Si and Al–3.1 Mg–Si alloy. The tensile properties of both the sheets have been evaluated by testing laser-cut tensile specimens according to ASTM E8M standard at room temperature. The experimental results indicate that the Al–3.1 Mg–Si alloy, with higher Mg content, exhibits significantly higher yield and tensile strengths, along with nearly double elongation compared to the Al–0.9 Mg–Si alloy. Also, the stretch forming tests revealed better formability in Al–3.1 Mg–Si alloy sheet. Electron backscatter diffraction analysis depicted that the annealed alloy sheet with higher Mg possessed fine equiaxed grains with uniform distribution of Mg_2Si particles, contributing to its higher yield and tensile strengths. After plastic deformation, both the sheet samples exhibited elongated grains with a slight reduction in grain size. Pole figure maps indicated that the Al–3.1 Mg–Si alloy has a stronger texture than the Al–0.9 Mg–Si alloy. After the tensile deformation, the texture of Al–3.1 Mg–Si alloy transformed into a very sharp and strong suggesting a better deformation behaviour. These findings provide valuable insights into how magnesium content influences the strain distribution during plastic deformation and microstructural changes in Al–Mg–Si alloys.

Keywords Al–Mg–Si alloy · Tensile properties · Formability · Forming limit diagram · Electron backscatter diffraction

✉ Vijay Gautam
vijaygautam@dce.ac.in

[1] Department of Mechanical Engineering, Delhi Technological University, Delhi 110042, India

1 Introduction

The development of various grades of aluminium alloys by incorporating alloying elements has been analysed by design engineers with respect to the various requirements of properties in the manufacturing of the sheet metal components for automotive and aerospace industries. The incorporation of each constituent in the alloy imparts unique characteristics, and the combination of these constituents has varied effects on its mechanical properties [1]. Al–Si alloy sheets are widely utilized in diverse technical applications due to their favourable attributes, such as low density, high strength and robust corrosion resistance. The addition of Mg into the alloy is an important key to improve its ability to undergo heat treatment and results in a highly respectable technical alloy. The positive impact of incorporating a secondary phase, such as the Mg_2Si precipitate, via a heat treatment, on the mechanical characteristics of the alloy has been extensively reported in many investigations [2–5]. The growing popularity of Al–Mg–Si alloys in the field of lightweight structures has created a higher need for extrusions in complex shapes that exhibit high strength, durable and toughness. Also, these alloys are required to meet precise criteria for tensile properties, while demonstrating advantageous characteristics required for excellent formability [6]. The utilization of the 6xxx-series Al–Mg–Si wrought alloys has experienced a notable rise in popularity within the architectural and structural components, as opposed to the 2xxx and 7xxx Al alloys [7]. Their attractive characteristics, such as combination of ease of welding and forming, cost-effectiveness, and ability to resist stress-corrosion cracking [8–10], are the main factors contributing to this. The incorporation of the Mg_2Si intermetallic compound into the Al alloys yields significant enhancements in both mechanical and corrosion resistance characteristics [11]. Magnesium plays a significant role as a key alloying element in Al–Mg–Si alloys,

Published online: 11 January 2025

Gmail Rakesh Kumar <rakeshkumar.ry9776@gmail.com>

Consideration for publication in IJME

Editor SI <specialissue@unibuckinghampress.com> Mon, Apr 6, 2026 at 6:24 PM
To: Rakesh Kumar <rakeshkumar.ry9776@gmail.com>

Title: OPTIMIZATION OF LASER BUTT WELDING PARAMETERS FOR Al-3Mg-Si ALUMINIUM ALLOY SHEET USING RESPONSE SURFACE METHODOLOGY

Dear R Kumar, V Gautam

I am pleased to inform you that your paper "**OPTIMIZATION OF LASER BUTT WELDING PARAMETERS FOR Al-3Mg-Si ALUMINIUM ALLOY SHEET USING RESPONSE SURFACE METHODOLOGY**" has been accepted for publication. After the recommendation of learned reviewer comments submitted by you, the article will be published by INTERNATIONAL JOURNAL OF MARITIME ENGINEERING. The article will be published by the University of Buckingham Press in a Special Issue as- Emerging Technologies in Research and Innovation.

You will receive proofreading file for final checking, after this step, no changes can be accepted.

Please share the plagiarism report.

Copyright form is attached herewith; same may be duly filled and submitted at the earliest.

Sincerely,

Editor
Special Issue, IJME
(Emerging Technologies in Research and Innovation)
https://www.intmaritimeengineering.org/index.php/ijme/index

From: Editor SI <specialissue@unibuckinghampress.com>
Sent: Monday, April 6, 2026 12:07 PM
To: Rakesh Kumar <rakeshkumar.ry9776@gmail.com>
Subject: Re: Consideration for publication in IJME

[Quoted text hidden]

Copyright Form_IJME Special Issue.docx
23K

DELHI TECHNOLOGICAL UNIVERSITY
(Formerly Delhi College of Engineering)
Bawana Road, Delhi-110042

Department of Mechanical Engineering
and
Centre for Energy & Environment

Sl. No. RAMMTE-2022/ PR/T8-10

Paper ID 182

Certificate of Presentation

This is to certify that Prof./Dr./Mr./Ms. ..... RAKESH KUMAR ..... has participated in the **3rd International Conference** on "**Recent Advances in Materials, Manufacturing and Thermal Engineering (RAMMTE-2022)**" organized by the Department of Mechanical Engineering, Delhi Technological University, Delhi during 8th & 9th July 2022. He/She has also presented the paper titled, Design consideration of laser power source for welding aluminium alloy sheet metal : A Review ..... We wish him/her a bright success in all his/her future endeavors.

Dr. M. Zuniad
Organizing Secretary

Dr. Anil Kumar
Convener

Prof. Amit Pal
Conference Chair

DRONACHARYA
Group of Institutions

Scopus

2nd International Conference on Optimization Techniques in Engineering and Technology

AIP Conference Proceedings

ICOTET-2024

Certificate of Participation

This certificate is awarded to Prof./Dr./Mr./Ms. RAKESH KUMAR for participating/presenting a paper titled The Effect of Magnesium Content on the Microstructure and Mechanical Properties of Al-Mg-Si Alloys.
In International Conference On Optimization Techniques In Engineering & Technology,
Organized by Dronacharya Group of Institutions, Gr. Noida, (U.P), India.
During 14th-15th June,2024

Prof. (Dr.) Arpita Gupta
Director

Prof. (Dr.) Shailesh Kr. Singh
Convener

Prof. (Dr.) Pawan Sharma
Organizing Chair

BIO DATA

Mr. Rakesh Kumar is currently working as a Research Scholar in the Department of Mechanical Engineering at Delhi Technological University, Delhi, India. His research focuses on the formability of tailor welded blanks of aluminium alloys under warm working conditions. His areas of research include laser welding, tailor welded blanks (TWBs), warm sheet metal forming, aluminium alloys, finite element analysis, and microstructural characterization using Electron Backscatter Diffraction. His research integrates experimental investigations, numerical simulations, and microstructural analysis to improve the formability and performance of lightweight welded structures for automotive applications. He has authored two SCIE-indexed journal publications and one Springer book chapter. He has also presented six research papers at national and international conferences.